FLEXURAL BEHAVIOR OF REINFORCED CONCRETE BEAMS STRENGTHENED WITH EXTERNALLY BONDED HYBRID SYSTEMS

by

Abubakr Ahmed Abdelall Mohammed

A Thesis Presented to the Faculty of the
American University of Sharjah
College of Engineering
in Partial Fulfillment
of the Requirements
for the Degree of

Master of Science in
Civil Engineering

Sharjah, United Arab Emirates

December. 2017

Acknowledgements

I would like to express my sincere gratitude to my supervisors, Dr. Jamal A. Abdalla and Dr. Rami Hawileh, for their continuous support during my MSc dissertations writing, but also their patience, encouragement and guidance.

Many thanks as well to the College of Engineering, Department of Civil Engineering at the American University of Sharjah for providing me with the teaching assistantship program throughout my postgraduate studies.

I would like also to make special thanks to my dearest mother, brothers, sisters and my love who encouraged me and greatly supported me throughout the writing of the dissertation and made this achievement possible.

Dedication

This thesis is dedicated to the soul of my beloved late father.

© 2017 Abubakr Ahmed Abdelall Mohammed. All rights reserved

Abstract

The demand for strengthening of aging reinforced concrete (RC) structures are continuously rising. Carbon fiber reinforced polymers (CFRP) are the most widely used externally bonded-reinforcing (EBR) materials for strengthening and retrofitting of RC structural members. The use of high strength galvanized steel mesh (GSM) strengthening material has recently gained some acceptance. However, Both CFRP and GSM have high strength but have low ductility. Recently developed aluminum alloys (AA) have high ductility and some desirable characteristics that may overcome some of the shortcomings of CFRP and GSM. Combining AA with CFRP and GSM will result in a hybrid material with balanced strength and ductility. Therefore, the major aim of this research is to develop a hybrid ductile and strong retrofitting system by combining AA plates with GSM and CFRP laminates to strengthen RC beams in flexure. A comprehensive experimental program was carried out to determine the tensile strength and the bond strength of the hybrid system. Fifteen-coupon specimens were tested for tensile strength, six specimens of concrete prisms for bond strength and 25 T-beam specimens for flexural strength under a four-point loading. Results showed an increase in the flexural capacity of the strengthened specimen ranging from 10% to 77% compared to the control beam and a decline in ductility of 13% to 59% compared to the un-strengthened specimen. Furthermore, analytical models based on ACI 440.2R-08 guidelines were employed to capture the flexural behavior of the tested specimens. Experimental results correlated well with the analytical predictions in a range of 30% of the experimental values. The study concluded that the newly proposed hybrid systems are promising systems for the improvement of the flexural behavior (strength and ductility) of RC beams.

Search Terms: ***Flexural strengthening, Externally bonded reinforcing material, AA, GSM, CFRP and Reinforced Concrete Prism.***

Table of Contents

Abstract 6

List of Figures 9

List of Tables 13

Chapter 1: Introduction 14

1.1 Background 14
1.2 Research Significant 15
1.3 Research Objectives 16
1.4 Thesis Organization 16

Chapter 2: Literature Review 18

2.1 CFRP 18
2.2 Steel Mesh 19
2.3 Aluminum 20
2.4 Hybrid System 21
2.5 Externally Bonded Prims 22

Chapter 3: Experiential Program 24

3.1 Test specimens properties 24
3.2 Equivalent Matrix for Beams Strengthening 29
3.3 Materials 30
3.3.1 Concrete. 30
3.3.2 Steel rebar. 31
3.3.3 Aluminum. 33
3.3.4 Epoxy. 33
3.3.5 CFRP. 34
3.3.6 Steel Mesh. 34
3.3.7 Hybrid. 35
3.4 Strengthening procedure and test setup 39
3.4.1 Instrumentation (Strain Gauges) 40
3.4.2 Flexural bond tests (small concrete prisms) 41

Chapter 4: Experimental Results 46

4.1 Load versus Mid-span Deflection Relationships 46
4.1.1 Group [GA] 47

4.1.2 Group [GB] 59
4.2 Results Discussion 72
4.2.1 Group A. 72
4.2.2 Group B. 82
Chapter 5: Analytical Prediction 93
5.1 Flexibility Model 93
5.2 Predicted Graphs for the Tested Specimen 95
5.2.1 Group [GA]: 95
5.2.2 Group [GB] 101
5.3 Summary of Predicted Deflection vs Experimental Deflection 107
5.3.1 Group A 107
5.3.2 Group B 108
5.4 Results Discussion 108
Chapter 6: Summary and Conclusion 110
References 112
Vita 116

List of Figures

Figure 2-1: Types of bond test methods [20]. 23
Figure 3-1: Control beam with no EBR materials (Ø12) 24
Figure 3-2: Control beam with no EBR materials (Ø16) 25
Figure 3-3: Test matrix grouping 25
Figure 3-4: Steel rebar tensile test 31
Figure 3-5: Stress strain curves for tested steel rebars. 32
Figure 3-6: Aluminum alloy plate 33
Figure 3-7: ADESILEX PG2 SP and mixed Epoxy [45]. 33
Figure 3-8: CFRP sheet. 34
Figure 3-9: Galvanized steel mesh. 34
Figure 3-10: Dimensions for the aluminum plate and hybrid to be tested [38]. 35
Figure 3-11: Coupon specimen. 36
Figure 3-12: The testing machine configuration 37
Figure 3-13: Strengthening material and hybrid coupon test results. 38
Figure 3-14: Preparing grids for concrete bottom surface 39
Figure 3-15: Prepared FRP's laminates 39
Figure 3-16: Mixing the epoxy resin 40
Figure 3-17: Appling of epoxy resin over the concrete surface. 40
Figure 3-18: Installing steel strain gauge before casting 40
Figure 3-19: Flexural bond test setup 41
Figure 3-20: Specimen test preparation 41
Figure 3-21: Prisms test configuration. 42
Figure 3-22: Internal stresses in beam specimen 43
Figure 3-23: Prism strengthened with AA failure mode. 43
Figure 3-24: Prism strengthened with CFRP failure mode. 44
Figure 3-25: Prism strengthened with GSM failure mode. 44
Figure 3-26: Prism strengthened with CFRP+AA failure mode 44
Figure 3-27: Prism strengthened with GSMAA failure mode. 45
Figure 3-28: Load-deflection curve for all prisms 45
Figure 3-29: Variation of average bond strength of prisms. 45
Figure 4-1: [GA-Control Beam] - Load-deflection curve. 47
Figure 4-2: Failure mode of Beam A-Control. 48
Figure 4-3: Beam A1-A - Load-deflection curve. 48

Figure 4-4: Failure mode of strengthened Beam A1-A.....49
Figure 4-5: Beam A1-C: Load-deflection curve. 49
Figure 4-6: Failure mode of strengthened Bam A1-C.....50
Figure 4-7: Beam A1-S: Load-deflection curve.....50
Figure 4-8: Failure mode of strengthened Bam A1-S. 51
Figure 4-9: Beam A1-CA - Load-deflection curve. 51
Figure 4-10: Failure mode of strengthened Beam A1-CA. 52
Figure 4-11: Beam A1-SA: Load-deflection curve. 52
Figure 4-12: Failure mode of strengthened Beam A1-SA. 53
Figure 4-13: Beam A1-CA-W Load-deflection curve. 53
Figure 4-14: Failure mode of strengthened Beam A1-CA-W. 54
Figure 4-15: Beam A2-A Load-deflection curve. 54
Figure 4-16: Failure mode of strengthened Beam A2-A. 55
Figure 4-17: Beam A2-C Load-deflection curve. 55
Figure 4-18: Failure mode of strengthened Beam A2-C. 56
Figure 4-19: Beam A2-S Load-deflection curve. 56
Figure 4-20: Failure mode of strengthened Beam A2-S. 57
Figure 4-21: Beam A2-CA: Load-deflection curve. 57
Figure 4-22: Failure mode of strengthened Beam A2-CA. 58
Figure 4-23: Beam A2-SA Load-deflection curve. 58
Figure 4-24: Failure mode of strengthened Beam A2-SA. 59
Figure 4-25: Beam B-Control- Load-deflection curve. 59
Figure 4-26: Failure mode of strengthened Beam B-Control. 60
Figure 4-27: Beam B1-A: Load-deflection curve. 60
Figure 4-28: Failure mode of strengthened Beam B1-A. 61
Figure 4-29: Beam B1-C: Load-deflection curve. 61
Figure 4-30: Failure mode of strengthened Beam B1-C. 62
Figure 4-31: Beam B1-S: Load-deflection curve. 62
Figure 4-32: Failure mode of strengthened Beam B1-S. 63
Figure 4-33: Beam B1-CA: Load-deflection curve.....63
Figure 4-34: Failure mode of strengthened Beam B1-CA. 64
Figure 4-35: Beam B1-SA-Load-deflection curve. 64
Figure 4-36: Failure mode of strengthened Beam B1-SA.....65
Figure 4-37: Beam B1-CA-W: Load-deflection curve. 65

Figure 4-38: Failure mode of strengthened Beam B1-CA-W. 66
Figure 4-39: Beam B1-SA-W: Load-deflection curve. 66
Figure 4-40: Failure mode of strengthened Beam B1-SA-W. 67
Figure 4-41: Beam B2-A Load-deflection curve. 67
Figure 4-42: Failure mode of strengthened Beam B2-A. 68
Figure 4-43: Beam B2-C: Load-deflection curve. 68
Figure 4-44: Failure mode of strengthened Beam B2-C. 69
Figure 4-45: Beam B2-S: Load-deflection curve. 69
Figure 4-46: Failure mode of strengthened Beam B2-S. 70
Figure 4-47: Beam B2-CA: Load-deflection curve. 70
Figure 4-48: Failure mode of strengthened Beam B2-CA. 71
Figure 4-49: Beam B2-SA Load-deflection curve. 71
Figure 4-50: Failure mode of strengthened Beam B2-SA. 72
Figure 4-51: Load-deflection curve of all A1 beams. 73
Figure 4-52: Load-deflection of all A2 beams. 73
Figure 4-53: Load-deflection–Beams with one FRP layer of A1 74
Figure 4-54: Load-deflection–Beams with CFRP hybrid of A1. 74
Figure 4-55: Load-deflection–Beams with GSM hybrid A1. 75
Figure 4-56: Load-deflection–Beams with different hybrid of A1. 75
Figure 4-57: Load-deflection–Beams with one FRP layer of A2. 76
Figure 4-58: Load-deflection – Beams with CFRP hybrid of A2. 76
Figure 4-59: Load-deflection – Beams with GSM hybrid of A2. 77
Figure 4-60: Load-deflection – Beams with hybrid of A2. 77
Figure 4-61: Increase in load compared to control beam for A1. 78
Figure 4-62: Decrease in deflection compared to control beam of A1. 78
Figure 4-63: Increase in load compared to control beam of A2. 79
Figure 4-64: Decrease in deflection compared to control beam of A2. 79
Figure 4-65: Load-deflection of all beams with FRP B1. 83
Figure 4-66: Load vs. Deflection, all beams with FRP B2. 83
Figure 4-67: Load-deflection – Beams with one FRP layer B1. 84
Figure 4-68: Load-deflection – Beams with CFRP hybrid of B1. 84
Figure 4-69: Load-deflection – Beams with GSM hybrid of B1. 85
Figure 4-70: Load-deflection – Beams with different hybrid of B1. 85
Figure 4-71: Load vs. Deflection-Beams with one FRP layer of B2. 86

Figure 4-72: Load vs. Deflection, Beams with CFRP hybrid of B2. 86
Figure 4-73: Load-deflection – Beams with GSM hybrid of B2. 87
Figure 4-74: Load-deflection – Beams with different hybrid of B2. 87
Figure 4-75: Increase in load compared to control beam for B1. 88
Figure 4-76: Decrease in deflection vs control beam for B1. 88
Figure 4-77: Increase in load compared to control beam for B2. 89
Figure 4-78: Decrease in ductility compared to control beam for B2. 89
Figure 5-1: A-Control beam-experimental-theoretical results. 95
Figure 5-2: Beam A1-A-experimental-theoretical results. 95
Figure 5-3: Beam A1-C-experimental-theoretical results. 96
Figure 5-4: Beam A1-S-experimental-theoretical results. 96
Figure 5-5: Beam A1-CA-experimental-theoretical results. 97
Figure 5-6: Beam A1-SA -experimental-theoretical results. 97
Figure 5-7: Beam A1-CA-W -experimental-theoretical results. 98
Figure 5-8: Beam A2-A -experimental-theoretical results. 98
Figure 5-9: Beam A2-C-experimental-theoretical results. 99
Figure 5-10: Beam A2-S -experimental-theoretical results. 99
Figure 5-11: Beam A2-CA-experimental-theoretical results. 100
Figure 5-12: Beam A2-SA-experimental-theoretical results. 100
Figure 5-13: Beam B-Control-experimental-theoretical results. 101
Figure 5-14: Beam B1-A -experimental-theoretical results. 101
Figure 5-15: Beam B1-C -experimental-theoretical results. 102
Figure 5-16: Beam B1-S -experimental-theoretical results. 102
Figure 5-17: Beam B1-CA -experimental-theoretical results. 103
Figure 5-18: Beam B1-S A -experimental-theoretical results. 103
Figure 5-19: Beam B1-CA-W -experimental-theoretical results. 104
Figure 5-20: Beam B1-SA-W -experimental-theoretical results. 104
Figure 5-21: Beam B2-A -experimental-theoretical results. 105
Figure 5-22: Beam B2-A -experimental-theoretical results. 105
Figure 5-23: Beam B2-S -experimental-theoretical results. 106
Figure 5-24: Beam B2-CA -experimental-theoretical results. 106
Figure 5-25: Beam B2-SA -experimental-theoretical results. 107

List of Tables

Table3-1 Group organization. 26
Table3-2: Test matrix configuration..... 27
Table3-3: Concrete compressive strength using cylinder standard. 30
Table3-4: Concrete compressive strength using cube standard. 31
Table3-5: Steel rebars dimensions 32
Table3-6: Steel rebars coupon test results 32
Table3-7: AA, GSM and CFRP Manufacture Properties. 35
Table3-8: Designation of tested coupon specimens 36
Table3-9: FRP laminate coupon test results 38
Table3-10: Ultimate load and failure mode 43
Table4-1: Summary of experimental results 80
Table4-2: Summary of ductility indices 81
Table4-3: Ultimate load capacity and mode of failure 82
Table4-4: Summary of experimental results 90
Table4-5: Summary of ductility indices 91
Table4-6: Ultimate load capacity and mode of failure 92
Table5-1: Difference in predicted and experimental deflection values (GA) 107
Table5-2: Difference in predicted and experimental deflection values (GB) 108

Chapter 1: Introduction

1.1 Background

Reinforced concrete (RC) structures are generally durable, however, they deteriorate over time due to environmental reasons. The increase in applied loads along with the changes in structure use, seismic damages or even changes in the design specifications, leads to the degradation in strength and ductility in RC structures and their members. As a result they need to be developed to retrofit their strength and stiffness.

Traditionally, RC members were maintained by enlarging the member's size and providing additional reinforcement. The main drawbacks of this traditional strengthening method are it increases the dead load, the additional reinforcement is prone to corrosion, it reduces the useable living space (head room and/or area) and it increases maintenance cost due to painting and coating of steel [1]. Accordingly, various techniques have been developed to sustain RC members. Steel plates were the dominated and the most widely used externally bonded reinforcing system for deficient reinforced concrete structure in the 1960's. In applying this technique, an adhesive was used as bonding material between the steel and the surface of the RC member. The adhesive layer between the two materials transfers shear forces between the concrete and the steel plate. However, steel as an externally bonded reinforcing material has been unfavorable after a period of time due to its susceptibility to corrosion and other shortcomings. Thus, the need for a new material to replace the steel plates for stronger and more durable structures became of vital importance. One of the most widely used strengthening techniques; is the use of Fiber Reinforced Polymers (FRP) as EBR materials. EBR is used mainly to enhance the tensile strength of the deteriorated RC members.

Over the years, several studies were conducted to explore the use of EBR materials, especially FRP. The success of using FRP as EBR materials is due to its superior qualities of high strength to weight ratio, high corrosion resistance, high stiffness and the ease of installation among other effective structural properties. Externally bonded FRP materials are usually connected to the tension side of flexural members like the

RC Beams and it carries the extra tensile stress that is transferred by the resin adhesive between the FRP and the RC Beam [1-10].

There are so many types of FRP materials that have been used as EBR materials to reinforce deteriorated RC structures; for instance, CFRP, Glass Fiber Reinforced Polymers (GFRP) and Basalt Reinforced Polymers (BFRP) [2]. However, over the last two decades, CFRP was the most commonly used EBR material due to the characteristics previously mentioned, yet it has some limitations such as low-temperature resistance and deboning issues [3]. Recently, AA plates were introduced for the same purpose. The use of this novel material (AA) and hybrids instead of other conventional materials seemed to be very promising in enhancing both the strength and ductility of the strengthened specimen [1–15].

CFRP, GSM and AA composite materials behave in linear elastic manner until failure. Usually beams re-reinforced with CFRP sheets illustrate lower ductility and high strength than those strengthened with AA plates. Moreover, CFRP and GSM composites have superior properties that include high tensile strength, high modulus of elasticity and relatively low elongation at failure. On the other hand, AA has a lower tensile strength, a reasonable modulus of elasticity and high elongation. Therefore, a hybrid system of CFRP, GSM and AA been proposed to efficiently utilize the mechanical properties of each FRP sheet and to ensure a steady rather than a sudden failure of the composites.

In Summary, the main objective of this study is to investigate the performance of the combined hybrid of AA, GSM and CFRP as new EBR materials for RC beams deficient in flexure.

1.2 Research Significant

The need for strengthening aged RC structure has recently increased due to many reasons and resulted in the development of many new strengthening techniques. One of the widely used techniques involves the use of FRP composite materials as EBR. The use of such material has many advantages as well as some disadvantages. Over the last two decades, CFRP emerged as the most widely used as EBR material, lately high strength AA and GSM with high tensile strength have been introduced as more devolved materials. Moreover, AA Plates have many advantageous features that may

be combined with the desirable feature of GSM and CFRP to produce hybrid Interface with large ductility and relatively low strength compared to GSM and CFRP that have high strength and low ductility. Combining AA with GSM and CFRP will likely result in hybrid materials that may have practically attractive.

In this study, the viability and effectiveness of using AA, CFRP and GSM and their hybrid combinations as new EBR materials for RC T-Beams was explored. A predicted model of ACI 440.2R-08 design guidelines used and developed based on the experimental results, has been developed to simulate the bond slip-stress and the flexural behaviors of the strengthened T-Beams. Therefore, the significance of this research study will result in advancing the knowledge in the field of strengthening, repairing and retrofitting using hybrid combination of AA, GSM, and CFRP as new EBR materials.

1.3 Research Objectives

This research study focused on exploring and understanding the effectiveness of using AA, CFRP, GSM and their hybrid combinations as a new EBR materials for RC beams that are deficient in flexure. Therefore, the primary objectives of this research study are:

1) Determining the mechanical properties of the hybrid combinations of AA, GSM, and CFRP.
2) Study the behavior of AA, GSM, and CFRP externally bonded to concrete prisms.
3) Evaluate the performance of RC T-Beams externally bonded with AA, GSM, CFRP and their hybrid combinations, and evaluate their flexural performance.
4) Develop analytical models to predict and capture the flexural response and behavior of the tested T-Beams specimens using the ACI318-11 and ACI 440.2R-08 guidelines.

1.4 Thesis Organization

Chapter 2 of this thesis provides a literature review on the different types of FRP materials that have been used for strengthening RC beams. Chapter 3 illustrates a very detailed experimental program including specimens' preparation, materials used, test

matrix, and testing setup. Chapter 4 explains the experimental results and discusses the effect on flexural performance of using AA, CFRP, GSM and their hybrid combinations. Chapter 5 shows the developed analytical models using the ACI318-11 and ACI 440.2R-08 guidelines to predict the Load-deflection curve response and compare that to the actual tested data. Chapter 6 summarizes the key findings of this research study, and provides future suggestions.

Chapter 2: Literature Review

Over the years several materials have been used as EBR. Including CFRP, GSM, AA, hybrid among others. The techniques of strengthening RC beams externally in flexural by bonding FRP sheets and plates to the beam's soffit via epoxy had shown a considerable enhancement in increasing the load carrying capacity and stiffness of the strengthened specimens. The following sections present some of the significant work in using EBR materials in flexural strengthening.

2.1 CFRP

CFRP is considered as the most widely used externally bonded material due to their various advantages in increasing the load carrying capacity of aging RC structures. However, CFRP has been developed and used as an EBR material as well as a replacement to steel, and this is due to many required characteristics of CFRP's such as high tensile strength, high corrosion resistance, low density, high durability and ease of installation. Nevertheless, the use of CFRP as externally bonded material has some shortcomings as well. These include low-temperature resistance, deboning and degradation due to environmental factors [16]–[18].

Several investigators studied the use of CFRP as EBR for beams deficient in flexure: Ashour et al. [18] studied the flexural strengthening of 16 RC continuous beams using CFRP laminates, they used different combinations of both reinforcing steel bars and external bonded CFRP laminates. They found out that most of the tested beams resulted in increasing the load capacity of the beams, but the ductility index was lower than the controlled beam. Moreover, they concluded that the main failure mode of the 16 tested beams was delamination which was a brittle cracking failure of the concrete cover next to the CFRP laminates.

Dong et al. [19] examined the structural behavior of 14 RC beams in total with external flexural and flexural–shear strengthening using CFRP and GFRP sheets. Seven beams were strengthened in flexure at the bottom face, and the rest of the beams were strengthened for both flexure and shear, where the CFRP sheets were at the bottom and side of the beams. They concluded that the flexural strength capacity of the strengthened beams increased from 41% to 125% over the control specimen. They also

observed that the CFRP and GFRP sheets not only improved the stiffness and the strength of the beams but also enhanced the beam's ductility.

Esfahani et al. [20] investigated the flexural performance of 12 RC beams strengthened in flexure using CFRP sheets. They divided the beams into three different groups based on their reinforcement ratio, they observed that the stiffness and the flexural strength of the strengthened beams were increased appreciably compared to the control beams. They also observed that the analytical prediction, based on AC and ISIS Canadian Standards, are more accurate compared to the experimental results when the reinforcement ratio is maximum and less accurate when the reinforcement ratio is low.

Aboutaha et al. [21] investigated the behavior of nine RC beams strengthened with CFRP sheets. The parameters used were the amount of tension reinforcing steel bars, steel reinforcing yield strength and CFRP type of anchorage. They observed that the flexural ductility of the strengthened beams low when the reinforcement ratio is low, and demonstrated CFRP anchoring techniques could significantly increase the flexural ductility of the strengthened beams while delaying or preventing the delamination of the CFRP sheets.

Toutanji et al. [22] studied the flexural performance of eight RC beams strengthened externally with three to six layers of CFRP sheets and bonded with an inorganic resin. They found that by increasing the number of CFRP sheets, the load carrying capacity increased by up to 170% compared to the control beam, while the ductility of the strengthened beams was significantly reduced. Moreover, they observed that two failure modes happened for the tested beams strengthened with three and four layers of CFRP sheets, some failed by CFRP rupture, while those with five and six layers of CFRP sheets failed by CFRP delamination.

2.2 Steel Mesh

Recently, GSM has become one of the most promising and cost-effective externally bonded material in terms of strengthening reinforced concrete structure. GSM compared to GFRP and CFRP, has many advantages such as strength, less installation cost, ductility and resistance to flexure and shear[23], [24]. In spite of that, GSM hasn't been used widely and it is still an area of research. Using GSM as a hybrid combination with AA is some of the objective of this study.

Hawileh et al. [6] studied the flexural performance of reinforced concrete beams that been strengthened using hardwire steel fiber sheets. Two rectangular beams had been strengthened externally with one layer of medium and high cord density of 4.72 and 7.87 cords/cm. The specimens were tested under four-point loading, the test results showed an increase in the load carrying capacity by 44% and 48% for the medium and high cord density specimens respectively. Moreover, they concluded that the ductility of the tested specimen was much lower than that of the control beam due to concrete cover delamination.

De Felice et al. [24] carried out a comprehensive experimental program on the use of steel reinforced polymers (SRP) as external bonded material. Firstly, they studied the mechanical properties under tensile loading, the durability of steel textile, the shear bond performance and finally, they studied the applications of steel reinforced polymers that bonded to structural members which are made of concrete or masonry. Finally, they observed that using SRP as EBR is a very practical option for strengthening whether concrete or masonry structural members. They also added that the use of SRP is much better than CFRP in terms of strengthening system and EBR materials.

Borri et al. [23] studied the flexural performance of wood beams strengthened with high strength steel cords using four-point load test. The bending tests on strengthened beams showed a non-linear behavior was observed during the experimental work. Generally, they concluded that the behavior of the strengthened specimen indicated significant increase in the capacity and ductility in comparison to control specimen. In some cases, the maximum load increased by more than 100% compared to un-strengthened beams.

Bashandy [25] studied the flexural behavior of RC beams strengthened in flexure using steel mesh and plastic mesh. They found out that using steel mesh increased the ultimate load by 11-25%. Moreover, the steel mesh enhanced the crack pattern compared to the plastic mesh.

2.3 Aluminum

Lately, developed AA with high tensile strength are promising candidates as EBR materials. They have a favorable feature, which makes it suitable for many applications. Moreover, they can overcome some of the shortcomings of other FRP materials like

CFRP and GSM when they are combined as hybrid EBR. The use of AA in engineering design and application is based on many factors related to its physical and mechanical properties [26], [27].

Aluminum metal is widely known for its high ductility. It has many advantages such as lightweight, corrosion resistance, high strength to weight ratio, ease of production, recyclability and relatively low cost. Therefore, combining AA with FRPs like CFRP and GSM using the epoxy will give the system some ductility and hence, the system will give an alert before failure under tension. Also, this combination technique will result in enhancing the Stress-Strain curve of the composite material to be much closer in characteristics to that of steel[3], [28], [29].

2.4 Hybrid System

Many studies have considered improving the mechanical characteristics of the FRP systems, as well as studying different techniques for different arrangements of materials [1, 3, 19-29]. Multiples studies combined GFRP with CFRP. The authors found that strengthened specimens with this hybrid material have shown an improved strength and ductility under flexure[1, 19, 20, 30-32]. Among them, Grace et al. developed a ductile hybrid of CFRP combined with GFRP. Eight concrete beams were tested under flexure, and the results were compared with similar beams strengthened with CRFP plates and sheets only. It was noted that the beams strength with the developed fibers achieved higher ultimate strength and ductility indices [30].

Similarly, Wu et al. [31] studied the effect of combining high strength and high modulus carbon sheets to form a new hybrid system. Fifteen beams were tested under tension in which these RC beams were strengthened with different configurations of the proposed hybrid system. The high modulus carbon sheets showed a large increase in the flexural stiffness, yielding load and ductility.

Hawileh et al. [6] studied the effect of combined CFRP and GFRP. Series of Strengthened RC beams were tested and an increase in the load capacity of them ranged from 30% to 98%, depending on the combination of fibers. It was also noted that the ductility at failure load of the strengthened beams is higher than that with a single carbon sheet.

Wu et al. [32] studied experimentally the tensile properties of hybrid FRP rods using carbon and E-glass fibers as well as vinyl ester and unsaturated polyester resins. The effect of hybridization on the tensile properties of FRP rods was obtained by comparing the results of the tensile test for the hybrid rods to those of the non-hybrid rods. The results of the test program indicated that the ultimate strain of the hybrid rod with the dispersed type was increased by up to 33%.

Xiong et al. [39] investigated the performance of six RC beams strengthened externally using two types of strengthening systems. One with hybrid CFRP/GFRP system, and the other one was CFRP only. They tested the beams using four-point loading test, and they found out that the beams with hybrid CFRP/GFRP system were 89.7% higher than those beams strengthened with CFRP only. Furthermore, the hybrid combination beams were 10 and 38% less in stiffness and cost compared to those CFRP beams. Also, they observed that the deflection ductility obtained by the hybrid combination beams were 16.2% less than the control beam.

Attari et al. [39] investigated the effectiveness of hybrid FRP sheets using unidirectional CFRP and GFRP which combined the high tensile strength of CFRP with the high ductility of the GFRP. Conducted results showed that using two layers of the hybrid FRP sheets of CFRP and GFRP increased the flexural strength capacity of the RC specimens by 114%, in addition, it showed a good sign of ductility for those specimens strengthened with the hybrid fibers over the control beam.

Throughout the recent years, it has been clear that the literature is lacking the information on using the GSM, AA in flexural or even the use of the hybrid system of CFRP sheets, GSM and AA in strengthening RC members. Therefore, this research will significantly increase understanding the effectiveness of using their hybrid combinations as new EBR materials for RC Beams by exploring and investigating the use of each material.

2.5 Externally Bonded Prims

Many studies have been carried out to develop the assessment of the bond capacity of the FRP bonded to the concrete soffit. As been discussed before there are several factors affecting the contribution of using externally bonded materials for strengthening purposes, especially epoxy adhesive plays a vital role in transferring the tensile stress

from the concrete surface to the external FRP materials. Moreover, surface preparation plays another major role in increasing the bond strength between the strengthening FRP materials and the concrete surface. Epoxy adhesive usually has lower tensile strength as compared to the externally bonded composite sheet or plate; therefore, failure will initiate at the FRP-concrete interface. Several FRP composite design codes showed that the design of CFRP composite depends on the bond characteristics between the concrete and the CFRP laminate [38]. A number of experimental investigations have been conducted to study the bond behavior between the CFRP and concrete interface. All the experimental results showed that CFRP composite laminates failed due to sheet de-bonding or delamination modes of failure [26]. Therefore, the externally bonded system failed before the laminates reach its ultimate tensile strength [10], [40].

Different test setups such as single shear, double shear and beam tests have been used to study the interfacial behavior between the CFRP and concrete. Studies have also shown that experimental results can vary significantly due to different types of setups. Flexural prisms bond tests have shown to be one of the most effective techniques to predict the bond strength between the strengthening material and concrete surface. Therefore, in this study flexural prisms bond tests have been used to study the bond behavior between the concrete and AA, CFRP, GSM and their combinations composites laminates [46].

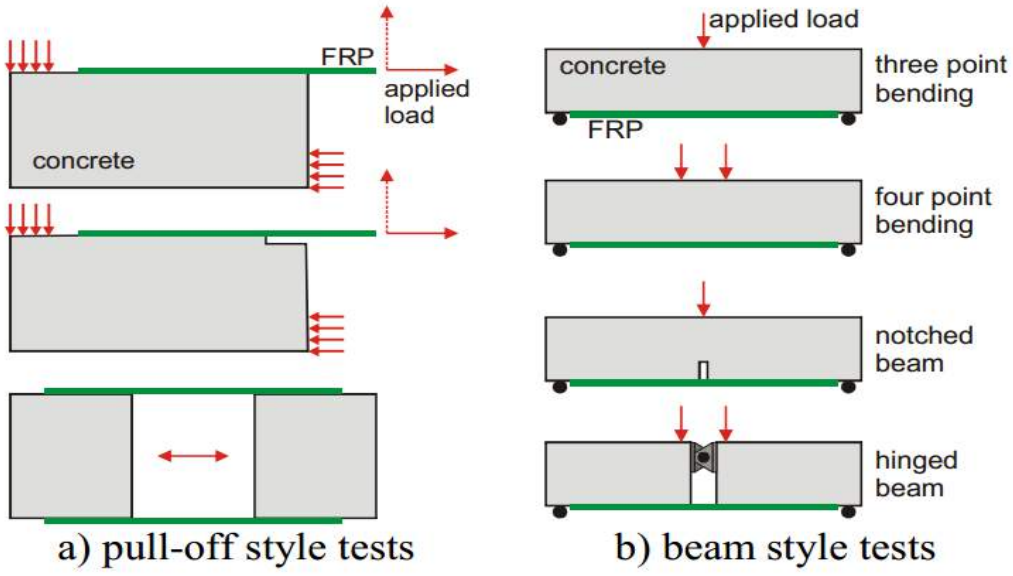

Figure 2-1: Types of bond test methods [20].

Chapter 3: Experiential Program

The experimental program conducted in this research mainly focused on studying the flexural behavior of RC T-beams externally strengthened with different combinations of AA, CFRP and GSM. In this program, the variables within each group are the steel reinforcement ratio (0.56% and 1.04%), number of strengthening layers and finally, the width of strengthening layers (50 mm and 100 mm).

3.1 Test specimens properties

A total of twenty five beams were casted with an average concrete strength (*f'c*) and steel yield strength (*fy*) of 45 and 560 MPa, respectively. They were T-section of 150 mm web wide, 450 mm flange wide, 300 mm deep and 2000 mm long. Four bars of 8 mm diameter were used as top reinforcement and 8 mm diameter bars were used as shear reinforcement at 100 mm spacing. There were two different group of bottom reinforcement, first 12 beams were reinforced with two bars of 12 mm diameter and the remaining 13 beams were reinforced with two bars of 16 mm diameter, details of the cross section are presented in Figures 3.1 and 3.2. Tables 3.1 and 3.2 display the beam specimens, designations and cross-section detailing that were used during the experimental program. The beam specimens were designed per the ACI318-14 [40] design beams, and the orientation of the FRP's layers were varied across the specimens as shown in Figure 3-3.

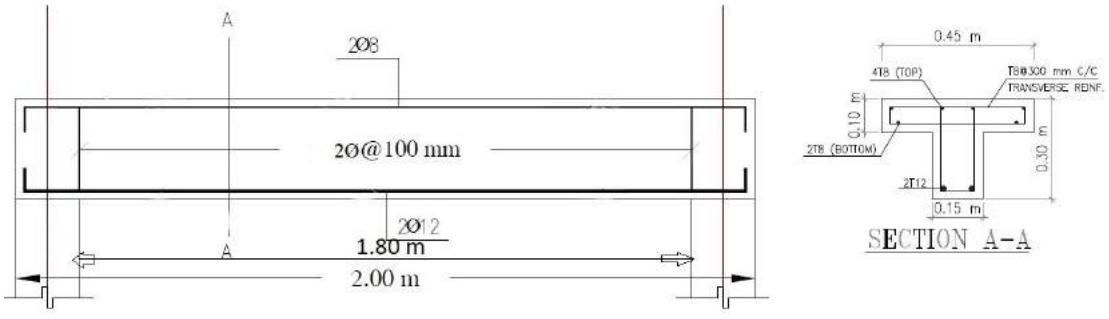

(a) Beam Elevation (b) Beam Section

Figure 3-1: Control beam with no EBR materials (Ø12)

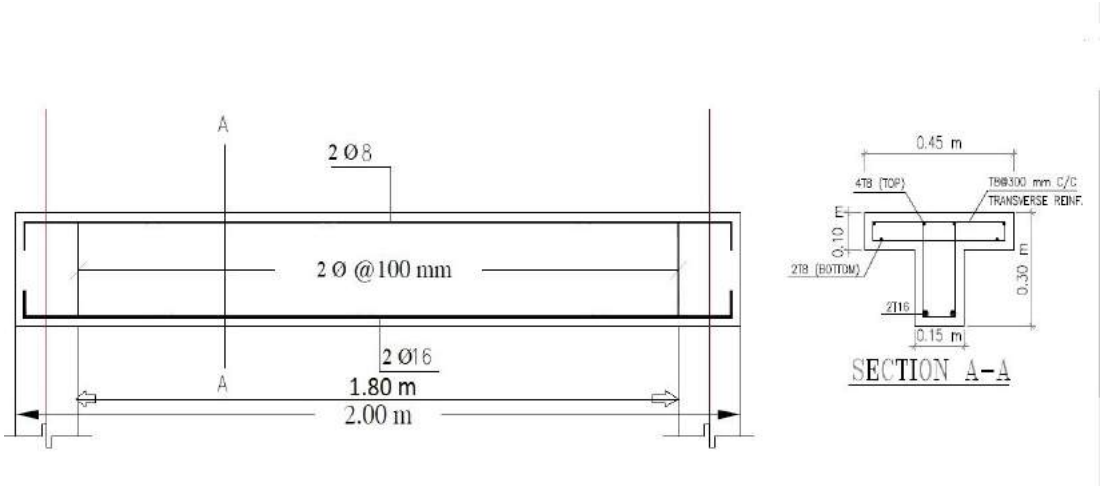

Figure 3-2: Control beam with no EBR materials (Ø16)

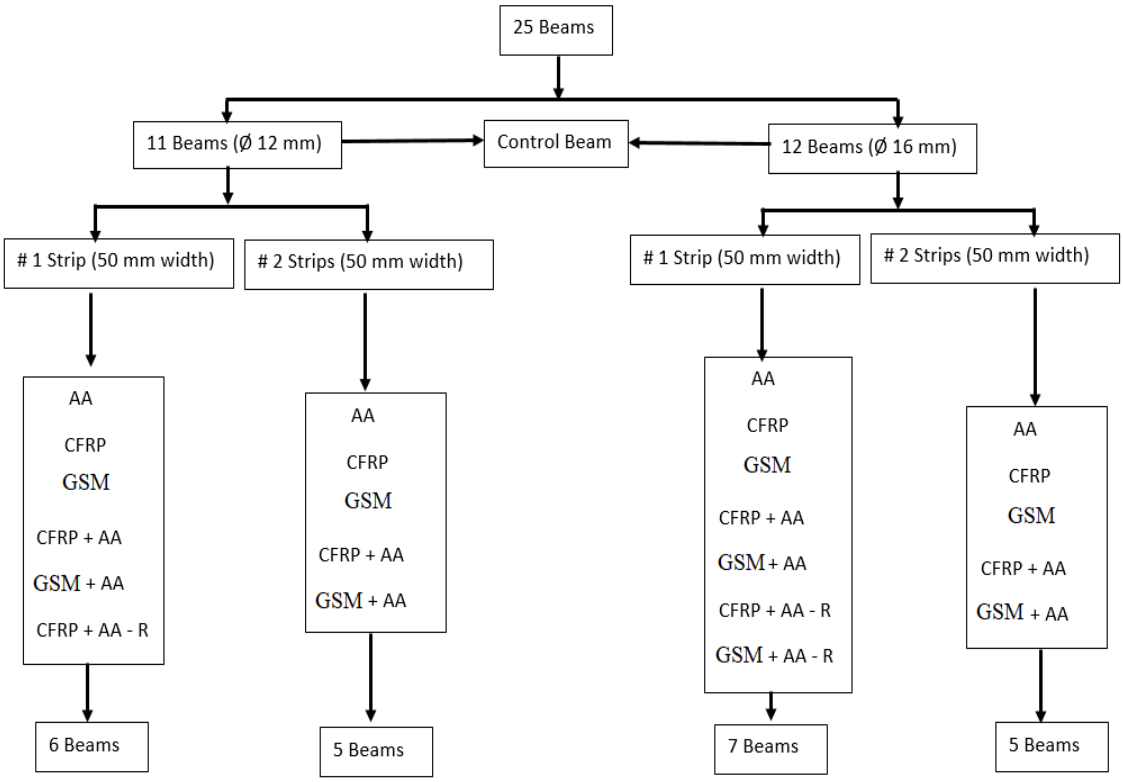

Figure 3-3: Test matrix grouping

Table3-1 Group organization.

Specimen	**Group A**	**Group B**
Quantity	12 x 2.0 m Beams	13 x 2.0 m Beams
Bottom Bar Size	12	16
Size (mm x mm)	450*150*300	450*150*300
Section Details	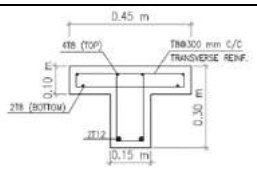	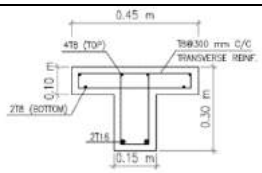
ρ % (mm^2 / mm^2)	0.5776	1.0352
f'c (MPa)	45.01	45.01
fy (MPa)	560	560
Number of Specimen	12	13

Table3-2: Test matrix configuration

Beam	Desgignation	Side view
Control Beam	A- Control , or B-Control	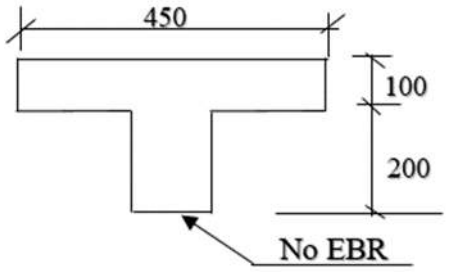
One layer of CFRP, AA or GSM bonded to the soffit.	A1-A A1-C A1-S	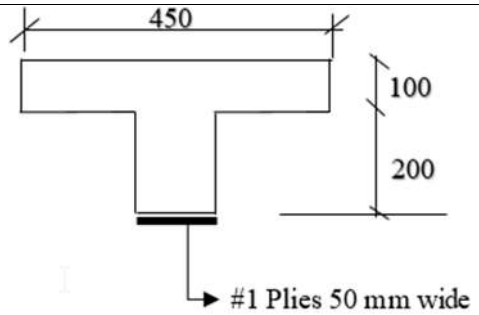
Hybrid of CFRP with AA, Or Hybrid of GSM with AA (50 mm layer width).	A1-CA A1-SA	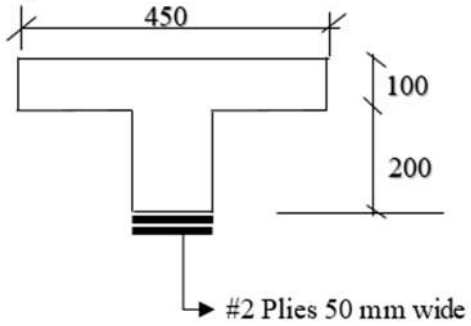

Hybrid of CFRP with AA wrapped in U shape with CFRP at both ends, Or Hybrid of GSM with AA wrapped in U shape with CFRP at both ends	A1-CA-W A1-SA-W	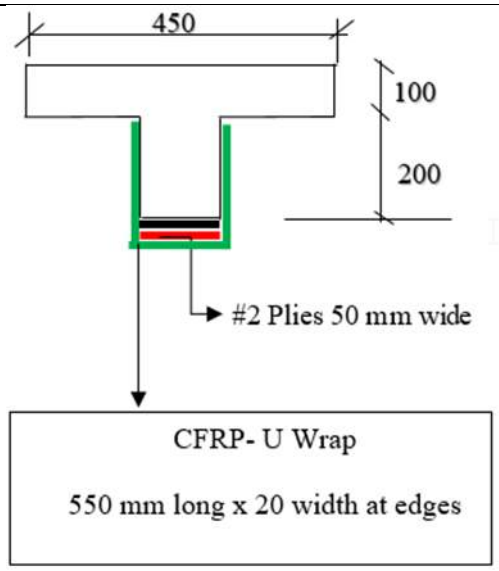
One layer of CFRP, AA or GSM bonded to the soffit.	B2-A B2-C B2-S	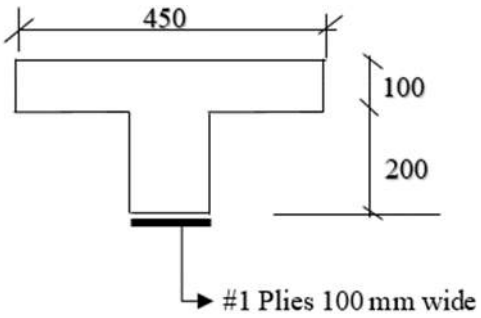
Hybrid of CFRP with AA, Or Hybrid of GSM with AA (100 mm layer width).	B2-CA B2-SA	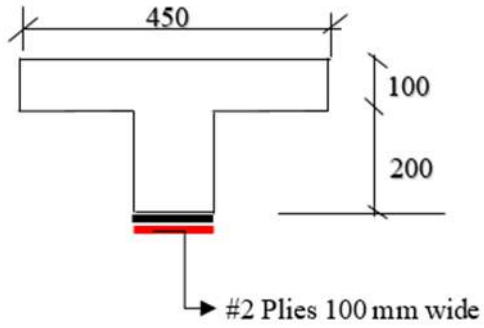

3.2 Equivalent Matrix for Beams Strengthening

In this section calculation for the equivalent test matrix for AA, GSM, CFRP and their hybrid combination will be developed using the ACI 440.2R-08. The FRP reinforcement ratio (ρ_{eq}), which illustrate the equivalent properties and forces that will be added by the FRP reinforcement to the concrete section based on the considerations for the stiffness of each hybrid material. Based on that, we need to confirm and compare how many layers of AA that are equivalent to the number of layers of CFRP and GSM individually, as well when it comes to hybrid layers versus each other's. As shown below, an example for each beam's group with the two strips of FRP material that had 100 mm width, and the same example goes for the 50 mm width.

❖ Group A

➢ (# 2 Strip, 100 mm width)

1. AA

$$\rho_{eq} = \rho_s + n\rho_f = \frac{A_s}{bd} + \frac{E_f}{E_s}\frac{A_f}{bd} = \frac{226.19}{150\times 261} + \frac{70}{200}\frac{100\times 3}{150\times 261} = 0.00846$$

2. GSM

$$\rho_{eq} = \rho_s + n\rho_f = \frac{A_s}{bd} + \frac{E_f}{E_s}\frac{A_f}{bd} = \frac{226.19}{150\times 261} + \frac{190}{200}\frac{100\times 0.254}{150\times 261} = 0.0064$$

3. CFRP

$$\rho_{eq} = \rho_s + n\rho_f = \frac{A_s}{bd} + \frac{E_f}{E_s}\frac{A_f}{bd} = \frac{226.19}{150\times 261} + \frac{59.93}{200}\frac{100\times 0.8}{150\times 261} = 0.00652$$

4. AA + GSM

$$\rho_{eq} = \rho_s + n\rho_f = \frac{A_s}{bd} + \frac{E_f}{E_s}\frac{A_f}{bd} = \frac{226.19}{150\times 261} + \frac{70}{200}\frac{50\times 3}{150\times 261} + \frac{190}{200}\frac{50\times 0.254}{150\times 261} = 0.00743$$

5. AA + CFRP

$$\rho_{eq} = \rho_s + n\rho_f = \frac{A_s}{bd} + \frac{E_f}{E_s}\frac{A_f}{bd} = \frac{226.19}{150\times 261} + \frac{70}{200}\frac{50\times 3}{150\times 261} + \frac{59.93}{200}\frac{50\times 0.8}{150\times 261} = 0.00749$$

❖ Group B

➢ (# 2 Strip, 100 mm width)

1. AA

$$\rho_{eq} = \rho_s + n\rho_f = \frac{A_s}{bd} + \frac{E_f}{E_s}\frac{A_f}{bd} = \frac{402.12}{150\times 259} + \frac{70}{200}\frac{100\times 3}{150\times 259} = 0.01305$$

2. GSM

$$\rho_{eq} = \rho_s + n\rho_f = \frac{A_s}{bd} + \frac{E_f}{E_s}\frac{A_f}{bd} = \frac{402.12}{150\times 259} + \frac{190}{200}\frac{100\times 0.254}{150\times 259} = 0.01097$$

3. **CFRP**

$$\rho_{eq} = \rho_s + n\rho_f = \frac{A_s}{bd} + \frac{E_f}{E_s}\frac{A_f}{bd} = \frac{402.12}{150\times 259} + \frac{59.93}{200}\frac{100\times 0.8}{150\times 259} = 0.0111$$

4. AA + GSM

$$\rho_{eq} = \rho_s + n\rho_f = \frac{A_s}{bd} + \frac{E_f}{E_s}\frac{A_f}{bd} = \frac{402.12}{150\times 259} + \frac{70}{200}\frac{50\times 3}{150\times 259} + \frac{190}{200}\frac{50\times 0.254}{150\times 259} = 0.01201$$

5. AA + CFRP

$$\rho_{eq} = \rho_s + n\rho_f = \frac{A_s}{bd} + \frac{E_f}{E_s}\frac{A_f}{bd} = \frac{402.12}{150\times 259} + \frac{70}{200}\frac{50\times 3}{150\times 259} + \frac{59.93}{200}\frac{50\times 0.8}{150\times 259} = 0.01201$$

3.3 Materials

3.3.1 Concrete. Total of 25 RC beams were casted using a ready-mix concrete supplied by RAK Precast Company, the average compressive strength was 45 MPa, three different cylinders and cubes were tested and we got the value of the exact compressive strength of the RC beams, as shown in the Tables 3-3 and 3-4.

Table3-3: Concrete compressive strength using cylinder standard.

Specimen	Compressive strength (MPa)
Cylinder 1	45.0
Cylinder 2	44.9
Cylinder 3	45.1
Average	45.01

Table3-4: Concrete compressive strength using cube standard.

Specimen	Compressive strength (MPa)
Cube 1	58.0
Cube 2	58.7
Cube 3	52.2
Average	56.3

3.3.2 Steel rebar. A three steel rebars were tested at room temperature in the laboratory under tension to get the mechanical properties of the used steel in this research study, at a rate of 2 mm/min using an INSTRON Universal Testing Machine (UTM), each coupon specimen was gripped at the same distance from the specimen's both ends, thus making a clear gauge length of 100 mm, as shown in Figures 3-4 and 3-5 and Tables 3-5 and 3-6.

Figure 3-4: Steel rebar tensile test

Table3-5: Steel rebars dimensions

Bar Size	Density	Nominal	Cross-Sectional Area
8	0.395	8.0	50.265
12	0.888	12.0	113.097
16	1.579	16.0	201.062

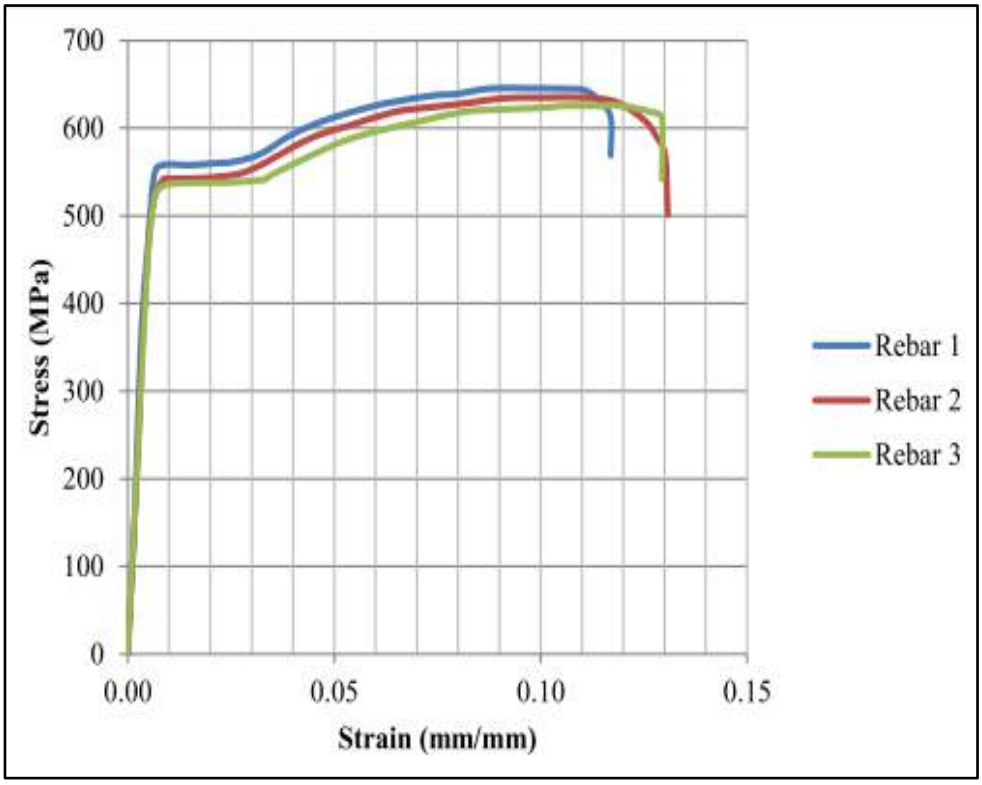

Figure 3-5: Stress strain curves for tested steel rebars.

Table3-6: Steel rebars coupon test results

Specimen	Yield Strength (MPa)	Tensile Strength (MPa)	Modulus of Elasticity (GPa)
Rebar [1]	558.38	655.22	199.93
Rebar [2]	548.78	633.08	200.01
Rebar [3]	547.28	632.21	199.98
Average	551.47	640.17	199.97

3.3.3 Aluminum. They are different types of AA, but mainly what will be used in this study is a member of the AA5083 family as presented in Figure 3-6. Because this type of AA has many features and advantages, one of them is high tensile strengths almost equal to 288 MP as shown in the mechanical properties Table3-7.

Figure 3-6: Aluminum alloy plate

3.3.4 Epoxy. Many studies showed that the epoxy (resin) used as adhesive to bond the sheets/plates to the bottom face of RC beams in order to transfer the stress between the tension face of RC beams and the FRP laminates [42]. Generally, epoxy materials are formed from two parts, the hardened part and liquid part which needs to be mixed together within a certain mix ratio and here in this research study it's 1:3, all of this depends on the type of the epoxy that commercially available in the market. In this research study, ADESILEX PG2 SP is the epoxy used for bonding the FRP sheets to the RC beams as shown in Figure 3-7. The mechanical properties that specified by the manufactured are 80 MPa, 40 MPa, 8000 MPa, 4000 MPa and 30 MPa for Compressive strength (ASTM D-695) , flexural strength (ISO-178), Modulus of elasticity under compression (ASTM D-695), Modulus of elasticity in flexural (ISO-178), and tensile strength (ASTM D-638), respectively [45].

(a) Adesilex Pg2 SP (b) Mixed Epoxy

Figure 3-7: ADESILEX PG2 SP and mixed Epoxy [42].

3.3.5 CFRP. The CFRP used in this project was SikaWrap-300 C/60, a unidirectional woven carbon fiber used for dry or wet application processes, as shown in Figure 3-8. It can be used for flexural and shear strengthening of concrete structures, brickwork and timber. SikaWrap-300 C/60 is a lightweight material with a total areal weight of 300 g/m2 ± 15 g/m2, which contains black carbon fibers (99% of total areal weight) woven by white thermoplastic heat-set fibers (1% of total areal weight). The manufacturer specifies a fiber design thickness of 0.166 mm. The manufacturer also provides the dry fiber properties, which include tensile strength, tensile elastic modulus and elongation at break which equals 3900 N/mm2, 230000 N/mm2 and 1.5%, respectively [43].

Figure 3-8: CFRP sheet.

3.3.6 Steel Mesh. Galvanized steel mesh (GSM) fabric with high tensile strength which is composed of high carbon steel cords with a micro-fine zinc galvanized coating [47] will be used. The high tensile strength GSM fabrics with high, medium, and low cord densities of 7.09, 4.72 and 1.57 cord/cm will be explored. The mechanical properties of GSM are shown in Table3-7, but we end up using only the high steel mesh cords because of the good results that been found in the pilot study compared to the other twos GSM, as presented in Figure 3-9.

Figure 3-9: Galvanized steel mesh.

Table3-7: AA, GSM and CFRP Manufacture Properties.

Material	Thickness (mm)	Tensile Strength (MPa)	Modulus of Elasticity (GPa)
Aluminum	3.0	288	70.3
GSM	0.38	2800	190
CFRP	0.17	310	70-250

3.3.7 Hybrid. Fifteen different types of coupon laminates were prepared and tested in this experimental investigation to examine the mechanical properties of hybrid FRP laminates. The sample included different combinations of Carbon, Aluminum, and Steel Mesh. All coupon laminates were prepared according to ASTM (D 638 - 02a) [48] had a width and a gauge length of 45 mm and 100 mm, respectively. The thickness of the coupon varied between 0.91 mm to 3.21 mm depending on the type of laminate and number of FRP layers, except the control specimen, it was 2.98 mm thickness. All composite laminate coupon samples were prepared in such a way to resemble real application when externally bonded to concrete surfaces. This was achieved by applying a layer of epoxy adhesive on a smooth surface of Aluminum, followed by the CFRP sheet. The Same procedure was done with steel Mesh. As shown in Figure 3-10 and 3-11

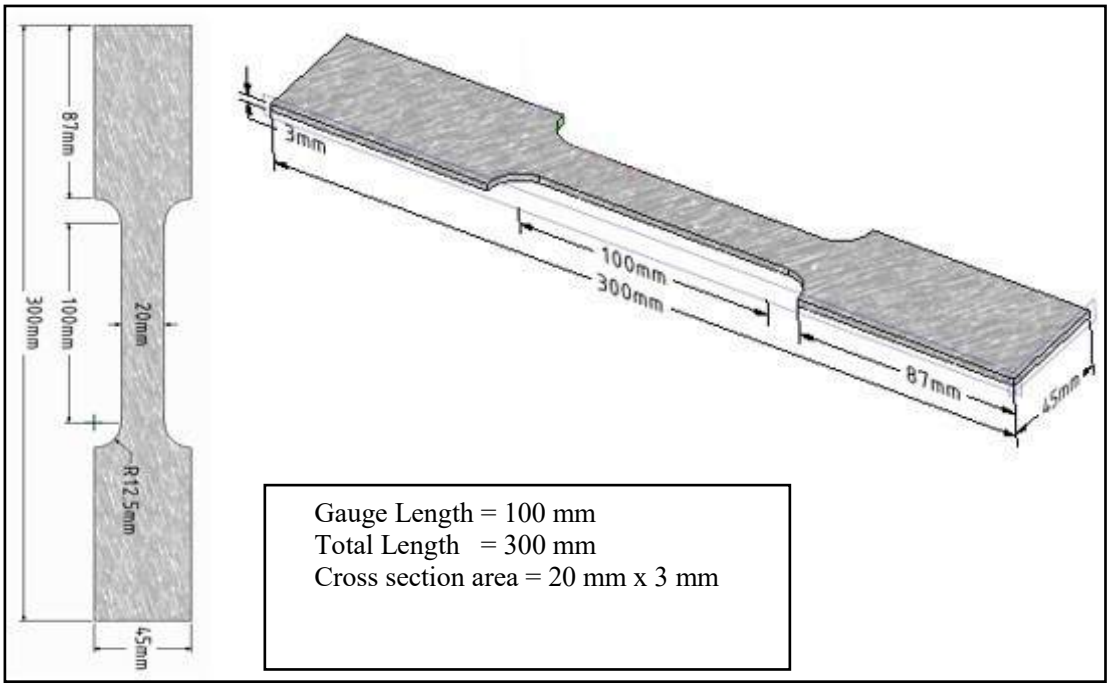

Figure 3-10: Dimensions for the aluminum plate and hybrid to be tested [38].

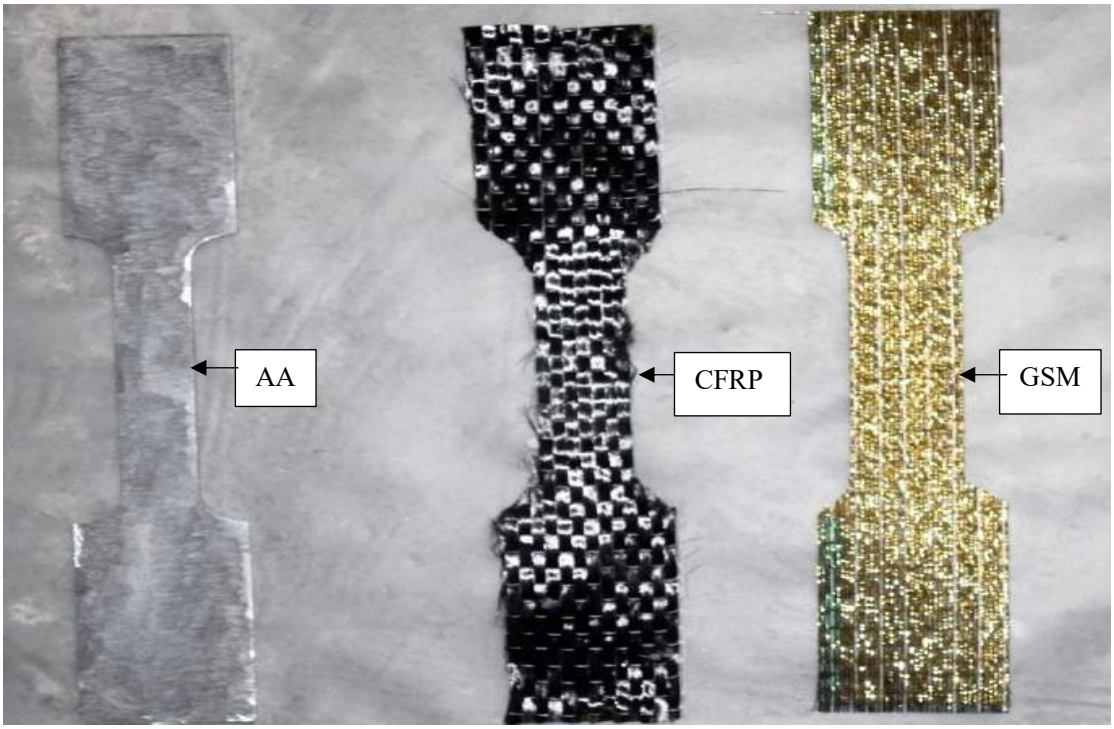

Figure 3-11: Coupon specimen.

Table3-8: Designation of tested coupon specimens

Label	**Name**
CFRP-S	stand for CFRP - Sheet
GSM-H	stand for Steel Mesh – High Density
AA	stand for Aluminum Alloy plate
CFRPAA	stand for hybrid of CFRP and AA
GSMAA	stand for hybrid of GSM and AA

The fifteen coupon specimens were tested at room temperature in the laboratory under tension (see Figure (3-12)), at a rate of 2 mm/min using an INSTRON Universal Testing Machine (UTM). A load of 100 kN. Each coupon specimen gripped at the same distance from the specimen's both ends, thus making a clear gauge length of 100 mm.

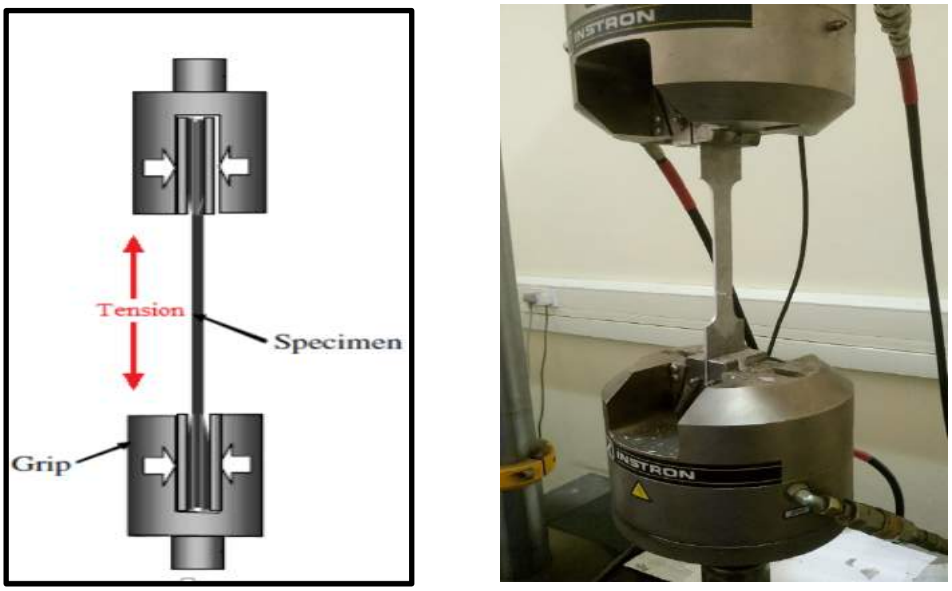

Figure 3-12: The testing machine configuration

The tensile strength of laminates was calculated using Equation below, where the maximum force was divided by the net fiber area of the hybrid FRP laminate. The elastic modulus was obtained by measuring the slope of the linear elastic segment of the stress-strain curve. Moreover, it was observed that failure of all specimens occurred within the gauge length, as:

Tensile strength equation:

$$\sigma = \frac{P\ max}{A}$$

Where:

σ = Tensile Strength (MPa)

P_{max} = Maximum load prior failure (N)

A = Average cross-sectional area (mm^2)

Figure 3-13 shows the stress–strain relationships of the coupon specimens. It is clear from the Figures that the curve of the specimens has yielding properties, as well as that; the curves are similar in shape to that of structural steel. Moreover, the Elasticity modulus of all curves is measured. Table 3-9 Summarizes the average calculated results of thickness, tensile strength, the elastic modulus (E), and the Strain for AA, AA+CFRP-sheet and AA+SM laminates, respectively.

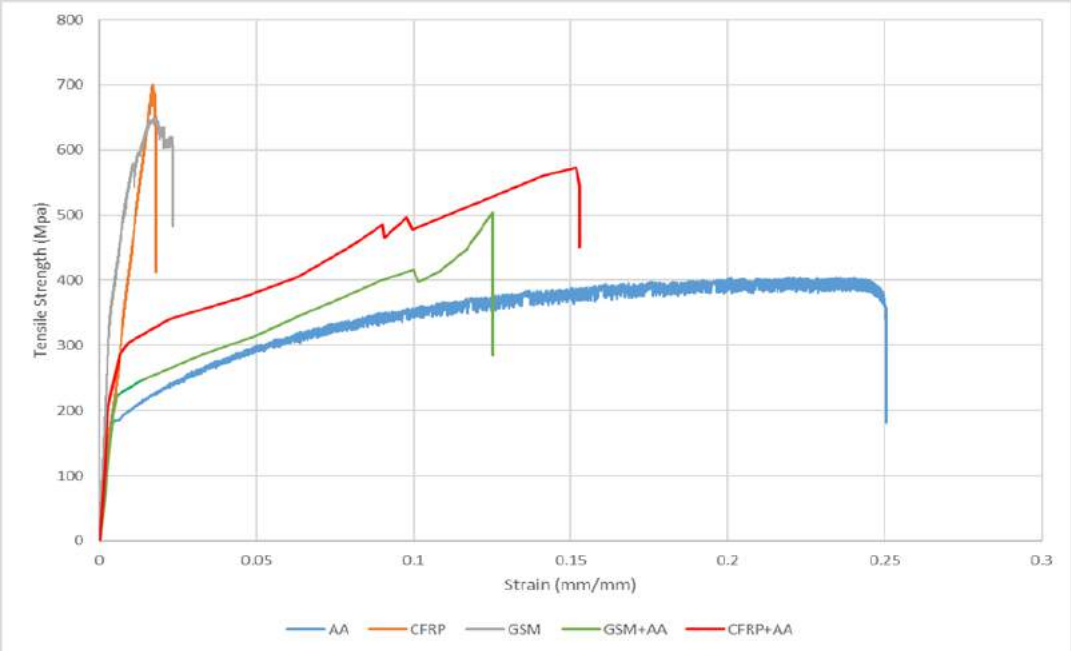

Figure 3-13: Strengthening material and hybrid coupon test results.

Table3-9: FRP laminate coupon test results

FRP Laminate	Thickness (mm)	Elastic Modulus (GPa)	Tensile Strength (MPa)	Ultimate Strain (%)
AA	2.980	70.3	288.6	20.9
CFRP	0.897	56.7	675.9	1.97
GSM	0.941	62.3	626.1	1.79
CFRPAA	4.310	60.4	538.9	15.9
GSMAA	4.610	58.1	504.6	12.5

3.4 Strengthening procedure and test setup

First, we cleaned the surface of the bottom side of the Concrete beams then a consistence groves been made using a mechanical grinder exactly at the middle of the beam, which was 50 mm for the width and 200 mm for the span length as shown on the Figure 3-14. Then we smoothed the surface after finishing the grooving and cleaned the surface using a standard vacuum to take away all the dust, afterward FRPs sheets been prepared exactly the way described in texting matrix as shown in figure 3-14. After that a layer of mixed ADESILEX PG2 SP epoxy been applied, next we installed the FRP sheet to the bottom side of the beam as shown in designation of Table3-2. Attaching the FRPs layer and the Aluminum shown in the figures 3-15.

Figure 3-14: Preparing grids for concrete bottom surface

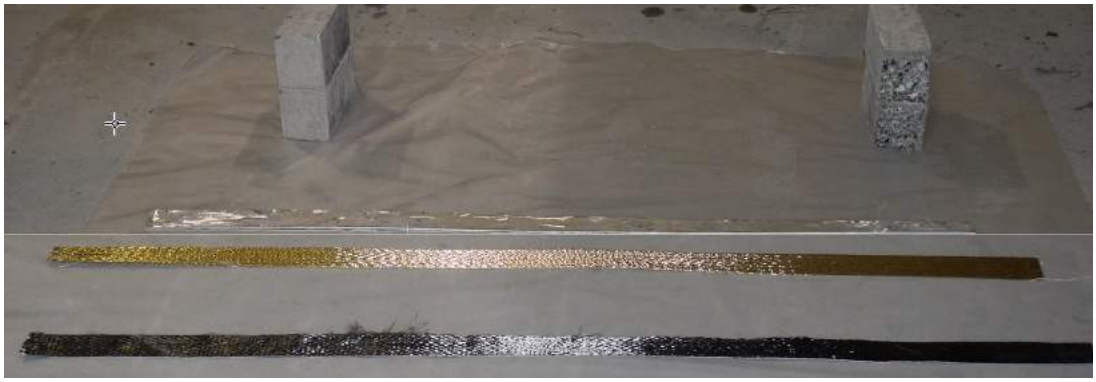

Figure 3-15: Prepared FRP's laminates

Figure 3-16: Mixing the epoxy resin

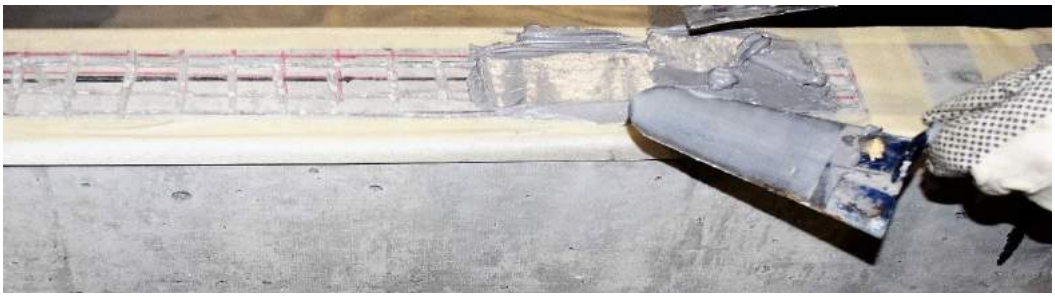

Figure 3-17: Appling of epoxy resin over the concrete surface.

3.4.1 Instrumentation (Strain Gauges). Figure 3-18 shows the locations of the strain gauges on the all specimen. Strain gauges were installed primarily on the concrete, steel, and FRP materials along the horizontal axis of the beam specimen at the beam's mid-span.

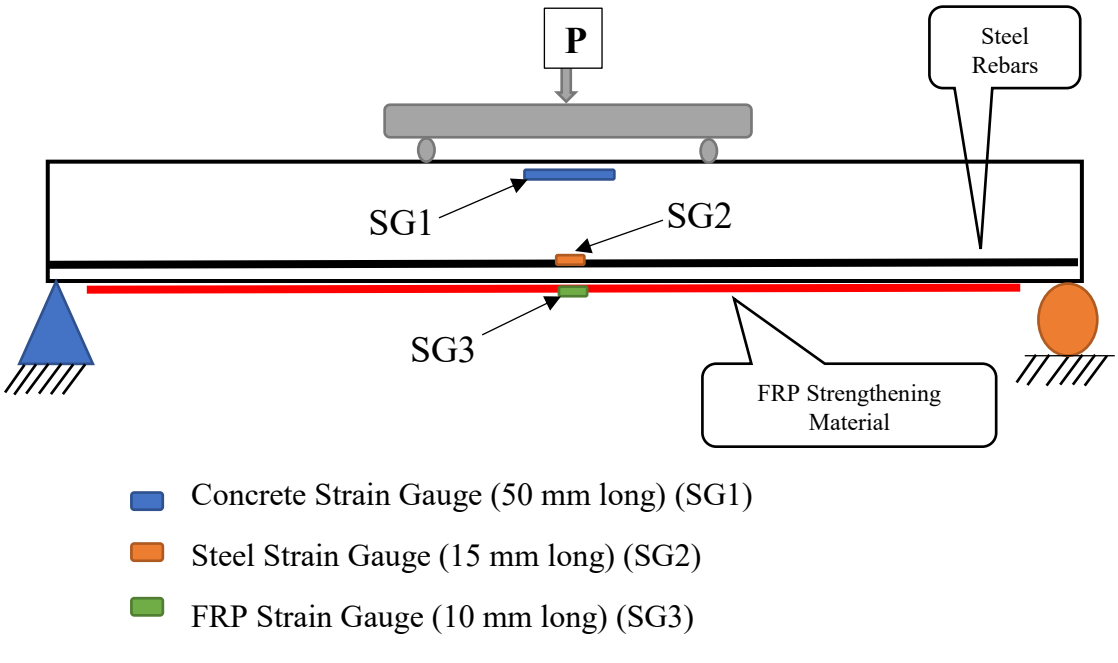

Figure 3-18: Installing steel strain gauge before casting

3.4.2 Flexural bond tests (small concrete prisms)

3.4.2.1 ***Test Setup.*** Three-point bending tests conducted on the prisms using SANS compression machine that has a capacity of 3000 kN. The loading applied at a rate of 0.25 mm/min. Load-deflections readings were continuously recorded until the failure of the specimen. Figures 3-19 and 3-20 show the experimental setup:

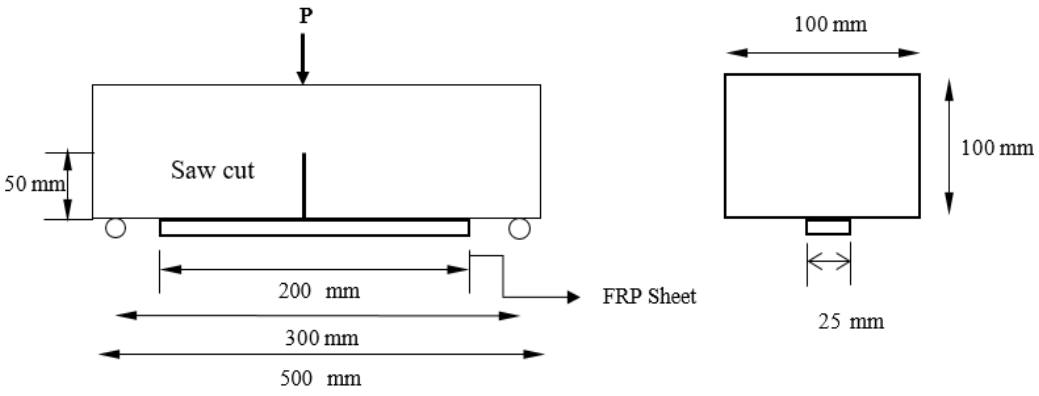

(a) Elevation View (b) Section View

Figure 3-19: Flexural bond test setup

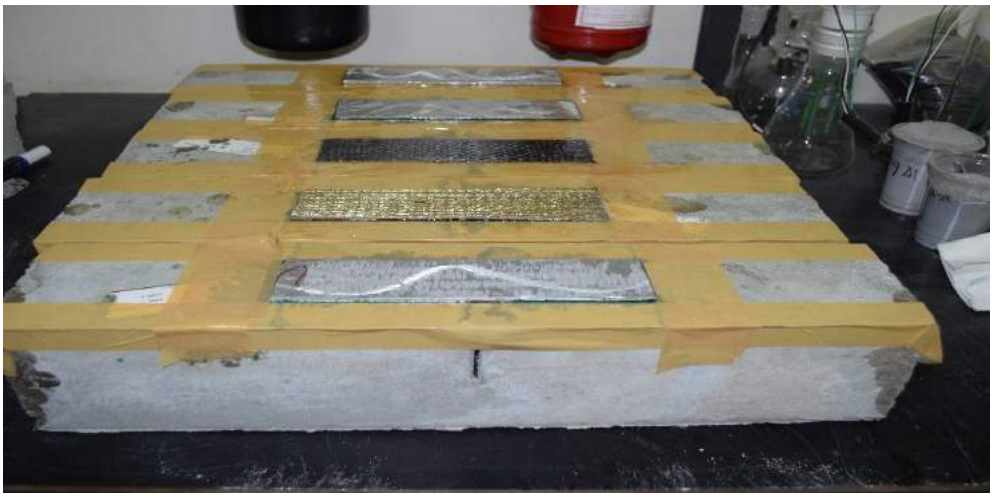

Figure 3-20: Specimen test preparation

(a) Stain Gauge instruments (b) Prism under loading

Figure 3-21: Prisms test configuration.

3.4.2.2 ***Test results and discussion.*** This section presents results obtained from testing the bond between AA, CFRP, GSM and their hybrid combination to the concrete surface; such as failure mode and average bond strength compared to control specimen. All beams tested in three-point flexure over a span of 500 mm. Load was applied at a constant rate until failure. Table 3-10 summaries the applied load, average bond strength, deflection at ultimate and failure results. The average bond strength determined using equation (1) [48]. Figure 3-28 show the load versus mid-span deflection response curves of the tested specimens. Cohesive failure (concrete cover separation) mode observed for the specimens strengthened with AA and GSM, whereas adhesive failure mode (debonding) observed for the specimens strengthened with CFRP. Specimen strengthened with hybrid CFRPAA and GSMAA observed shear failure mode, as presented in Figures 3-23 to 3-27. It is clear from Figure 3-28 that all curves are linear up to concrete cracking and the post cracking behavior depends on the stiffness of the adhesive. It is quite evident from Figures 3-28 and 3-29 beside Table 3-10 that Specimen strengthen with hybrid CFRPAA and GSMAA showed high values in terms of bond strength, almost 3 times the control specimen.

$$\tau = (3PL)/(5hws) \qquad (1)$$

Where:

T: Average bond strength in FRP

P: Applied load at mid span

L: Span of the beam

h: Overall beam depth

w: width of FRP

s: length of FRP

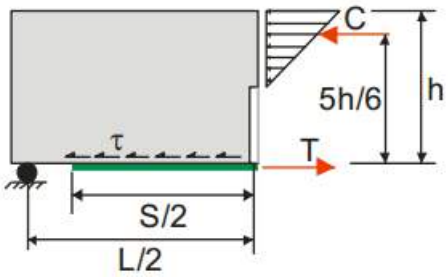

Figure 3-22: Internal stresses in beam specimen

Table3-10: Ultimate load and failure mode

System	P_u	Pu/Pu_c	τ (Mpa)	δ_u (mm)	δ_f (mm)	Failure Mode
Control	6.78	-	2.03	0.306	0.683	Flexural
AA	16.279	140.1	4.88	0.188	0.401	Delamination
CFRP	13.592	100.5	4.08	0.719	0.866	De-bonding
GSM	11.729	73.0	3.52	0.495	0.601	De-bonding
CFRP	33.352	391.9	10.01	0.954	1.119	Shear
GSMA	29.238	331.2	8.77	0.789	0.893	Shear

Figure 3-23: Prism strengthened with AA failure mode.

Figure 3-24: Prism strengthened with CFRP failure mode.

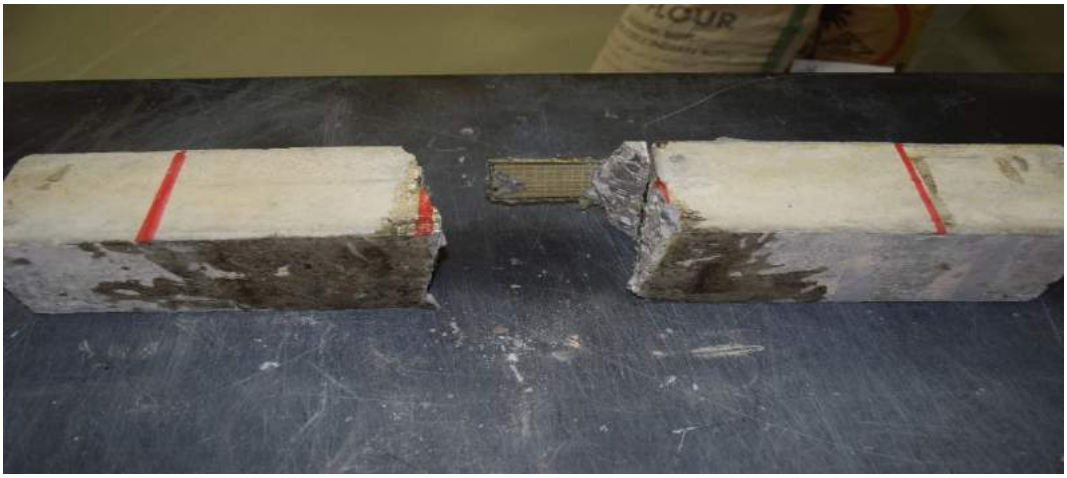

Figure 3-25: Prism strengthened with GSM failure mode.

Figure 3-26: Prism strengthened with CFRP+AA failure mode

Figure 3-27: Prism strengthened with GSMAA failure mode.

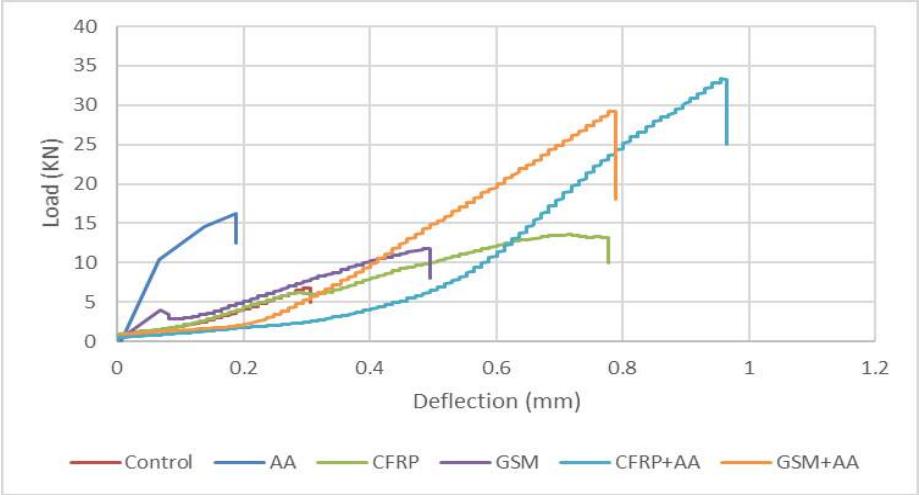

Figure 3-28: Load-deflection curve for all prisms

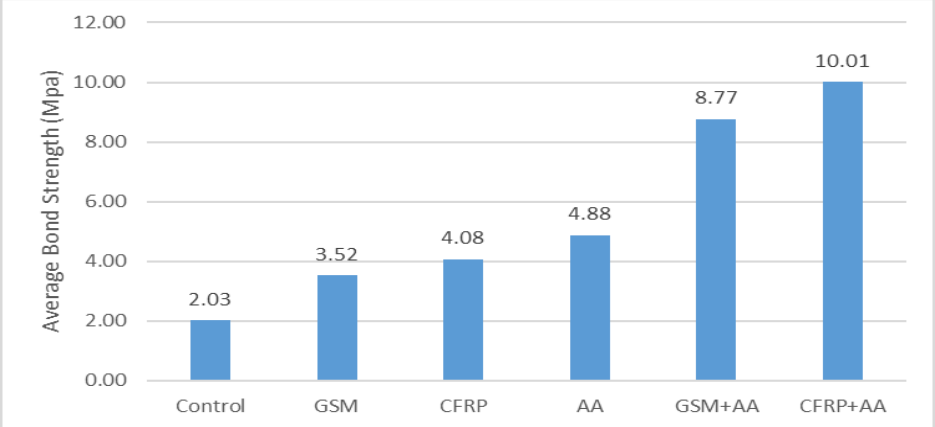

Figure 3-29: Variation of average bond strength of prisms.

Chapter 4: Experimental Results

In this chapter, results of experimental test of specimen strengthened with AA, CFRP, GSM and their hybrid combination are presented. Load versus mid-span deflection curves, along with modes of failure and strains are presented as well. Discussion and analysis of results, showing the effect of hybrid strengthening on strength and ductility of the tested specimens are given.

4.1 Load versus Mid-span Deflection Relationships

The load versus mid-span deflection is presented and discussed in this section. Results that obtained from the experimental program show the ultimate bearing capacity, the deflection at yield point, the ultimate deflection at mid-span and the deflection at failure for all strengthened specimen and their control beams. The ultimate load capacity defined as ($P_{u)}$ which is the ultimate load that the beam can carry before failure. The deflection corresponded to the ultimate load is noted as the ultimate deflection ($\delta_{ultimate}$). The load at the yield point were the internal steel rebars reaches the yielding stage defined as (P_y). Therefore, the deflection corresponded to the yield load is noted as the deflection at yield (δ_{yield}). The deflection at failure point is defined as the maximum deflection that RC beam can reach ($\delta_{failure}$).

The performance of the strengthened specimen been evaluated by finding the percentage increase in the load carrying capacity and the ductility of the RC beams compared to the un-strengthened specimen. The increase in the load carrying capacity found as the ratio of the ultimate load of the strengthened beam to the ultimate load of the control beam.

To evaluate the ductility of the strengthened specimen, the increase in the strengthened system's ductility was measured based on considering the yield point of steel rebars as a benchmark point. Therefore, two ratios been considered as a ductility index. Firstly, the ratio of beam's deflection at ultimate load to beam's deflection at yield point ($\delta_{ultimate} / \delta_{yield}$), and secondly, the ratio of beam's deflection at failure load to beam's deflection at yield point ($\delta_{failure} / \delta_{yield}$).

Lastly, the failure mode for each strengthened beam are discussed in this sector. Generally, the failure for most of the strengthened RC beams included flexural cracks,

concrete crushing, FRP de-bonding, FRP delamination (concrete cover separation) and rupture of FRP.

4.1.1 Group [GA]. This group contains twelve beams reinforced with 2Ø12 bars as main reinforcement. One beam is the control beam, which is left un-strengthened as a reference point to the behavior of conventionally strengthened specimen. All other eleven beams strengthened with different variables such as type of EBR material, number of EBR layers and width of strengthening layers (50 mm and 100 mm).

4.1.1.1 ***Beam A-Control.*** The control beam's test results used as a benchmark point to evaluate the performance of RC beams strengthened with different combinations of AA, CFRP and GSM. The control beam yielded an ultimate load of 99.7 KN with corresponding deflection of 22.8 mm. the deflection value at failure was equal to 29.2 mm. The beam failed in a typical flexural mode where the steel rebars yielded followed by crushing of concrete at the top face of the beam in the mid span region, as shown in Figures 4-1 and 4-2.

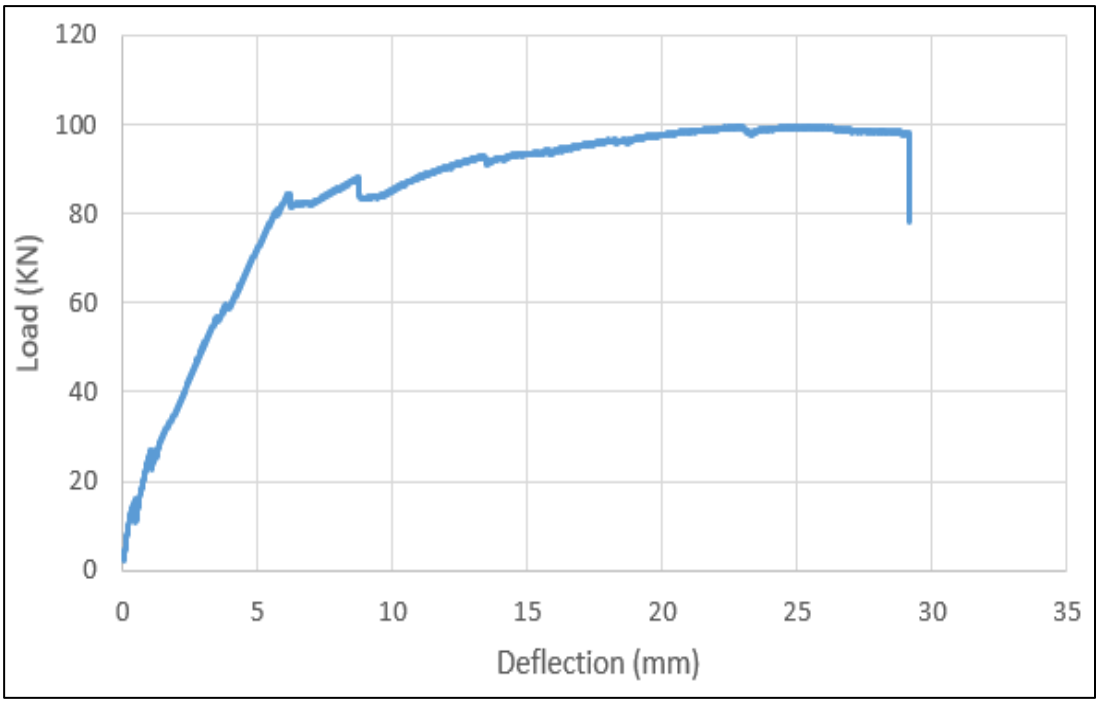

Figure 4-1: [GA-Control Beam] - Load-deflection curve.

Figure 4-2: Failure mode of Beam A-Control.

4.1.1.2 ***Beam A1-A.*** This beam strengthened with one layer of AA composite plate of width 50 mm. The ultimate load obtained was equal to 157.3 kN with corresponding deflection of 18.2 mm. The mid-span deflection value at failure was equal to 18.4 mm. The percentage increase in load carrying capacity was equal to 57.8% over the control specimen. The percentage decrease in ultimate and failure deflection was equal to 20.2% and 37% respectively. The beam failed by yielding of the steel rebar, followed by de-bonding of the FRP plate, and crushing of concrete at mid-span as shown in Figures 4-3 and 4-4.

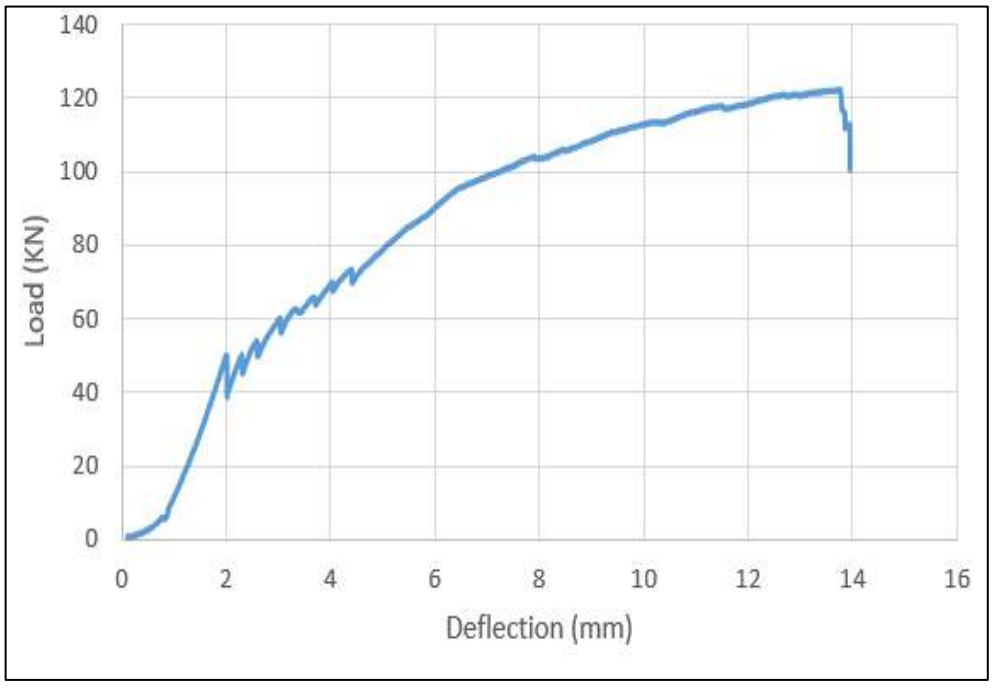

Figure 4-3: Beam A1-A - Load-deflection curve.

Figure 4-4: Failure mode of strengthened Beam A1-A

4.1.1.3 ***Beam A1-C.*** This beam strengthened with one layer of CFRP composite sheet of width 50 mm. The ultimate load obtained was equal to 122.1 kN with corresponding deflection of 14.1 mm. The mid-span deflection value at failure was equal to 18.4 mm. The percentage increase in load carrying capacity was equal to 22.5 % over the control specimen. The percentage decrease in ultimate and failure deflection was equal to 38.2% and 37% respectively. The beam failed by yielding of the steel rebar, followed by rapture of the FRP sheet, and crushing of concrete at mid-span as shown in Figures 4-5 and 4-6.

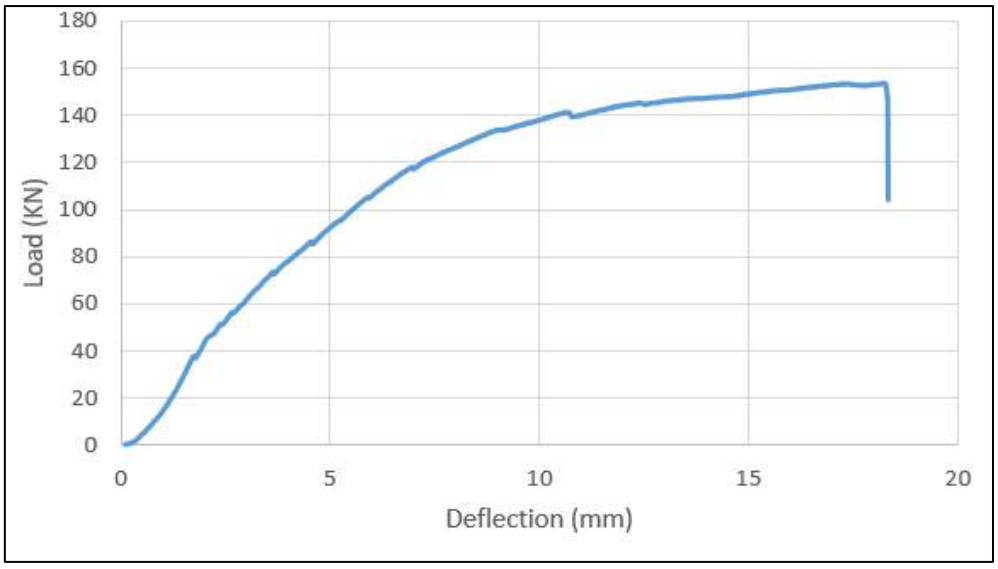

Figure 4-5: Beam A1-C: Load-deflection curve.

Figure 4-6: Failure mode of strengthened Bam A1-C.

4.1.1.4 Beam *A1-S.* This beam strengthened with one layer of GSM composite sheet of width 50 mm. The ultimate load obtained was equal to 154.3 kN with corresponding deflection of 18.1 mm. The mid-span deflection value at failure was equal to 18.2 mm. The percentage increase in load carrying capacity was equal to 54.8 % over the control specimen. The percentage decrease in ultimate and failure deflection was equal to 20.6% and 37.7% respectively. The beam failed by yielding of the steel rebar, followed by rupture of the FRP sheet, and crushing of concrete at mid-span as shown in Figures 4-7 and 4-8.

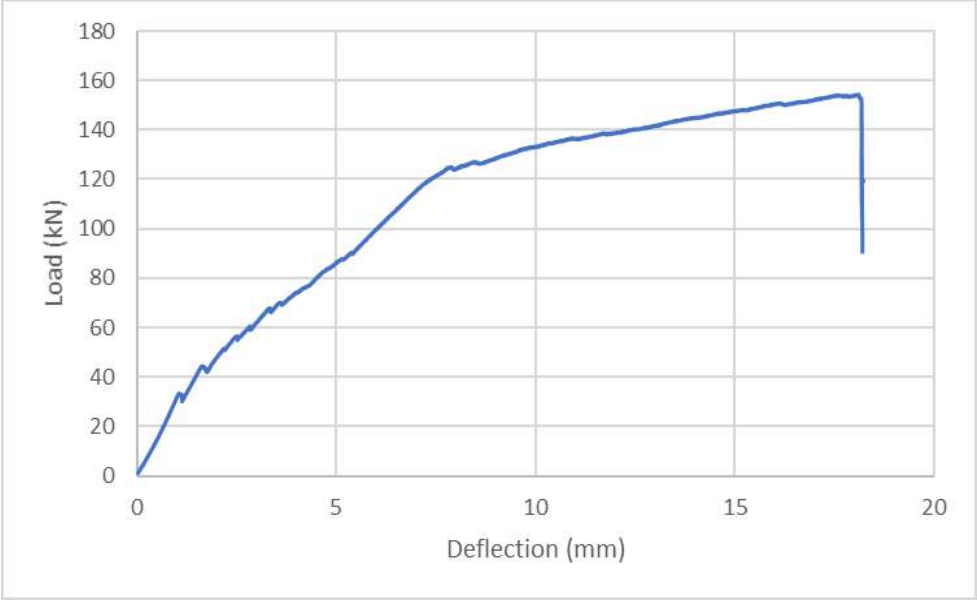

Figure 4-7: Beam A1-S: Load-deflection curve.

Figure 4-8: Failure mode of strengthened Bam A1-S.

4.1.1.5 ***Beam A1-CA.*** This beam strengthened with one layer of CFRP sheet and one layer of AA plate, both of width 50 mm. The ultimate load obtained was equal to 145.6 kN with corresponding deflection of 13.4 mm. The mid-span deflection value at failure was equal to 32.8 mm. The percentage increase in load carrying capacity was equal to 46.0 % over the control specimen. The percentage decrease in ultimate deflection was equal to 41.2% and 12.3% increase in failure deflection. The beam failed by yielding of the steel rebar, followed by de-bonding of the FRP hybrid, and crushing of concrete at mid-span as shown in Figures 4-9 and 4-10.

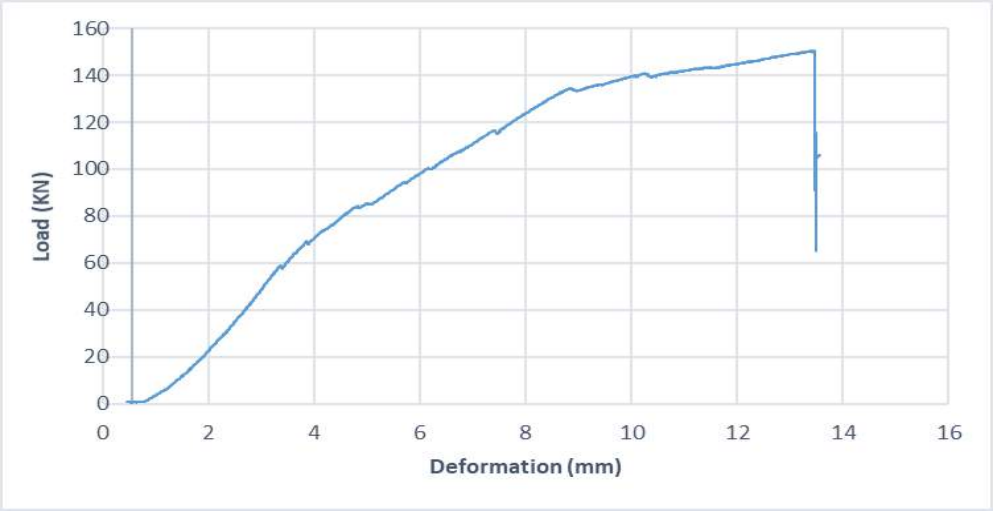

Figure 4-9: Beam A1-CA - Load-deflection curve.

Figure 4-10: Failure mode of strengthened Beam A1-CA.

4.1.1.6 ***Beam A1-SA***. This beam strengthened with one layer of GSM composite sheet of width 50 mm. The ultimate load obtained was equal to 150.4 kN with corresponding deflection of 13.4 mm. The mid-span deflection value at failure was equal to 13.6 mm. The percentage increase in load carrying capacity was equal to 50.9 % over the control specimen. The percentage decrease in ultimate and failure deflection was equal to 41.2% and 53.4% respectively. The beam failed by yielding of the steel rebar, followed by FRP delamination as shown in Figures 4-11 and 4-12.

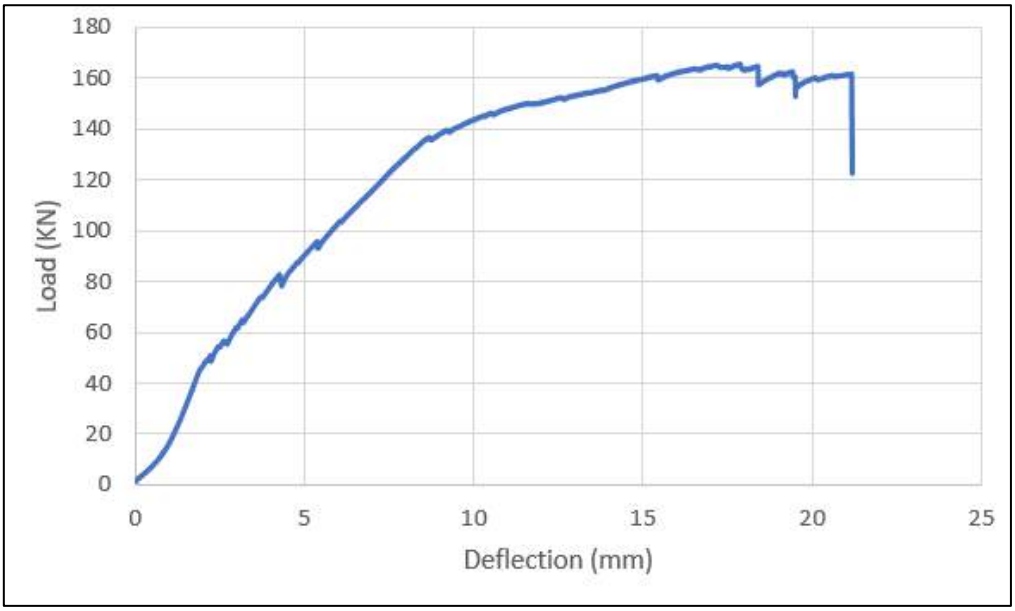

Figure 4-11: Beam A1-SA: Load-deflection curve.

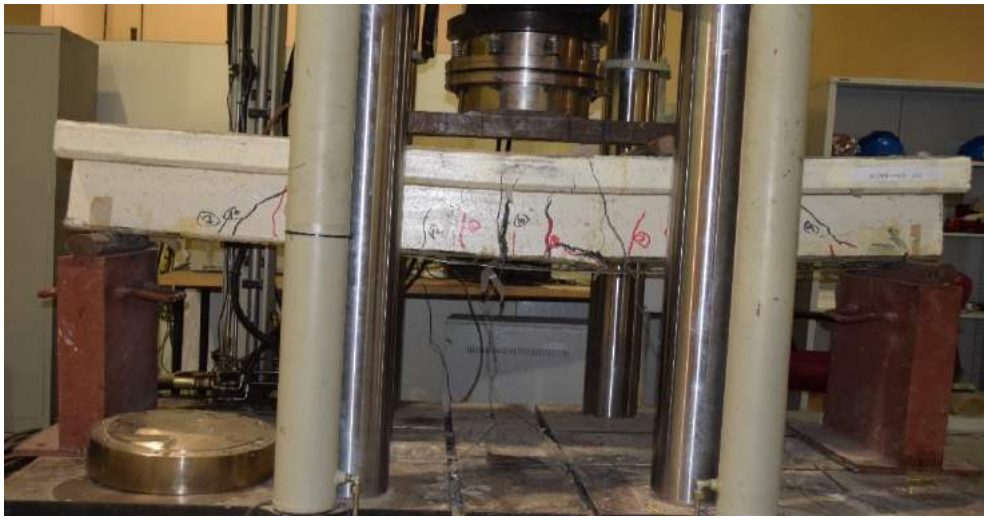

Figure 4-12: Failure mode of strengthened Beam A1-SA.

4.1.1.7 ***Beam A1-CA-W.*** This beam strengthened with one layer of CFRP sheet and one layer of AA plate, both of width 50 mm. the beam was U-wrapped at both ends using CFRP sheets of 50 mm width and 650 mm length. The ultimate load obtained was equal to 165.9 kN with corresponding deflection of 17.9 mm. The mid-span deflection value at failure was equal to 32.5 mm. The percentage increase in load carrying capacity was equal to 66.4 % over the control specimen. The percentage decrease in ultimate deflection was equal to 21.7% and 11.3% increase in failure deflection. The beam failed by yielding of the steel rebar, followed by de-bonding of the FRP hybrid, and crushing of concrete at mid-span as shown in figures 4-13 and 4-14.

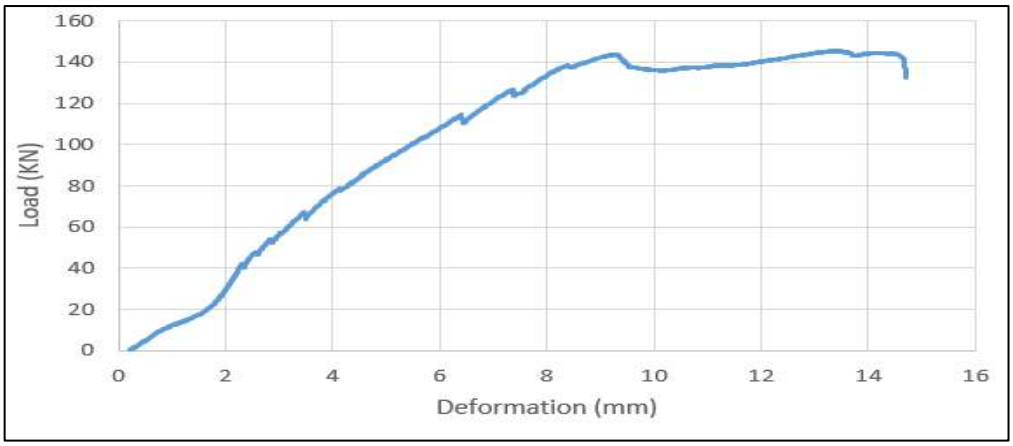

Figure 4-13: Beam A1-CA-W Load-deflection curve.

Figure 4-14: Failure mode of strengthened Beam A1-CA-W.

4.1.1.8 ***Beam A2-A.*** This beam strengthened with one layer of AA composite plate of width 100 mm. The ultimate load obtained was equal to 151.9 kN with corresponding deflection of 29.2 mm. The mid-span deflection value at failure was equal to 30.0 mm. The percentage increased in load carrying capacity was equal to 52.4% over the control specimen. The percentage decreased in ultimate deflection was equal to 28.2% and 2.7% increase in failure deflection. The beam failed by yielding of the steel rebar, followed by de-bonding of the FRP plate, See Figures 4-15 and 4-16.

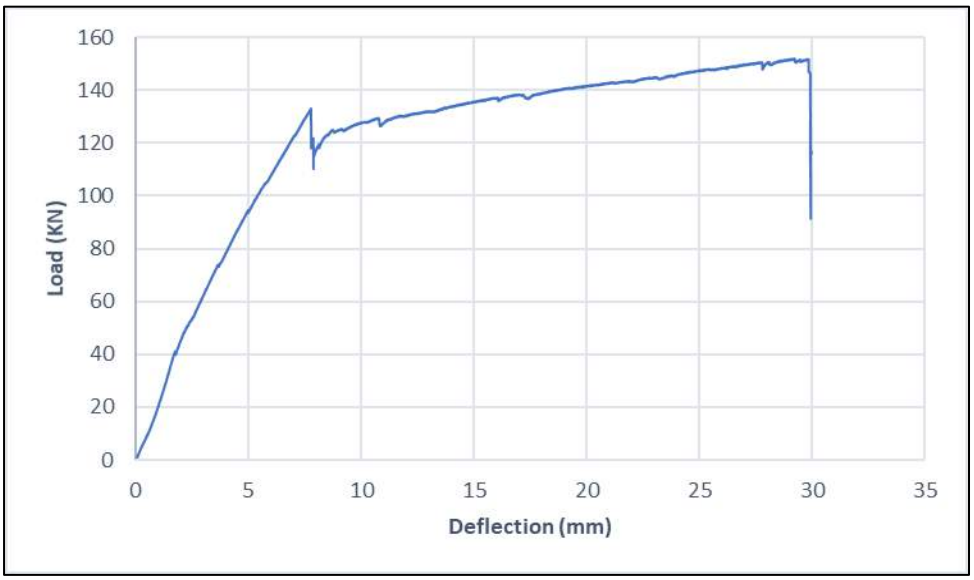

Figure 4-15: Beam A2-A Load-deflection curve.

Figure 4-16: Failure mode of strengthened Beam A2-A.

4.1.1.9 ***Beam A2-C***. This beam strengthened with one layer of CFRP composite sheet of width 100 mm. The ultimate load obtained was equal to 148.6 kN with corresponding deflection of 17.0 mm. the mid-span deflection value at failure was equal to 17.4 mm. The percentage increased in load carrying capacity was equal to 49.0 % over the control specimen. The percentage decreased in ultimate and failure deflection was equal to 25.3% and 40.4% respectively. The beam failed by yielding of the steel rebar, followed by rapture of the FRP sheet as shown in Figures 4-17 and4-18.

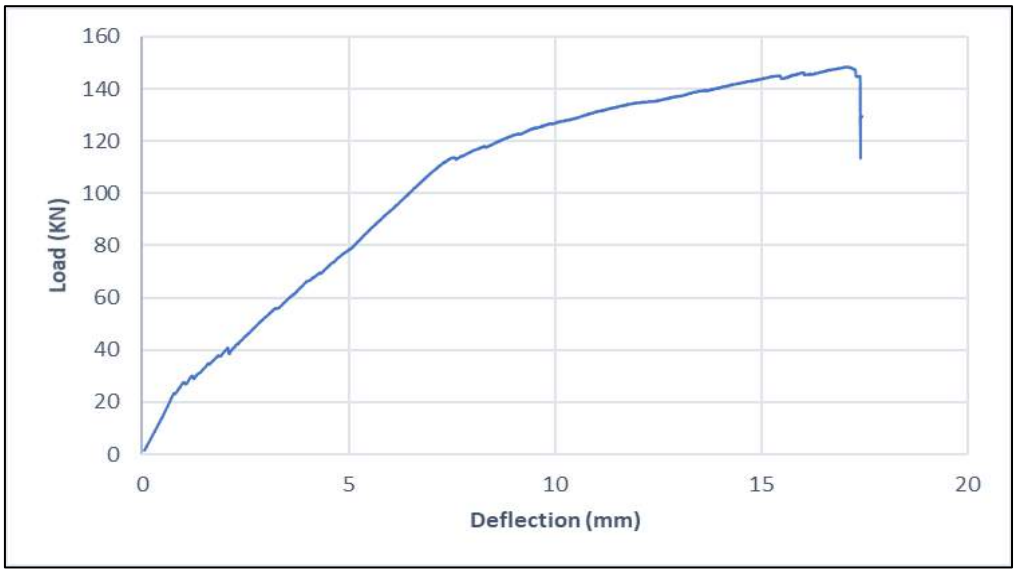

Figure 4-17: Beam A2-C Load-deflection curve.

Figure 4-18: Failure mode of strengthened Beam A2-C.

4.1.1.10 ***Beam A2-S.*** This beam strengthened with one layer of GSM composite sheet of width 100 mm. The ultimate load obtained was equal to 161.1 kN with corresponding deflection of 16.6 mm. the mid-span deflection value at failure was equal to 17.1 mm. The percentage increased in load carrying capacity was equal to 61.6 % over the control specimen. The percentage decreased in ultimate and failure deflection was equal to 27.2% and 41.4% respectively. The beam failed by yielding of the steel rebar, followed by rapture of the FRP sheet, and crushing of concrete at mid-span as shown in Figures 4-19 and 4-20.

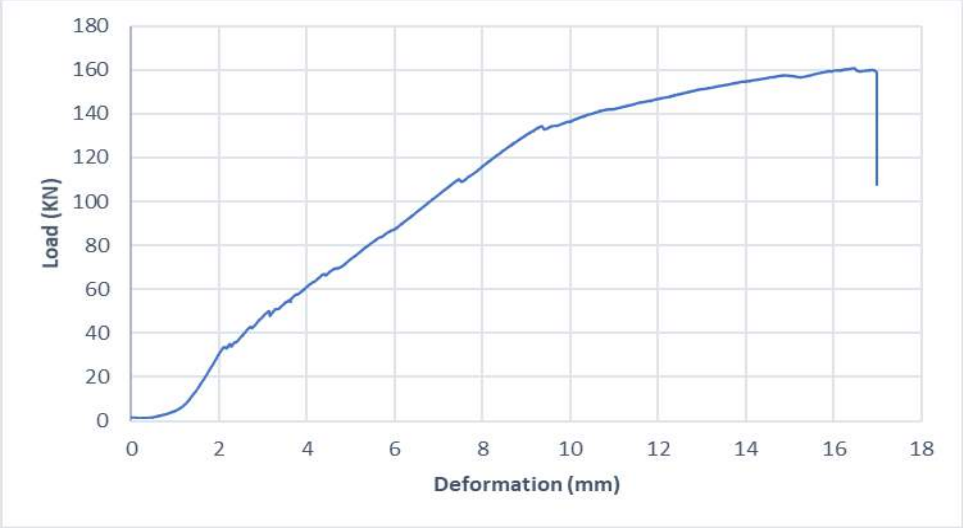

Figure 4-19: Beam A2-S Load-deflection curve.

Figure 4-20: Failure mode of strengthened Beam A2-S.

4.1.1.11 ***Beam A2-CA.*** This beam strengthened with one layer of CFRP sheet and one layer of AA plate, both of width 100 mm. The ultimate load obtained was equal to 176.4 kN with corresponding deflection of 11.7 mm. the mid-span deflection value at failure was equal to 11.9 mm. The percentage increased in load carrying capacity was equal to 76.9 % over the control specimen. The percentage decreased in ultimate and failure deflection was equal to 48.5% and 59.2% respectively. The beam failed by yielding of the steel rebar, followed by de-bonding of the FRP hybrid, and crushing of concrete at mid-span as shown in Figures 4-21 and 4-22.

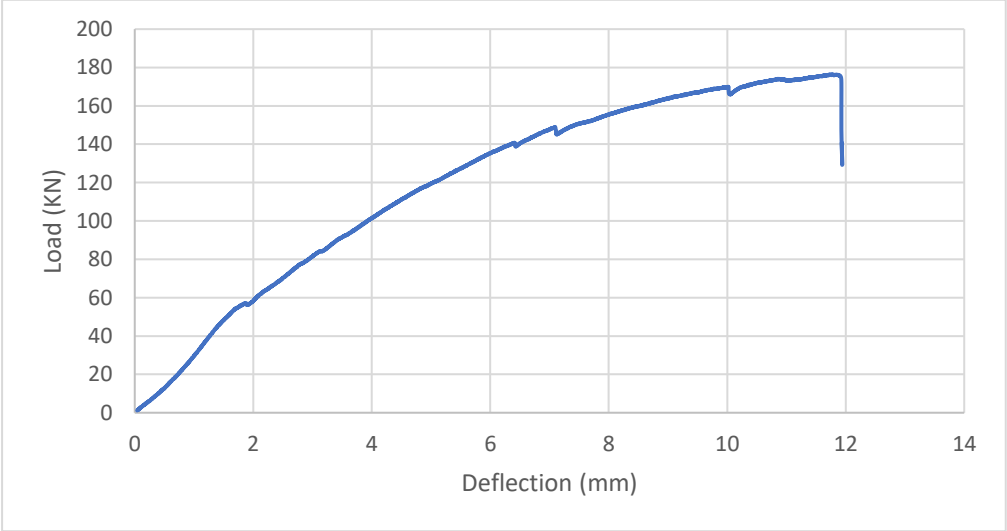

Figure 4-21: Beam A2-CA: Load-deflection curve.

Figure 4-22: Failure mode of strengthened Beam A2-CA.

4.1.1.12 ***Beam A2-SA.*** This beam strengthened with one layer of GSM sheet and one layer of AA plate, both of width 100 mm. The ultimate load obtained was equal to 162.9 kN with corresponding deflection of 8.6 mm. the mid-span deflection value at failure was equal to 16.6 mm. The percentage increased in load carrying capacity was equal to 63.4 % over the control specimen. The percentage decreased in ultimate deflection was equal to 62.2% and 43.2% increase in failure deflection. The beam failed by yielding of the steel rebar, followed by delamination of the FRP hybrid (concrete cover separation), and crushing of concrete at mid-span as shown in Figures 4-23 and 4-24.

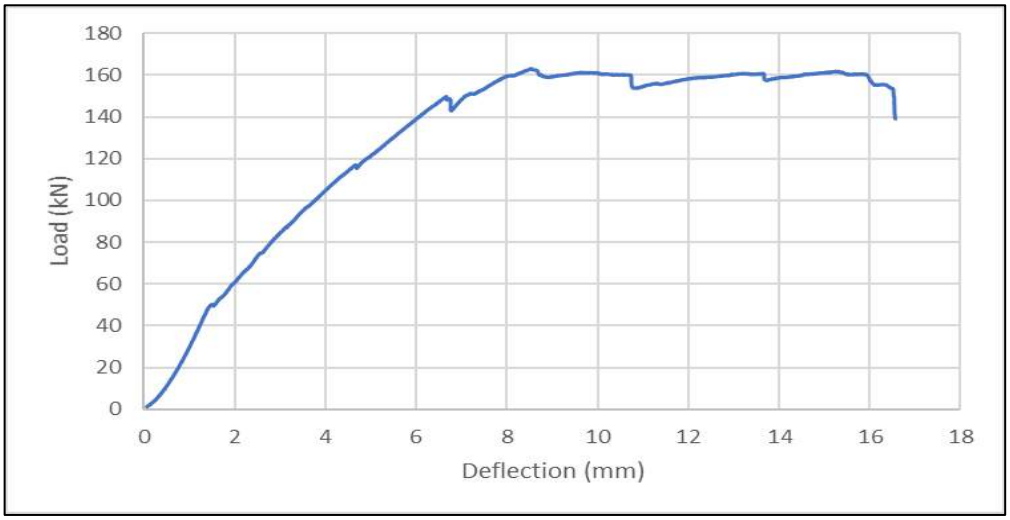

Figure 4-23: Beam A2-SA Load-deflection curve.

Figure 4-24: Failure mode of strengthened Beam A2-SA.

4.1.2 Group [GB]. This group contains twelve beams reinforced with 2T16 bars as main reinforcement. One beam is the control beam, which left un-strengthened to compare that to the behavior of conventionally strengthened specimen. All other eleven beams strengthened with different variables such as type of EBR material, number of EBR layers and width of strengthening layers (50 mm and 100 mm).

4.1.2.1 ***Beam B- Control.*** The control beam's test results used as a benchmark point to evaluate the performance of RC beams strengthened with different combinations of AA, CFRP and GSM. The control beam yielded an ultimate load of 179.9 KN with corresponding deflection of 17.6 mm. the deflection value at failure was equal to 31.5 mm. The beam failed in a typical flexural mode where the steel rebars yielded followed by crushing of concrete at the top face of the beam in the mid span region, as shown in Figures 4-25 and 4-26.

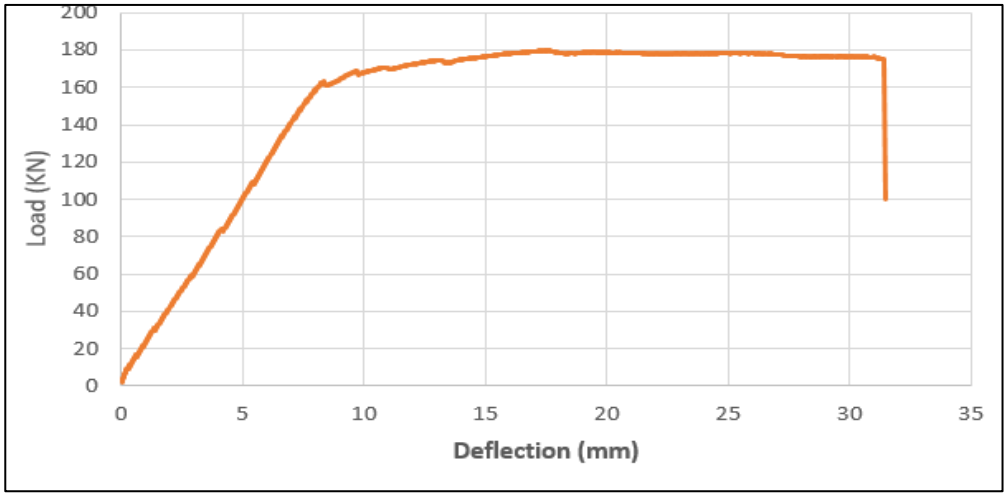

Figure 4-25: Beam B-Control- Load-deflection curve.

Figure 4-26: Failure mode of strengthened Beam B-Control.

4.1.2.2 ***Beam B1-A.*** This beam strengthened with one layer of AA composite plate of width 50 mm. The ultimate load obtained was equal to 217.6 kN with corresponding deflection of 16.4 mm. The mid-span deflection value at failure was equal to 16.5 mm. The percentage increased in load carrying capacity was equal to 21% over the control specimen. The percentage decreased in ultimate and failure deflection was equal to -6.8% and 47.6% respectively. The beam failed by yielding of the steel rebar, followed by de-bonding of the FRP plate, and crushing of concrete at mid-span as shown in Figures 4-27 and 4-28.

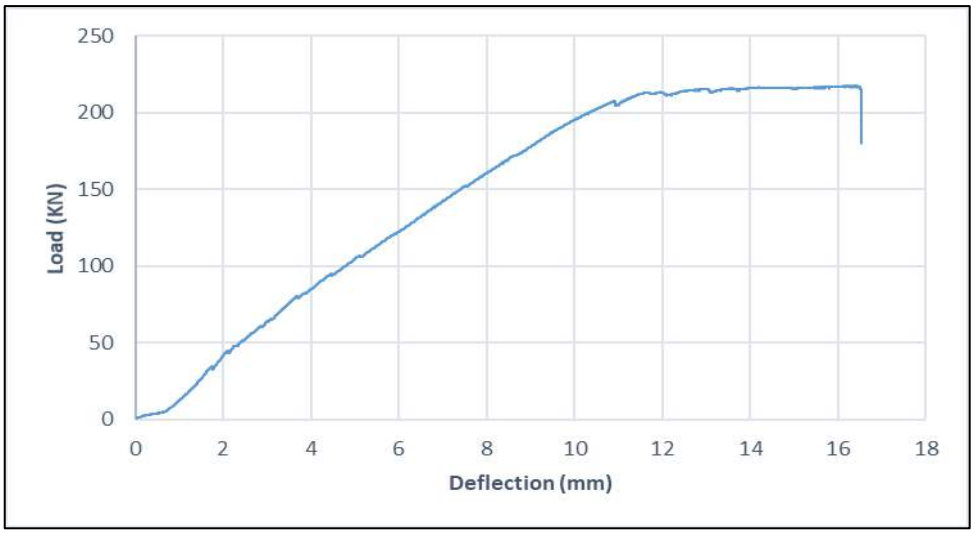

Figure 4-27: Beam B1-A: Load-deflection curve.

Figure 4-28: Failure mode of strengthened Beam B1-A.

4.1.2.3 ***Beam B1-C.*** This beam strengthened with one layer of CFRP composite sheet of width 50 mm. The ultimate load obtained was equal to 198.6 kN with corresponding deflection of 12.8 mm. the mid-span deflection value at failure was equal to 24.3 mm. The percentage increased in load carrying capacity was equal to 22.5 % over the control specimen. The percentage decreased in ultimate and failure deflection was equal to 27.3% and 22.9% respectively. The beam failed by yielding of the steel rebar, followed by rapture of the FRP sheet, and crushing of concrete at mid-span as shown in Figures 4-29 and 4-30.

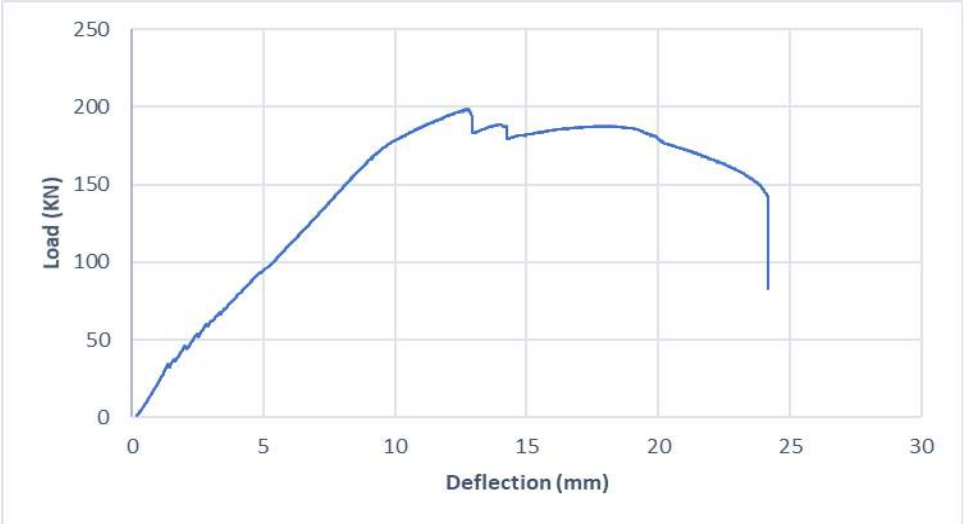

Figure 4-29: Beam B1-C: Load-deflection curve.

Figure 4-30: Failure mode of strengthened Beam B1-C.

4.1.2.4 ***Beam B1-S.*** This beam strengthened with one layer of GSM composite sheet of width 50 mm. The ultimate load obtained was equal to 201 kN with corresponding deflection of 14 mm. The mid-span deflection value at failure was equal to 14.3 mm. The percentage increased in load carrying capacity was equal to 11.7 % over the control specimen. The percentage decreased in ultimate and failure deflection was equal to 20.5% and 54.6% respectively. The beam failed by yielding of the steel rebar, followed by rapture of the FRP sheet, and crushing of concrete at mid-span as shown in Figures 4-31 and 4-32.

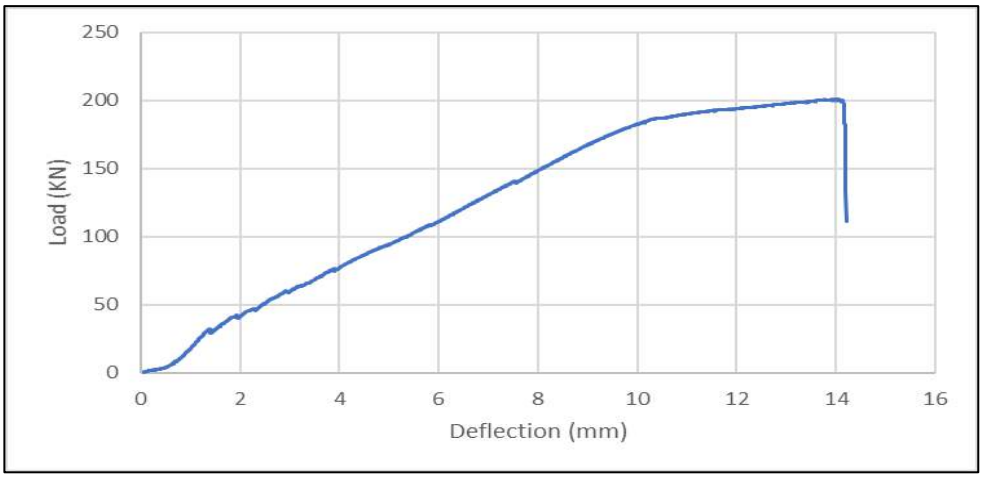

Figure 4-31: Beam B1-S: Load-deflection curve.

Figure 4-32: Failure mode of strengthened Beam B1-S.

4.1.2.5 ***Beam B1-CA***. This beam strengthened with one layer of CFRP sheet and one layer of AA plate, both of width 50 mm. The ultimate load obtained was equal to 211.6kN with corresponding deflection of 13.7 mm. the mid-span deflection value at failure was equal to 13.8 mm. The percentage increased in load carrying capacity was equal to 23.2 % over the control specimen. The percentage decreased in ultimate deflection was equal to 22.1% and 56.2% increase in failure deflection. The beam failed by yielding of the steel rebar, followed by de-bonding of the FRP hybrid, and crushing of concrete at mid-span as shown in Figures 4-33 and 4-34.

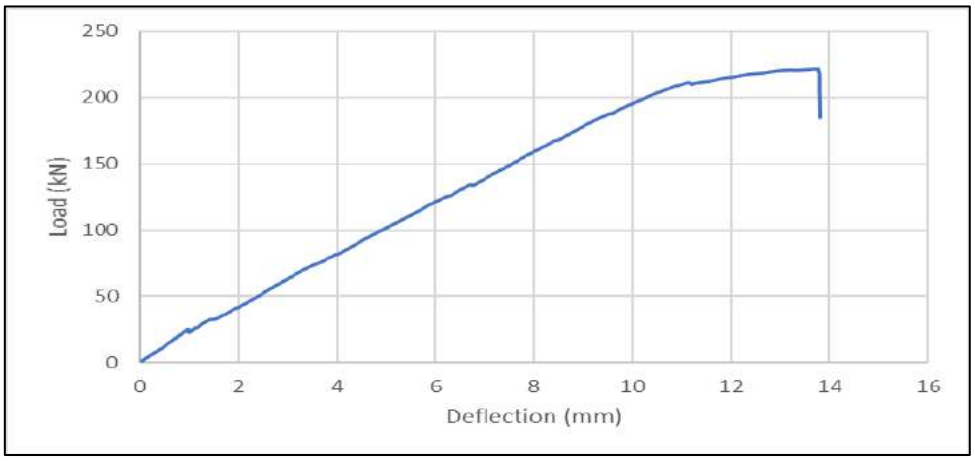

Figure 4-33: Beam B1-CA: Load-deflection curve.

Figure 4-34: Failure mode of strengthened Beam B1-CA.

4.1.2.6 ***Beam B1-SA***. This beam strengthened with one layer of GSM composite sheet of width 50 mm. The ultimate load obtained was equal to 218.7 kN with corresponding deflection of 12.5 mm. The mid-span deflection value at failure was equal to 13.1 mm. The percentage increased in load carrying capacity was equal to 21.6 % over the control specimen. The percentage decreased in ultimate and failure deflection was equal to 29% and 58.4% respectively. The beam failed by yielding of the steel rebar, followed by FRP delamination as shown in Figures 4-35 and 4-36.

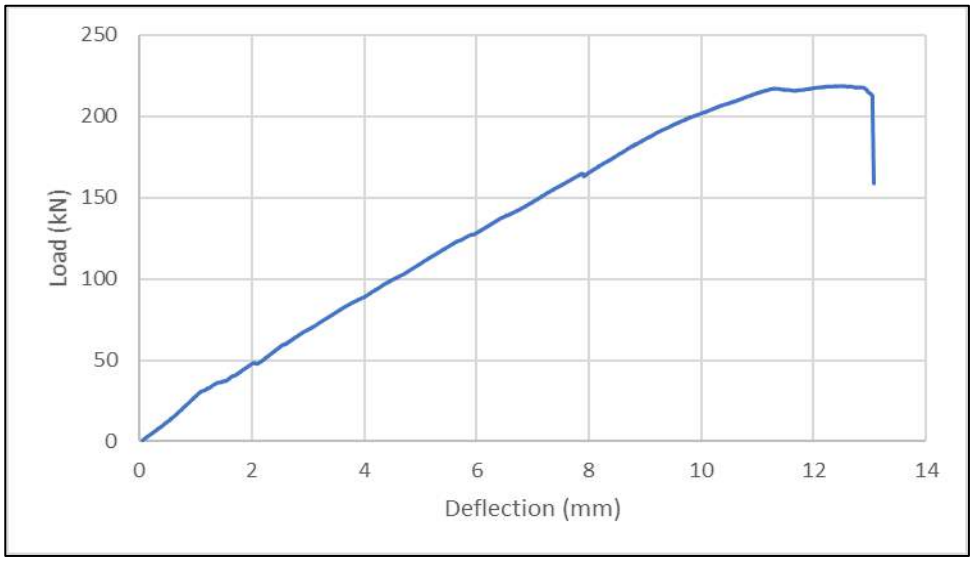

Figure 4-35: Beam B1-SA-Load-deflection curve.

Figure 4-36: Failure mode of strengthened Beam B1-SA.

4.1.2.7 ***Beam B1-CA-W.*** Beam strengthened with one layer of CFRP sheet and one layer of AA plate, both of width 50 mm. it was U-wrapped at both ends using CFRP sheets of 50 mm width and 650 mm length. The ultimate load obtained was 258.9 kN with corresponding deflection of 19.7 mm. the mid-span deflection value at failure was equal to 27.4 mm. The percentage increased in load carrying capacity was 43.9 % over the control specimen. The percentage decreased in ultimate deflection was equal to 11.8 % and 13.0 % increase in failure deflection. The beam failed by yielding of the steel rebar, followed by de-bonding of the FRP hybrid, and crushing of concrete at mid-span as shown in Figures 4-37 and 4-38.

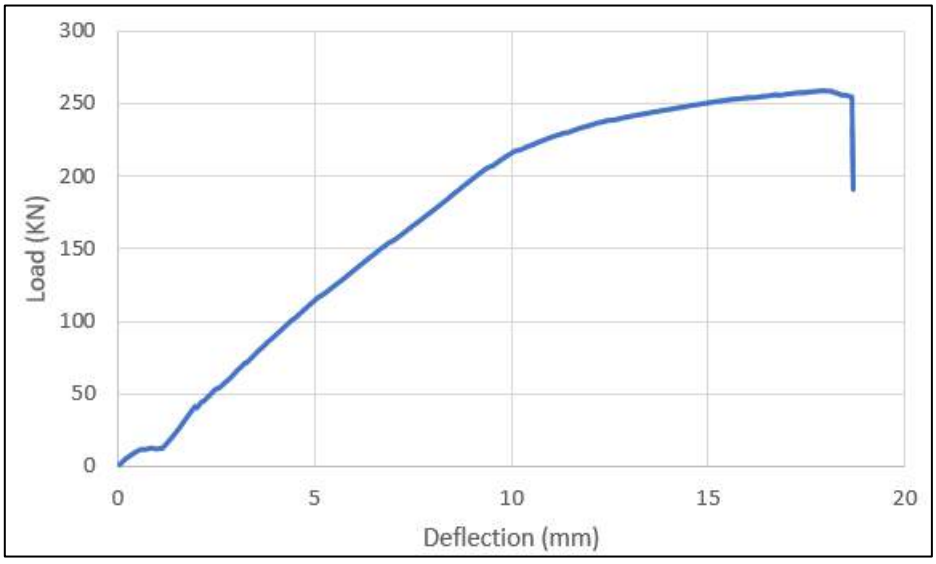

Figure 4-37: Beam B1-CA-W: Load-deflection curve.

Figure 4-38: Failure mode of strengthened Beam B1-CA-W.

4.1.3.8 ***Beam B1-SA-W***. This beam strengthened with one layer of GSM sheet and one layer of AA plate, both of width 50 mm. the beam was U-wrapped at both ends using CFRP sheets of 50 mm width and 650 mm length. The ultimate load obtained was equal to 252.7 kN with corresponding deflection of 17.8 mm. the mid-span deflection value at failure was equal to 20.3 mm. The percentage increased in load carrying capacity was equal to 40.4 % over the control specimen. The percentage decreased in ultimate deflection was equal to 2.1 % and 35.6 % increase in failure deflection. The beam failed by yielding of the steel rebar, followed by de-bonding of the FRP hybrid, and crushing of concrete at mid-span as shown in Figures 4-39 and 4-40.

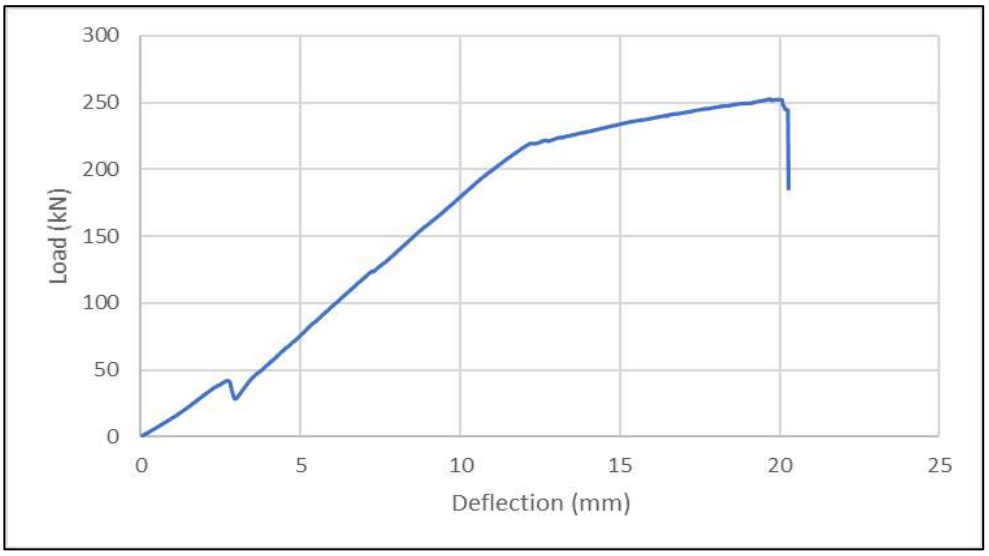

Figure 4-39: Beam B1-SA-W: Load-deflection curve.

Figure4-40: Failure mode of strengthened Beam B1-SA-W.

4.1.2.9 ***Beam B2-A.*** This beam strengthened with one layers of AA composite plate of width 100 mm. The ultimate load obtained was equal to 221.3 kN with corresponding deflection of 14.9 mm. the mid-span deflection value at failure was equal to 16.5 mm. The percentage increased in load carrying capacity was equal to 23 % over the control specimen. The percentage decreased in ultimate deflection was equal to 14.9 % and 47.6 % increase in failure deflection. The beam failed by yielding of the steel rebar, followed by de-bonding of the FRP plate, See Figures 4-41 and 4-42.

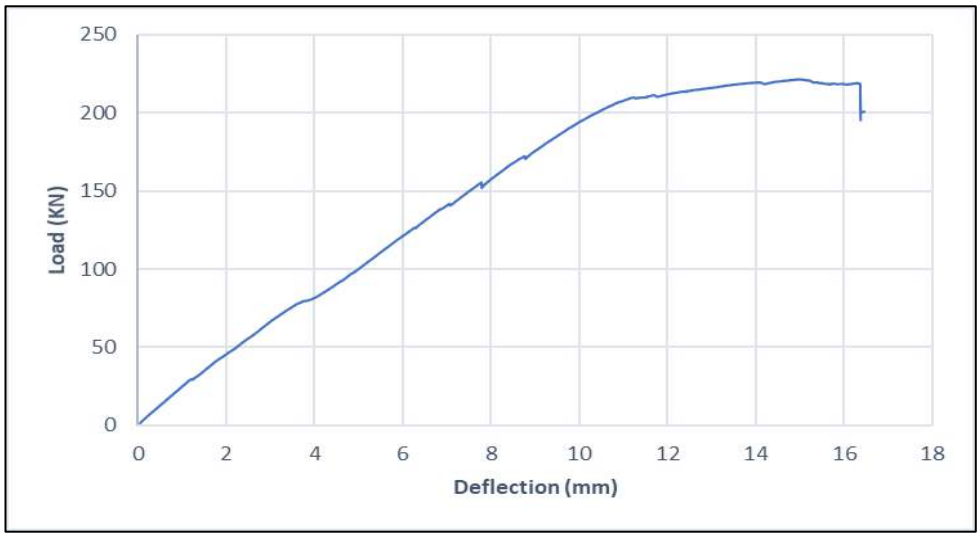

Figure 4-41: Beam B2-A Load-deflection curve.

Figure 4-42: Failure mode of strengthened Beam B2-A.

4.1.2.10 ***Beam B2-C.*** This beam strengthened with one layer of CFRP composite sheet of width 100 mm. The ultimate load obtained was equal to 223.4 kN with corresponding deflection of 161.1 mm. the mid-span deflection value at failure was equal to 18.8 mm. The percentage increased in load carrying capacity was equal to 24.2 % over the control specimen. The percentage decreased in ultimate and failure deflection was equal to 8.5 % and 40.3 % respectively. The beam failed by yielding of the steel rebar, followed by rapture of the FRP sheet as shown in Figures 4-43 and 4-44.

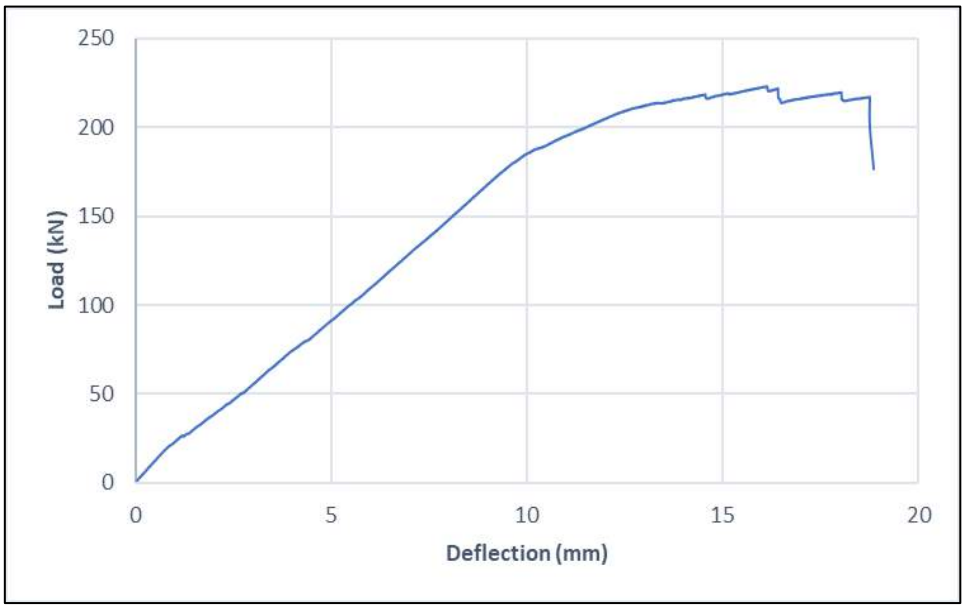

Figure 4-43: Beam B2-C: Load-deflection curve.

Figure 4-44: Failure mode of strengthened Beam B2-C.

4.1.2.11 ***Beam B2-S.*** This beam strengthened with one layer of GSM composite sheet of width 100 mm. The ultimate load obtained was equal to 275.2 kN with corresponding deflection of 27.1 mm. the mid-span deflection value at failure was equal to 2.3 mm. The percentage increased in load carrying capacity was equal to 53 % over the control specimen. The percentage decreased in failure deflection was equal to 28.2% and 2.7% increase in ultimate deflection. The beam failed by yielding of the steel rebar, followed by rapture of the FRP sheet, and crushing of concrete at mid-span as shown in Figures 4-45 and 4-46.

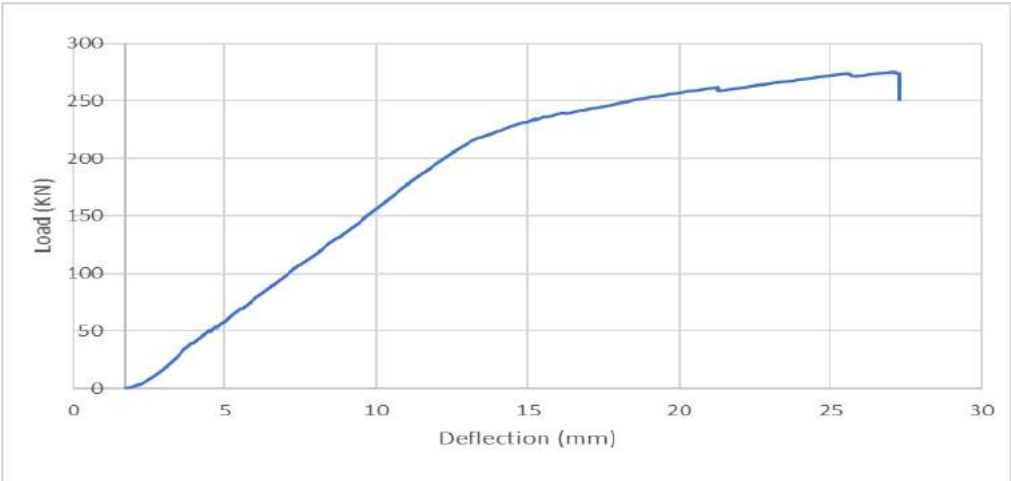

Figure 4-45: Beam B2-S: Load-deflection curve.

Figure 4-46: Failure mode of strengthened Beam B2-S.

4.1.2.12 ***Beam B2-CA.*** This beam strengthened with one layer of CFRP sheet and one layer of AA plate, both of width 100 mm. The ultimate load obtained was equal to 209.6 kN with corresponding deflection of 10.6 mm. the mid-span deflection value at failure was equal to 13.0 mm. The percentage increased in load carrying capacity was equal to 76.9 % over the control specimen. The percentage decreased in ultimate and failure deflection was equal to 40.7% and 58.7% respectively. The beam failed by yielding of the steel rebar, followed by de-bonding of the FRP hybrid, and crushing of concrete at mid-span as shown in Figures 4-47 and 4-48.

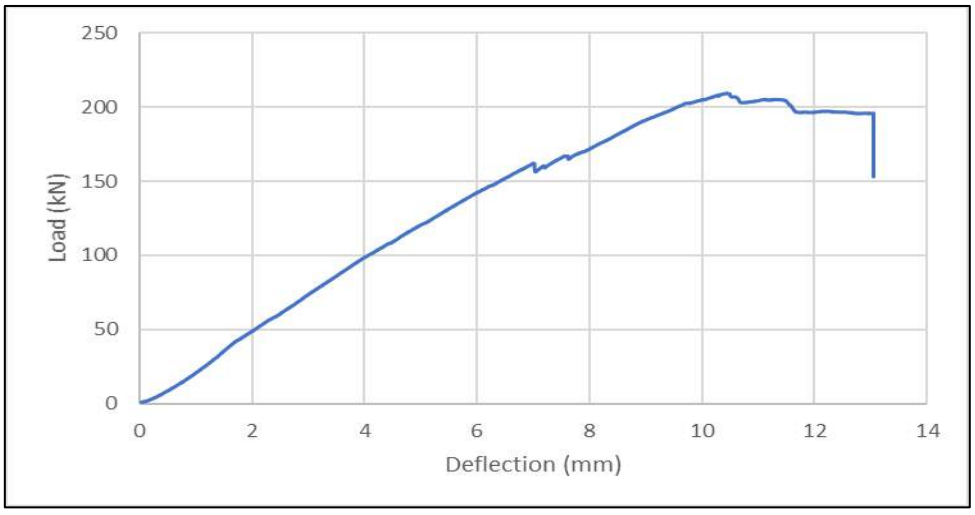

Figure 4-47: Beam B2-CA: Load-deflection curve.

Figure 4-48: Failure mode of strengthened Beam B2-CA.

4.1.2.13 ***Beam B2-SA.*** This beam strengthened with one layer of GSM sheet and one layer of AA plate, both of width 100 mm. The ultimate load obtained was equal to 256.2 kN with corresponding deflection of 15.7 mm. the mid-span deflection value at failure was equal to 16.4 mm. The percentage increased in load carrying capacity was equal to 42.4 % over the control specimen. The percentage decreased in ultimate and failure deflection was equal to10.8 % and 47.9 % respectively. The beam failed by yielding of the steel rebar, followed by delamination of the FRP hybrid (concrete cover separation), and crushing of concrete at mid-span as shown in Figures 4-49 and 4-50.

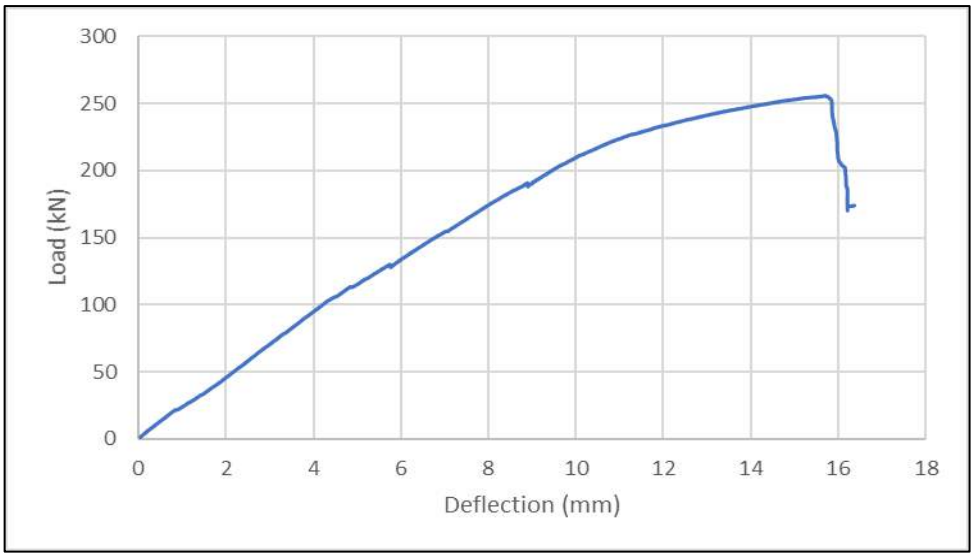

Figure4-49: Beam B2-SA Load-deflection curve.

Figure 4-50: Failure mode of strengthened Beam B2-SA.

4.2 Results Discussion

In this section, results from experimental testing program for T-beams are discussed and summarized. Tables and figures below, illustrate different behavior of beams strengthened with different combinations of FRP laminations.

4.2.1 Group A. This group was casted with 2T12 as main tension reinforcement, which is the lowest reinforcement ratio compared to the other group; however, it has high ultimate flexural capacity. Figures 4-51 to 4-64 show the load vs mid span deflection curve of the control and the strengthened specimen's in-group A. Results shown below illustrate that all specimens behaved in a same manner before reaching failure point; however, the increase in load and cracking lead to change in stiffness.

All tested specimen that strengthened with AA, CFRP, SM or hybrid system provided higher flexural bearing capacity from 18% to 77%, yet lower deflection values of ductility specimen in range of 27% to 59% in comparison to the control beam.

The results below illustrate the difference in flexural bearing capacity performance of RC T-beams that strengthened with hybrid system of CFRP with AA using U-Wrapping technique. It is observed that U-Wrapping technique had significantly increased the gap in ductility performance of the beam by 27% less than the control beam. In addition, the U-Wrapping technique had significantly increased

the flexural load capacity performance of the beam by 66% compared to the control specimen.

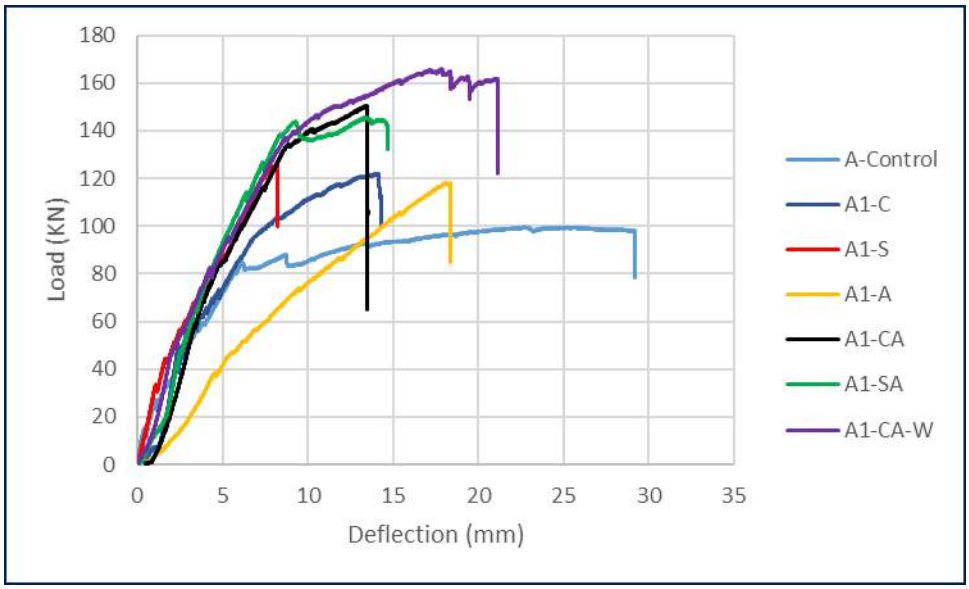

Figure 4-51: Load-deflection curve of all A1 beams.

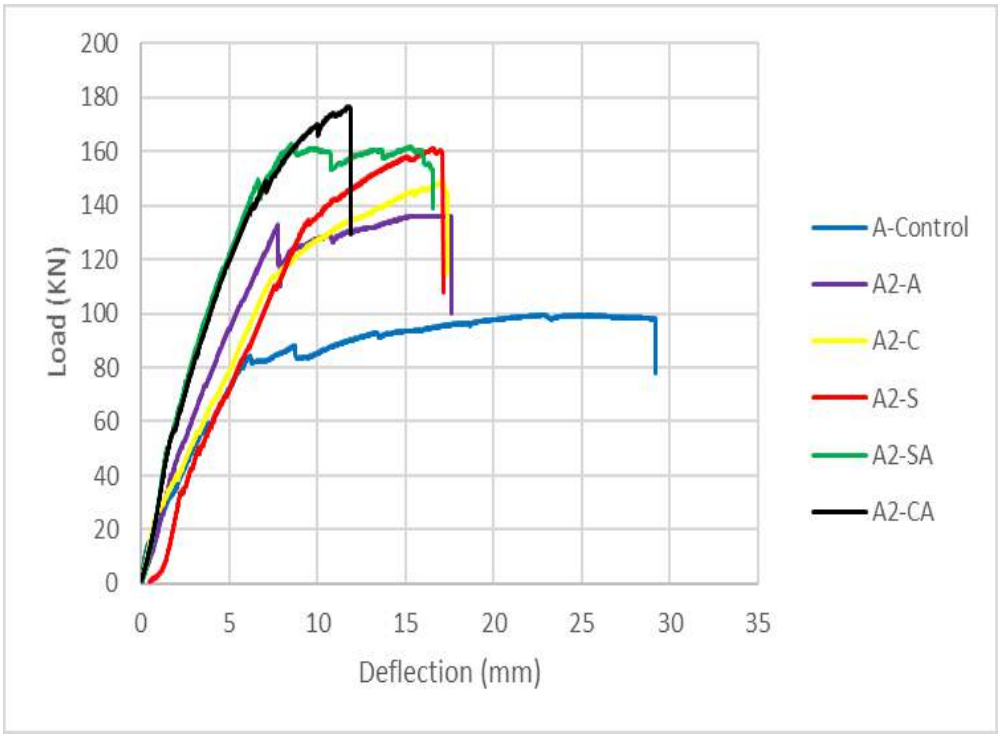

Figure 4-52: Load-deflection of all A2 beams.

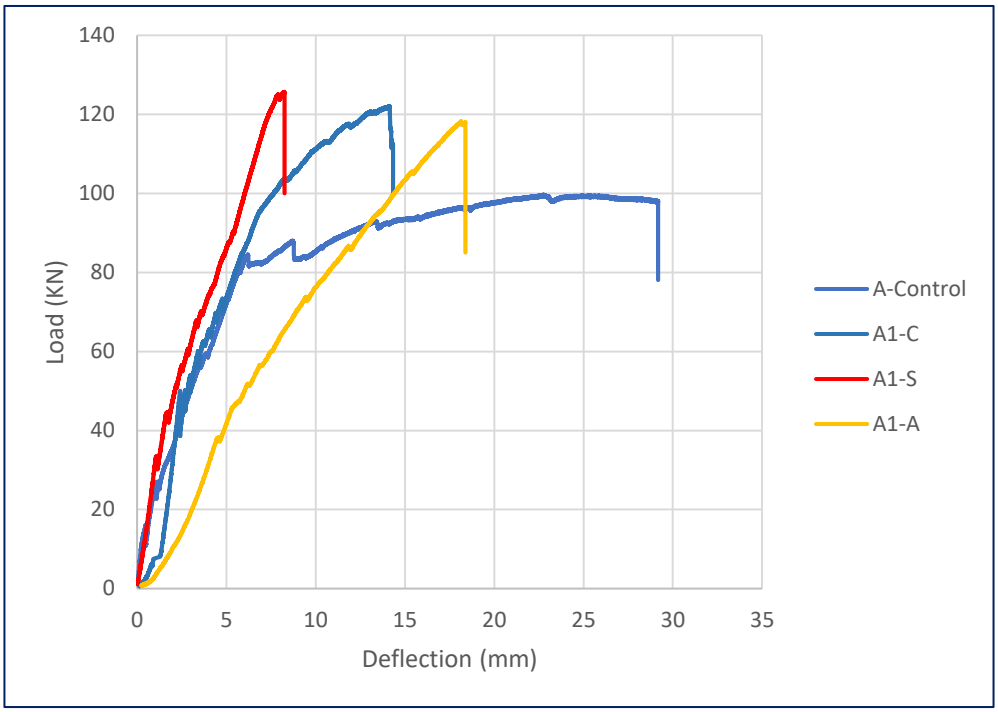

Figure 4-53: Load-deflection–Beams with one FRP layer of A1

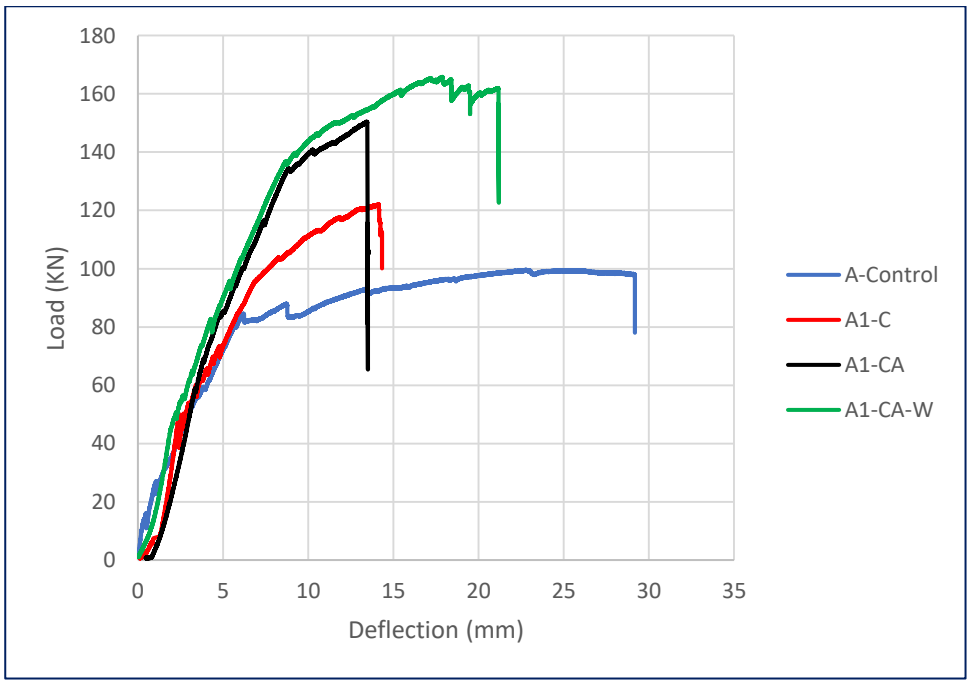

Figure 4-54: Load-deflection–Beams with CFRP hybrid of A1.

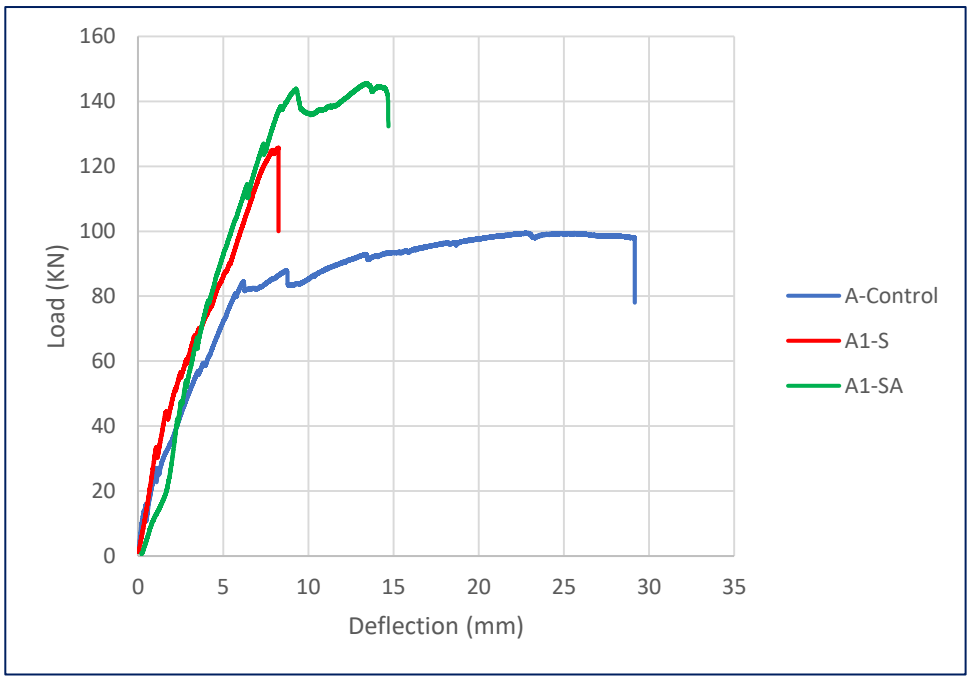

Figure 4-55: Load-deflection–Beams with GSM hybrid A1.

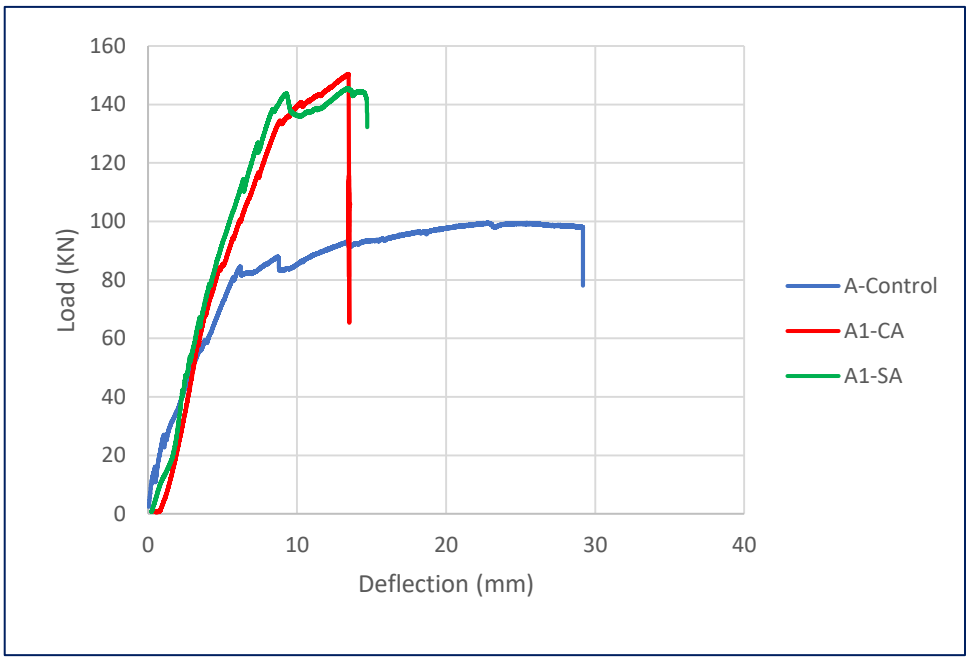

Figure 4-56: Load-deflection–Beams with different hybrid of A1.

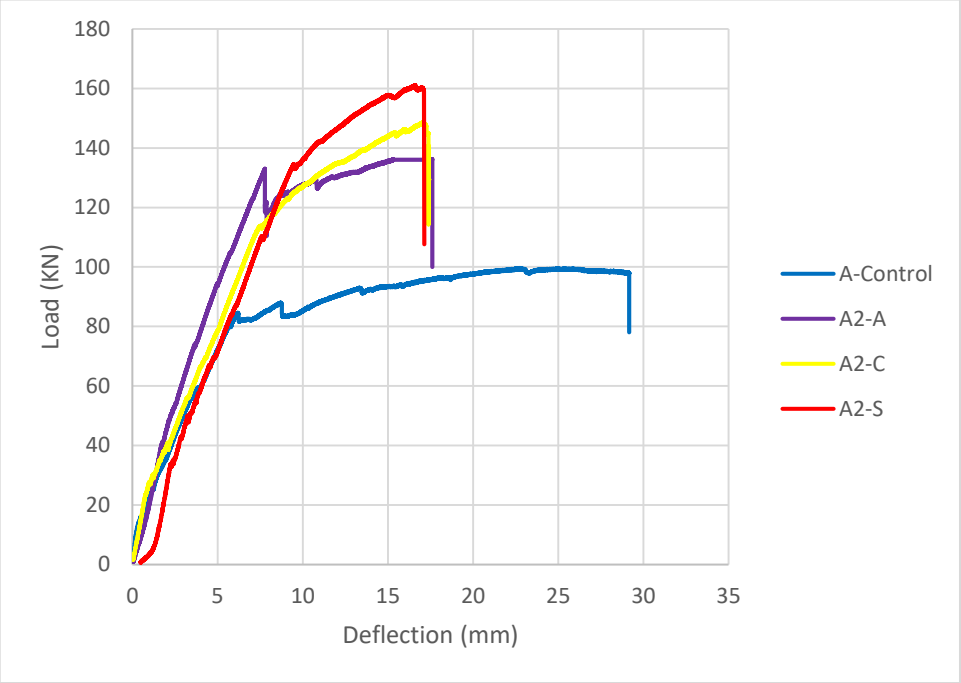

Figure 4-57: Load-deflection–Beams with one FRP layer of A2.

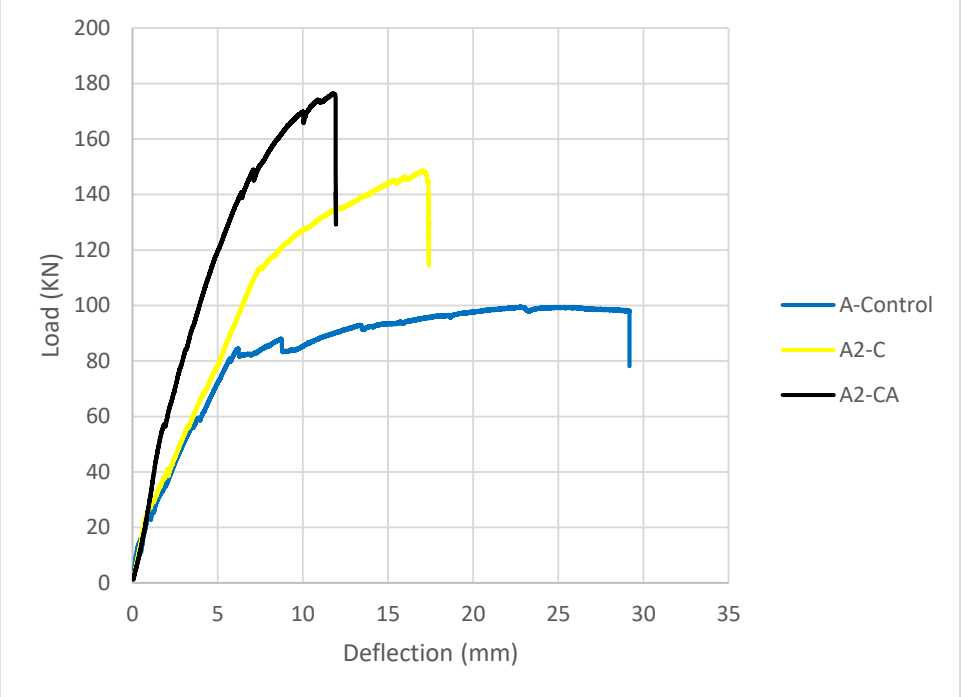

Figure 4-58: Load-deflection – Beams with CFRP hybrid of A2.

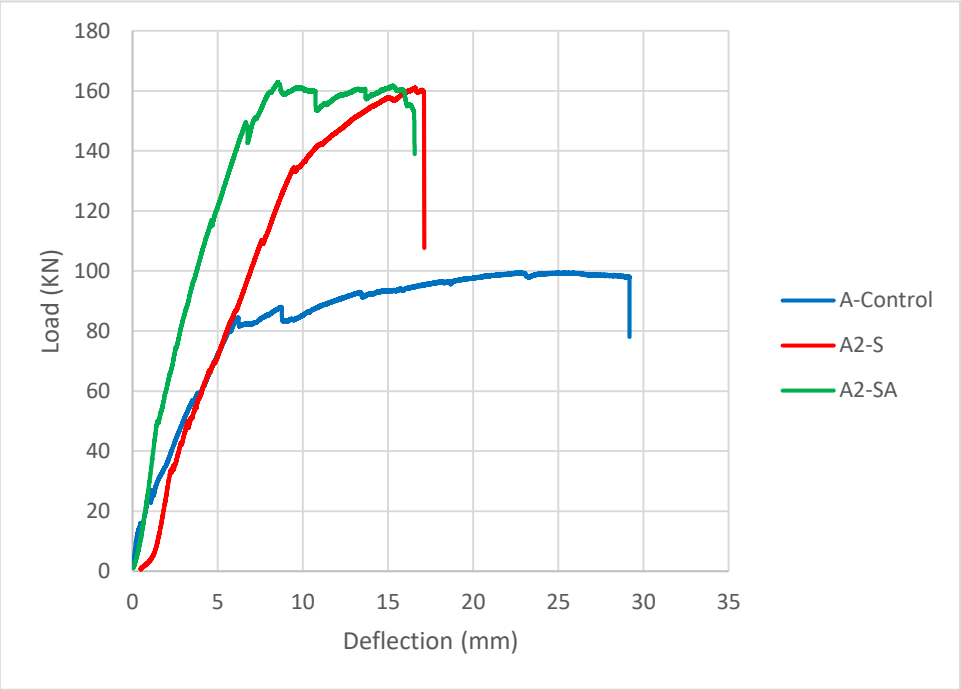

Figure 4-59: Load-deflection – Beams with GSM hybrid of A2.

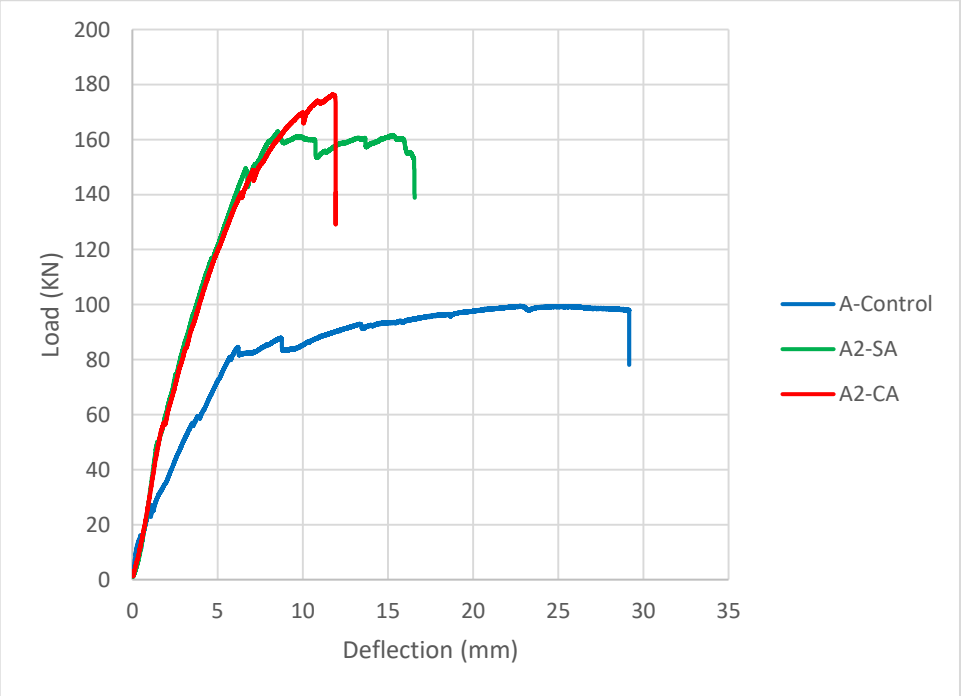

Figure 4-60: Load-deflection – Beams with hybrid of A2.

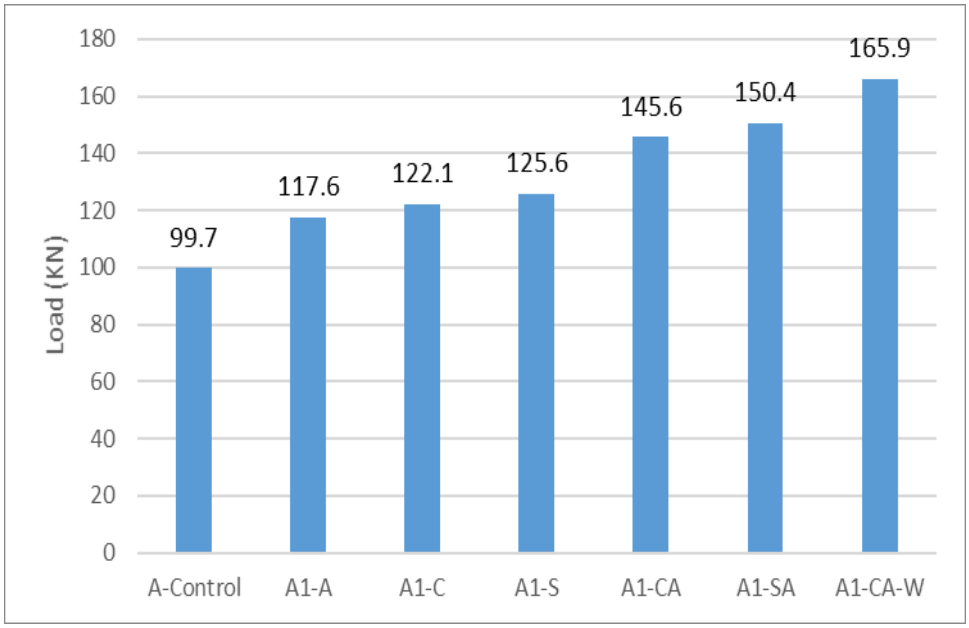

Figure 4-61: Increase in load compared to control beam for A1.

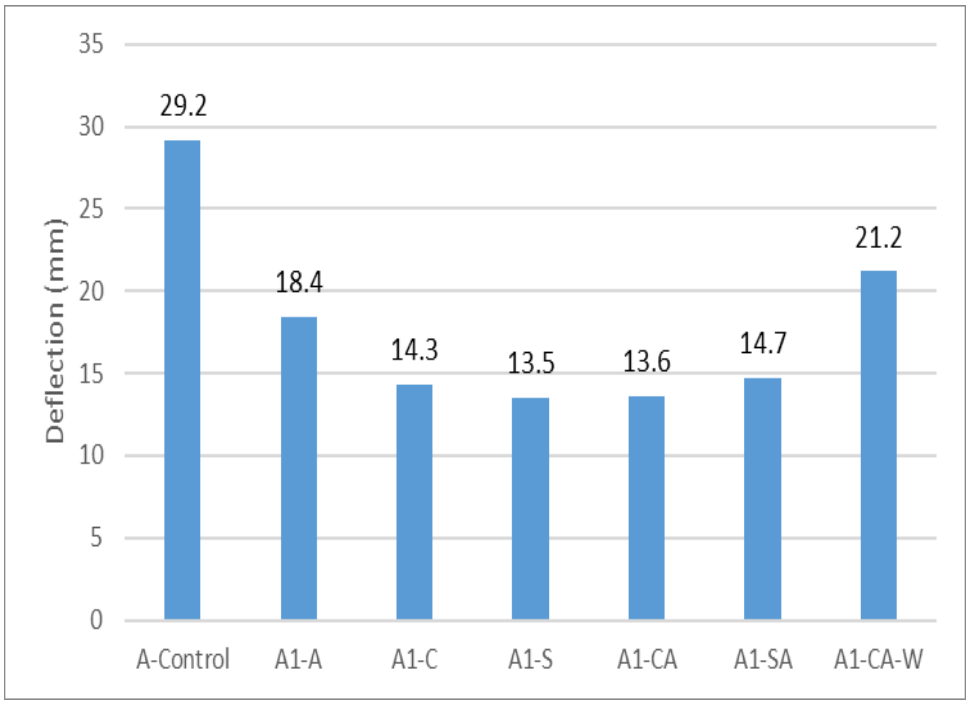

Figure 4-62: Decrease in deflection compared to control beam of A1.

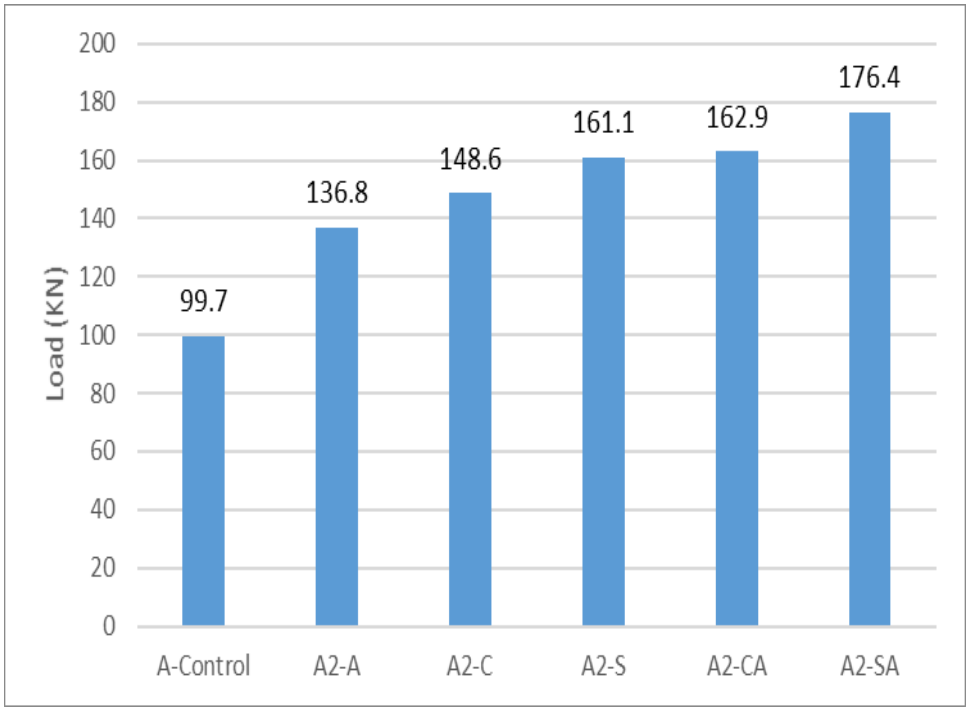

Figure 4-63: Increase in load compared to control beam of A2.

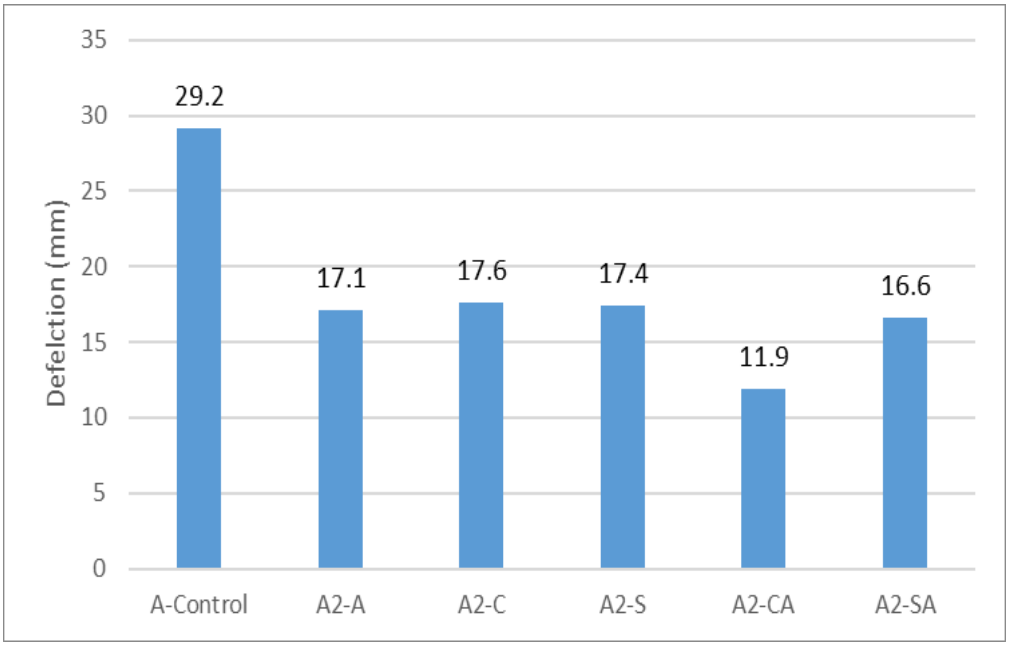

Figure 4-64: Decrease in deflection compared to control beam of A2.

Table4-1 shows the experimental results of the ultimate load, the ratio of the ultimate load of the strengthened beam to the ultimate load of the control beam, ultimate deflection, the ratio of the ultimate deflection of the strengthened beam to the ultimate

deflection of the control beam, failure deflection, and finally the ratio of the failure deflection of the strengthened beam to the failure deflection of the control beam.

Table 4-1 shows the stiffness of the strengthened beam as ratio between the load at steel yield point and the beam deflection at steel yield point *K* (*Py/δy*). On the other hand, Table 4-2 presents the ductility ratios to compare the flexural performance of the strengthened beams compared to the control beam, and summarize the ductility indices measured for all RC beams.

Table 4-1: Summary of experimental results

Specimen Designation	**P_y (KN)**	**δ_y (mm)**	**K***	**% K over BC**	**P_u (KN)**	**%P_u over BC**	**δ_u (mm)**	**%δ_u Decrease over BC**	**δ_f (mm)**	**%δ_f Decrease over BC**
A-Control	82.1	6.7	14.9	1.0	99.7	0.0	21.5	0.0	29.2	0.0
A1-A	97.6	5.3	22.2	1.5	117.6	18.0	17.8	17.2	18.4	37.0
A1-C	92.0	6.6	18.5	1.2	122.1	22.5	13.0	39.5	14.3	51.0
A1-S	95.3	5.7	22.0	1.5	125.6	26.0	7.9	63.3	13.5	53.8
A1-CA	133.7	8.0	18.8	1.3	150.4	50.9	13.1	39.1	13.6	53.4
A1-SA	133.4	8.9	16.4	1.1	145.6	46.0	9.4	56.3	14.7	49.7
A1-CA-W	99.4	5.8	28.6	1.9	165.9	66.4	17.2	20.0	21.2	27.4
A2-A	115.8	6.5	21.0	1.4	136.8	37.2	15.5	27.9	17.6	39.7
A2-C	100.3	6.5	22.9	1.5	148.6	49.0	16.6	22.8	17.4	40.4

A2-S	133.1	9.4	17.1	1.2	161.1	61.6	16.2	24.7	17.1	41.4
A2-CA	131.7	5.8	30.4	2.0	176.4	76.9	10.5	51.2	11.9	59.2
A2-SA	155.5	11.2	14.5	1.0	162.9	63.4	8.9	58.6	16.6	43.2

$K^* = (P_{y/} \delta_y)$

Table4-2: Summary of ductility indices

Specimen Designation	**δ_y (mm)**	**δ_u (mm)**	**δ_f (mm)**	**μΔu**	**μΔu/ (μΔu)B**	**μΔf**	**μΔf/ (μΔf)B**
A-Control	6.7	21.5	29.2	3.2	1.0	4.4	1.0
A1-A	5.3	17.8	18.4	3.4	0.9	3.5	0.8
A1-C	6.6	13.0	14.3	2.0	0.6	2.2	0.5
A1-S	5.7	7.9	13.5	1.4	0.4	2.4	0.5
A1-CA	8.0	13.1	13.6	1.6	0.5	1.7	0.4
A1-SA	8.9	9.4	14.7	1.1	0.3	1.7	0.4
A1-CA-W	5.8	17.2	21.2	3.0	0.9	3.7	0.9
A2-A	6.5	15.5	17.6	2.4	0.7	2.7	0.6
A2-C	6.5	16.6	17.4	2.6	0.8	2.7	0.6
A2-S	9.4	16.2	17.1	1.7	0.5	1.8	0.4
A2-CA	5.8	10.5	11.9	1.8	0.6	2.1	0.5
A2-SA	11.2	8.9	16.6	0.8	0.2	1.5	0.3

It can be noticed from Table 4-1 that the beams strengthened with one layer of FRP material exhibited 17% to 63% reduction in ductility at ultimate load compared to the un-strengthened beam. The beam strengthened with hybrid FRP materials like CFRP with AA, and SM with AA, both exhibited 39% to 59% less in ductility at ultimate load than the control beam. Beam of U- wrapped CFRP with AA exhibited

20% lower ductility at ultimate load than the control beam; which shows the effect of U-wrapping technique in reducing the gap in ductility compared to the control specimen. Table4-2, shows that the use of the hybrid system of CFRPAA with U-wrapping technique exhibited a ratio of 0.9 less in ductility at failure load compared to the control beam.

Table4-3: Ultimate load capacity and mode of failure

Specimen	P_U (KN)	Mode of failure
A-Control	99.7	Flexural (Steel yielding, Concrete crushing)
A1-A	117.6	S.y* followed by FRP debonding with f.c.
A1-C	122.1	S.y* followed FRP Concrete cover delamination
A1-S	125.6	S.y* followed FRP rupture then Concrete crushing
A1-CA	150.4	S.y* followed by FRP debonding with F.c
A1-SA	145.6	S.y* followed by FRP debonding with F.c.
A1-CA-W	165.9	F.c* followed by FRP partial delamination at ends
A1-SA-W	-	-
A2-A	136.8	F.c* followed by FRP rupture at the mid span
A2-C	148.6	F.c* followed by FRP partial delamination
A2-S	161.1	F.c* followed by FRP full delamination at ends
A2-CA	176.4	F.c* followed by FRP full delamination at one end
A2-SA	162.9	F.c* followed by FRP delamination at mid span

S.y*: Steel yielding.

F.c*: flexural cracks.

4.2.2 Group B. This group was casted with 2Ø16 as main tension reinforcement, which is the lowest reinforcement ratio compared to another group. However, it has high ultimate flexural capacity. Figure below shows the load vs mid span deflection curve of the control and the strengthened specimen's in-group B. Results shown below illustrates that all specimens behave in a same manner before reaching failure point; however, the increase in load and cracking lead to change in stiffness.

All tested specimen that strengthened with AA, CFRP, SM or hybrid system provided higher flexural bearing capacity from 10% to 53%, yet lower deflection values than that specimen which un-strengthened in range of 13% to 59% less in ductility compared to the control beam.

The results in Figures 4-65 to 4-78 illustrates the difference in flexural bearing capacity performance of RC T-beam that strengthened with hybrid system using U-Wrapping technique. It observed that U-Wrapping technique had significantly increased the gap in ductility performance of the beam by 13% to 36% less than the control beam. In addition, the U-Wrapping technique had significantly increased the flexural load capacity performance of the beam by 40% to 44% compared to the control specimen.

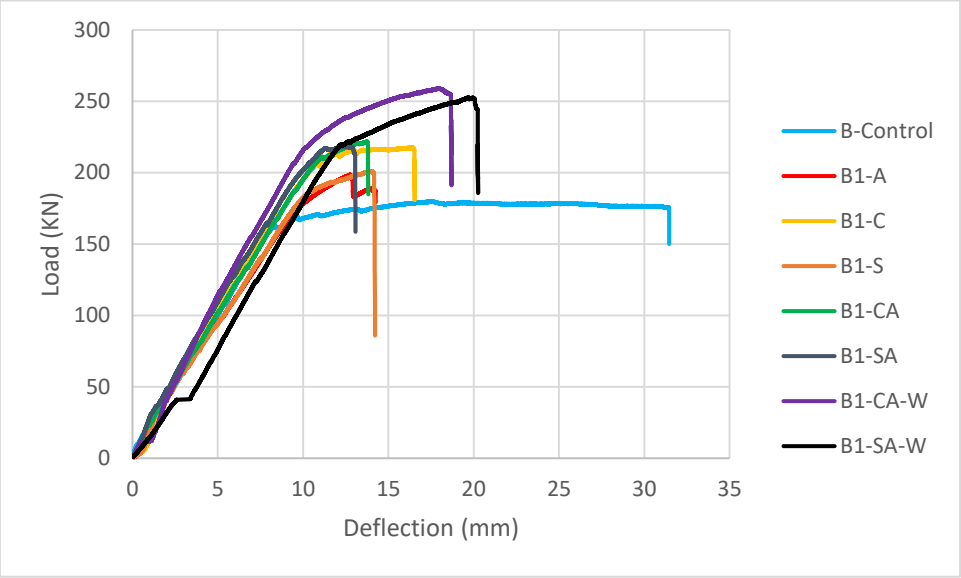

Figure 4-65: Load-deflection of all beams with FRP B1.

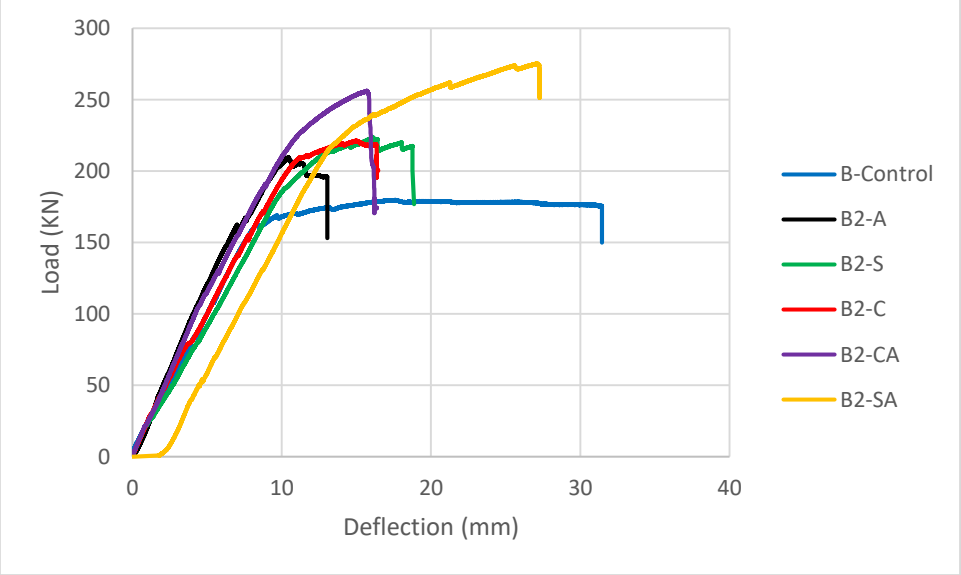

Figure 4-66: Load vs. Deflection, all beams with FRP B2.

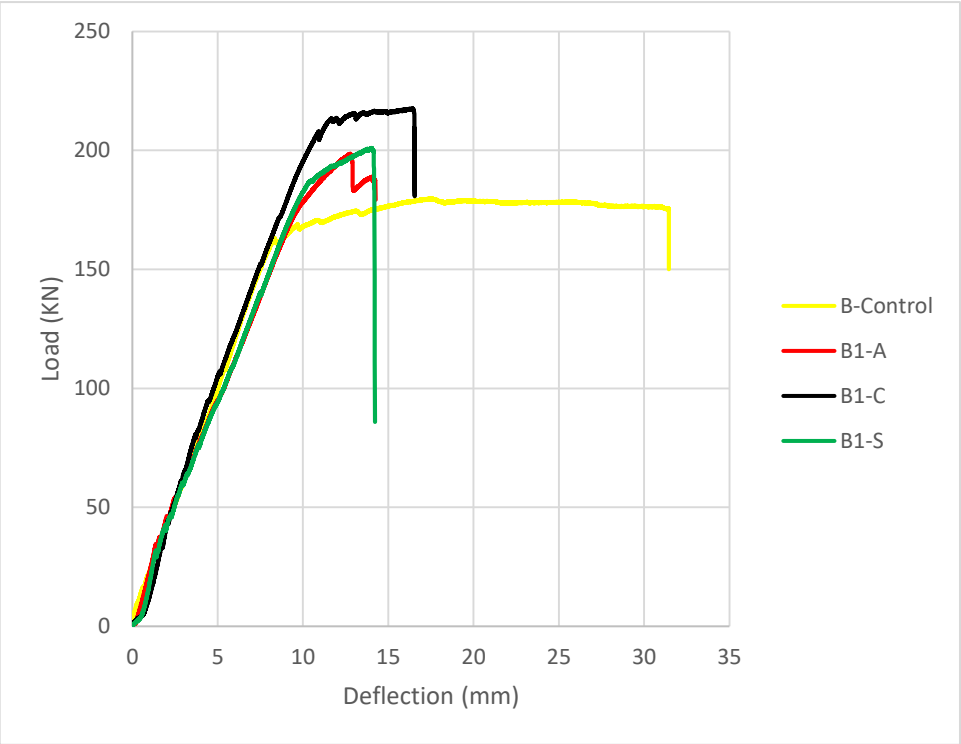

Figure 4-67: Load-deflection – Beams with one FRP layer B1.

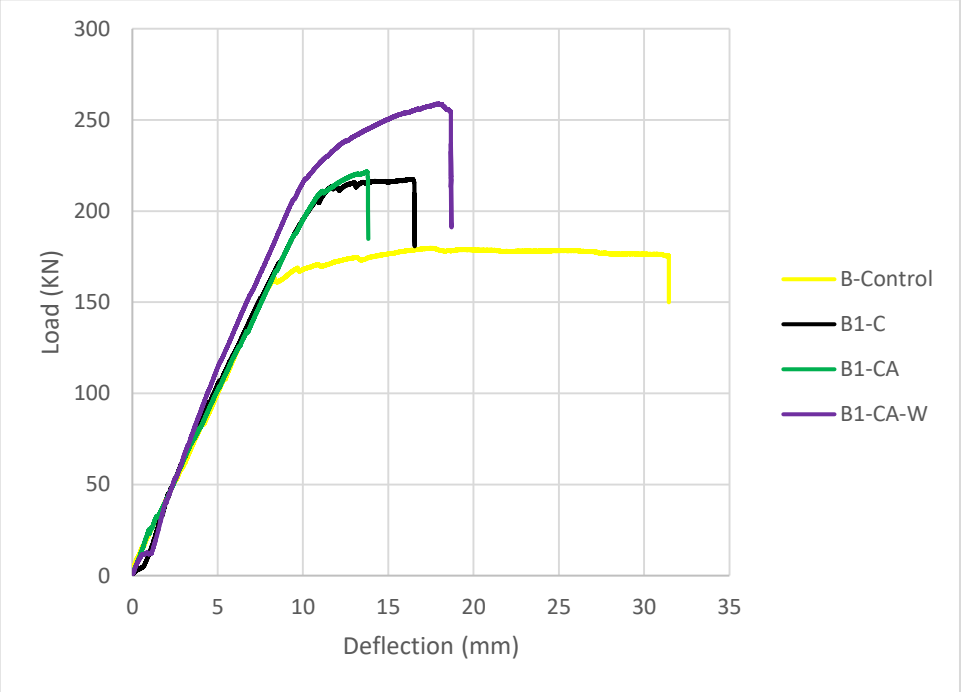

Figure 4-68: Load-deflection – Beams with CFRP hybrid of B1.

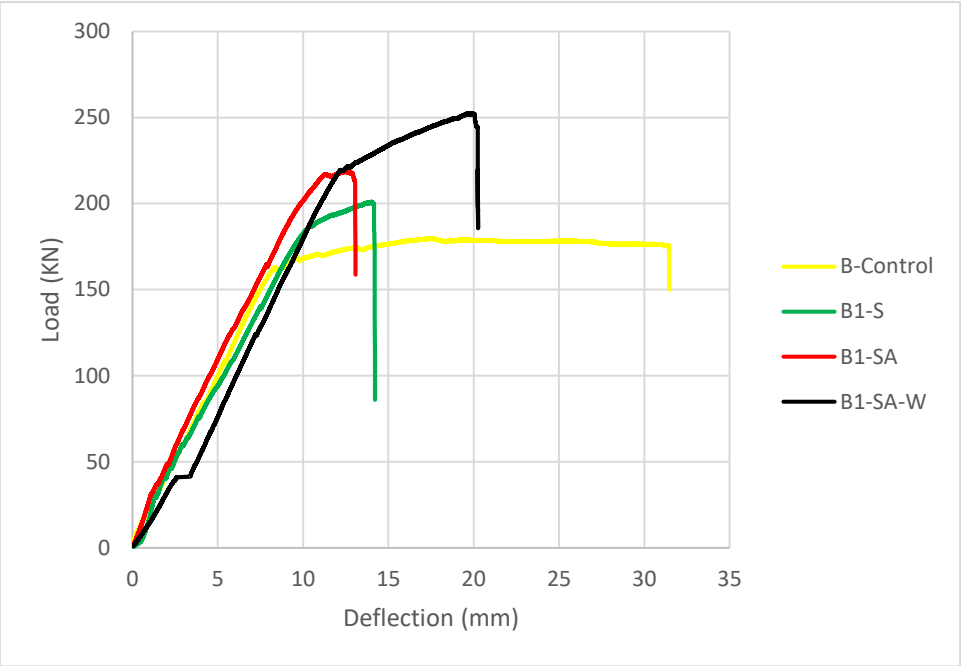

Figure 4-69: Load-deflection – Beams with GSM hybrid of B1.

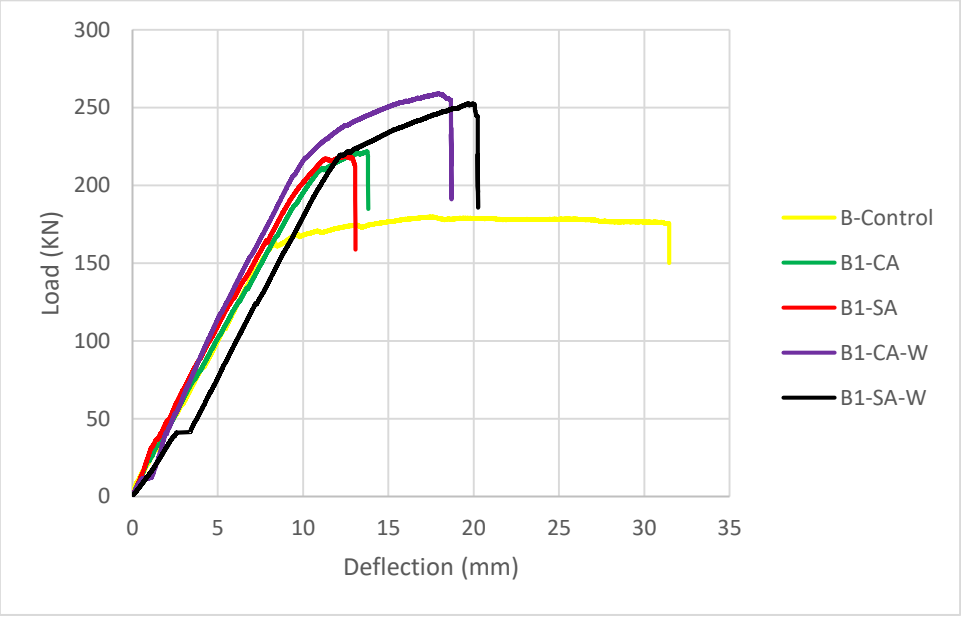

Figure 4-70: Load-deflection – Beams with different hybrid of B1.

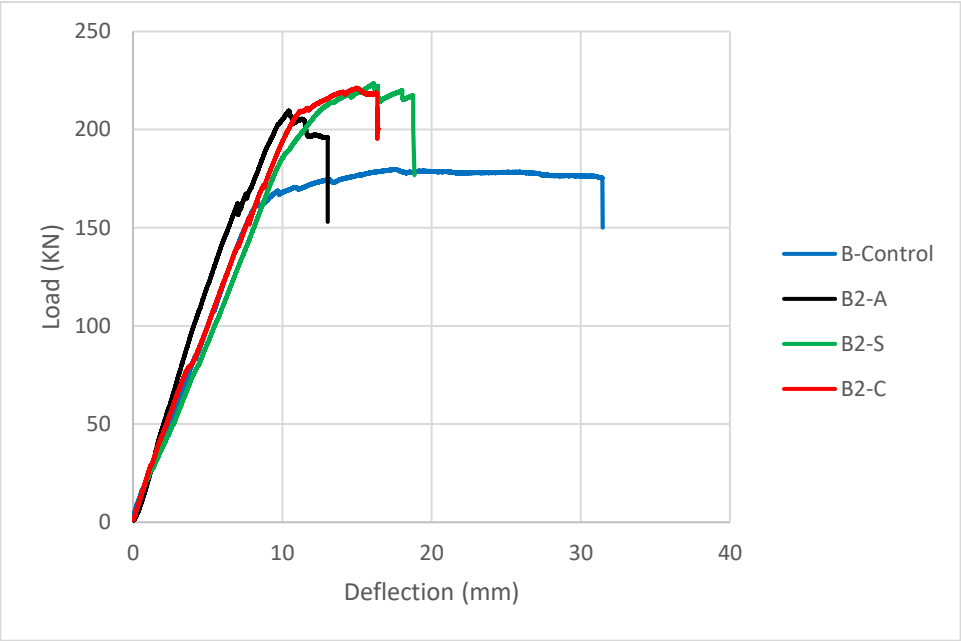

Figure 4-71: Load vs. Deflection-Beams with one FRP layer of B2.

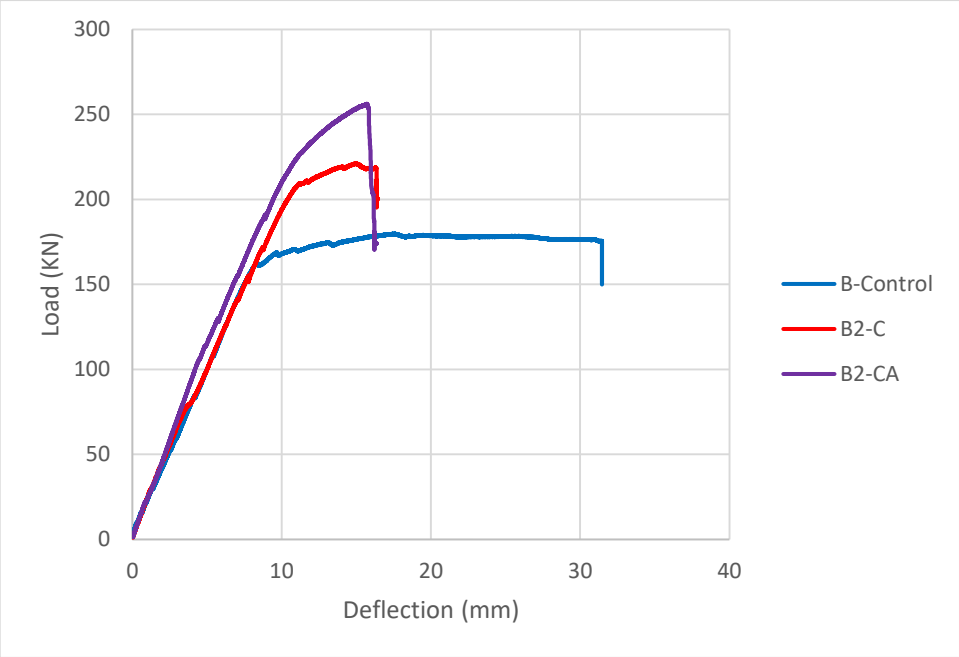

Figure 4-72: Load vs. Deflection, Beams with CFRP hybrid of B2.

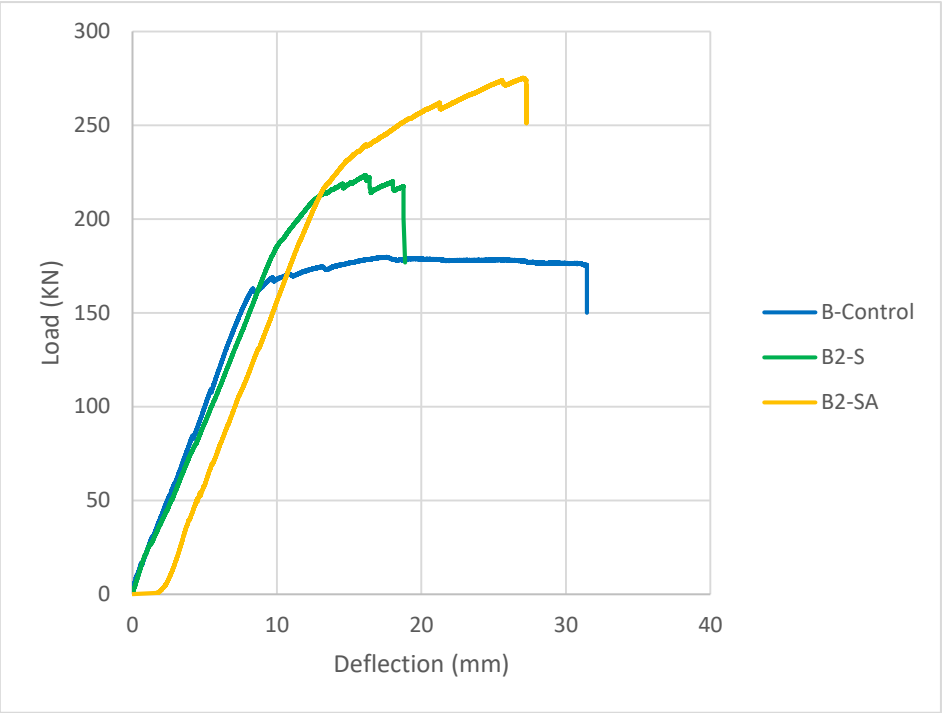

Figure 4-73: Load-deflection – Beams with GSM hybrid of B2.

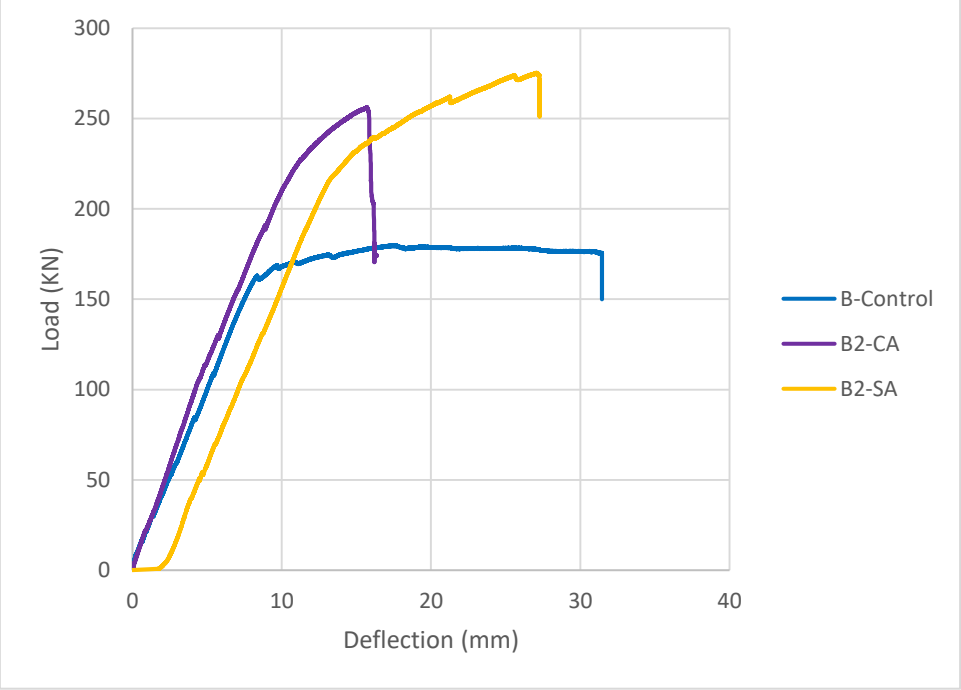

Figure 4-74: Load-deflection – Beams with different hybrid of B2.

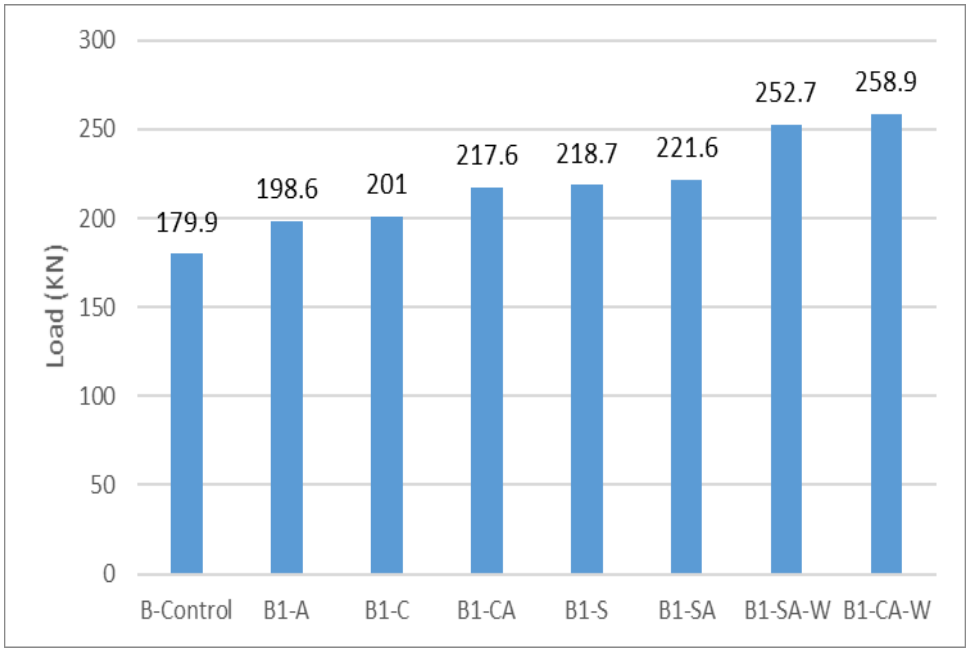

Figure 4-75: Increase in load compared to control beam for B1.

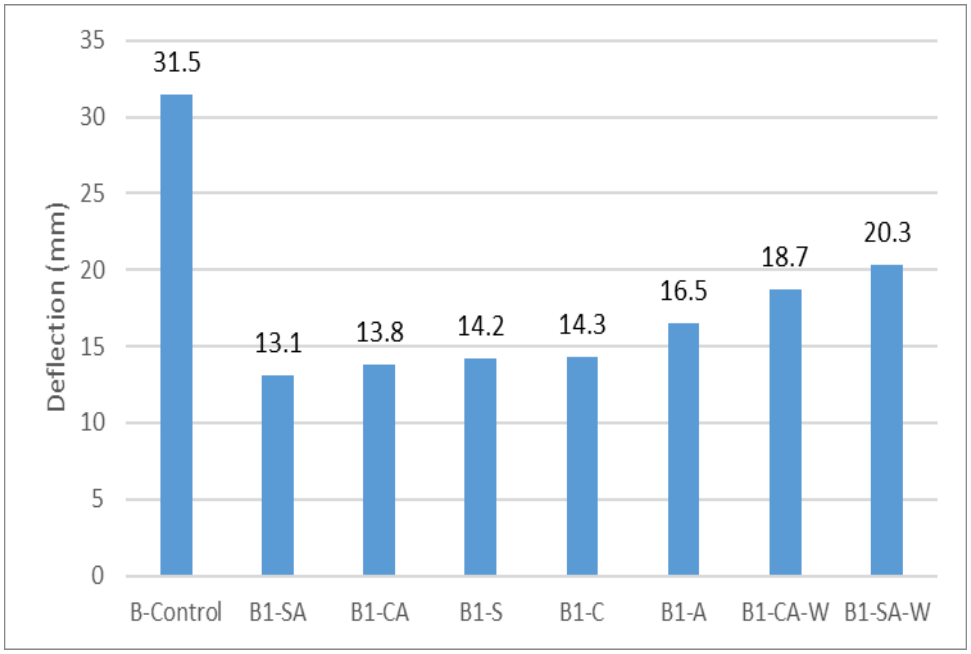

Figure 4-76: Decrease in deflection vs control beam for B1.

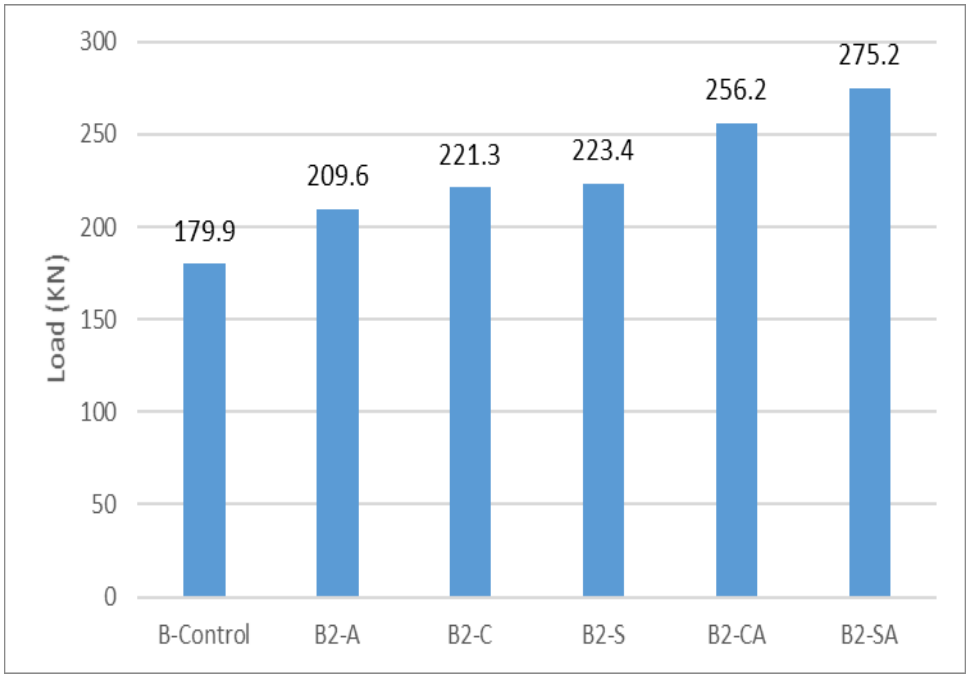

Figure 4-77: Increase in load compared to control beam for B2.

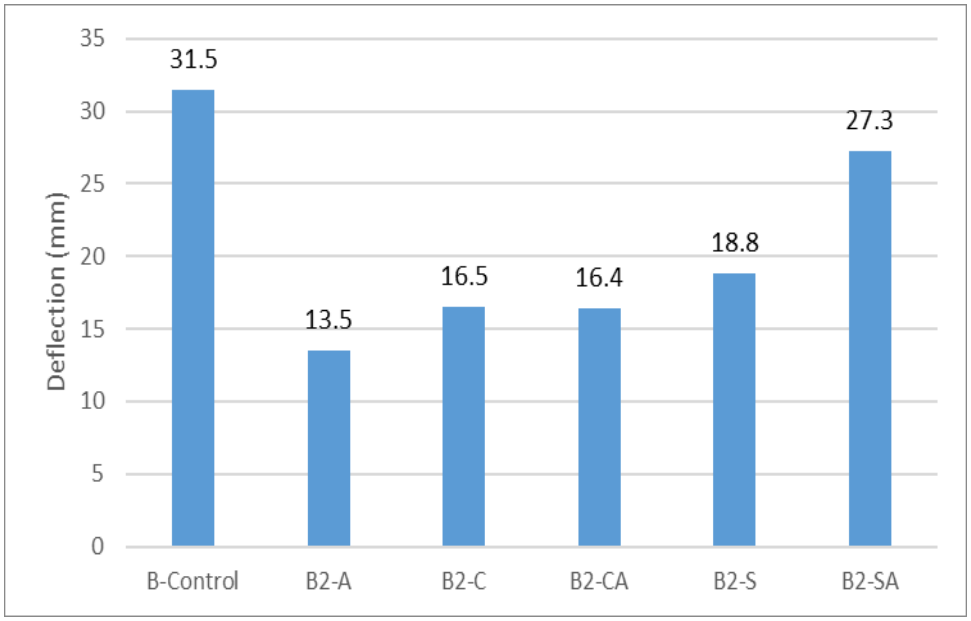

Figure 4-78: Decrease in ductility compared to control beam for B2.

Table 4-4 shows the stiffness of the strengthened beam as ratio between the load at steel yield point and the beam deflection at steel yield point K ($Py/\delta y$). On the other hand, Table 4-5 presents the ductility ratios to compare the flexural performance of the strengthened beams compared to the control beam, and summarize the ductility indices measured for all RC beams.

Table4-4: Summary of experimental results

Specimen Designation	P_y (KN)	δ_y (mm)	K*	% K over BC	P_u (KN)	%P_u over BC	δ_u (mm)	%δ_u Decrease over BC	δ_f (mm)	%δ_f Decrease over BC
B-Control	157.4	7.9	19.9	1.0	179.9	0.0	17.6	0.0	31.5	0.0
B1-A	167.6	9.2	18.2	0.9	198.6	10.4	12.8	27.3	16.5	47.6
B1-C	200.5	10.3	19.5	1.0	217.6	21.0	16.4	6.8	14.3	54.6
B1-S	184.3	10.2	18.1	0.9	201	11.7	14.0	20.5	14.2	54.9
B1-CA	190.6	9.8	19.4	1.0	221.6	23.2	13.7	22.2	13.8	56.2
B1-SA	163.2	7.9	20.7	1.0	218.7	21.6	12.5	29.0	13.1	58.4
B1-CA-W	217.7	10.2	21.3	1.1	258.9	43.9	19.7	-11.9	18.7	40.6
B1-SA-W	149.7	8.5	17.6	0.9	252.7	40.5	17.8	-1.1	20.3	35.6
B2-A	207.8	10.3	20.2	1.0	209.6	16.5	10.4	40.9	13.5	57.1
B2-C	169.9	8.6	19.8	1.0	221.3	23.0	14.9	15.3	16.5	47.6
B2-S	200.3	11.5	17.4	0.9	223.4	24.2	16.1	8.5	18.8	40.3
B2-CA	190.0	9.0	21.1	1.1	256.2	42.4	16.4	6.8	16.4	47.9
B2-SA	143.7	9.4	15.3	0.8	275.2	53.0	27.1	-54.0	27.3	13.3

Table 4-5: Summary of ductility indices

Specimen Designation	FRP Width	δ_y (mm)	δ_u (mm)	δ_f (mm)	μΔu	μΔu/ (μΔu)B	μΔf	μΔf/ (μΔf)B
B-Control	B1	7.9	17.6	31.5	2.2	1.0	4.0	1.0
B1-A	B1	9.2	12.8	16.5	1.4	0.6	1.8	0.4
B1-C	B1	10.3	16.4	14.3	1.6	0.7	1.4	0.3
B1-S	B1	10.2	14.0	14.2	1.4	0.6	1.4	0.3
B1-CA	B1	9.8	13.7	13.8	1.4	0.6	1.4	0.4
B1-SA	B1	7.9	12.5	13.1	1.6	0.7	1.7	0.4
B1-CA-W	B1	10.2	19.7	18.7	1.9	0.9	1.8	0.5
B1-SA-W	B1	8.5	17.8	20.3	2.1	0.9	2.4	0.6
B2-A	B2	10.3	10.4	13.5	1.0	0.5	1.3	0.3
B2-C	B2	8.6	14.9	16.5	1.7	0.8	1.9	0.5
B2-S	B2	11.5	16.1	18.8	1.4	0.6	1.6	0.4
B2-CA	B2	9.0	16.4	16.4	1.8	0.8	1.8	0.5
B2-SA	B2	9.4	27.1	27.3	2.9	1.3	2.9	0.7

It can be noticed from Table 4-4 that the beams strengthened with one layer of FRP material exhibited 7% to 41% less in ductility at ultimate load compared to the un-strengthened beam. The beam strengthened with hybrid FRP materials like CFRP with AA, and SM with AA, both exhibited 7% to 54% less in ductility at ultimate load than that of the control beam. Beam of U- Wrapped CFRP with AA exhibited -1% to -12 higher in ductility at ultimate load than that of the control beam; which shows the effect of U-wrapping technique in reducing the gap in ductility compared to the control specimen. Table 4-5 shows that the use of the hybrid system of CFRP with AA with U-wrapping technique, it exhibited around 0.5 to 0.6 as ratio of less in in ductility at failure load compared to the control beam. Table 4-6 shows the ultimate load capacity and mode of failure.

Table 4-6: Ultimate load capacity and mode of failure

Specimen	FRP Width	P_U (KN)	Mode of failure
B-C ontrol	B1	179.9	Flexural (Steel yielding, Concrete crushing)
B1-A	B1	198.6	S.y* followed by FRP debonding
B1-C	B1	217.6	S.y* followed FRP Concrete cover delamination
B1-S	B1	201	S.y* followed FRP rupture then Concrete crushing
B1-CA	B1	221.6	S.y* followed by FRP debonding with F.c
B1-SA	B1	218.7	S.y* followed by FRP debonding with F.c
B1-CA-W	B1	258.9	F.c* followed by FRP partial delamination
B1-SA-W	B1	252.7	F.c* followed by FRP rupture at the mid span
B2-A	B2	209.6	F.c* followed by FRP partial delamination
B2-C	B2	221.3	F.c* followed by FRP full delamination at ends
B2-S	B2	223.4	F.c* followed by FRP full delamination at one end
B2-CA	B2	256.2	F.c* followed by FRP full delamination at mid span
B2-SA	B2	275.2	F.c* followed by FRP rupture at the mid span

S.y*: Steel yielding.

F.c*: flexural cracks.

Chapter 5: Analytical Prediction

In this chapter an analytical model was derived to validate the results that have been obtained of the experimental testing of the reinforced concrete beams. The first analytical model driven based on the concept of the effective flexibility of cracked reinforced concrete element. The model was able to predict the theoretical behavior of the applied load versus the resulted deflection for each specimen based on the concept of strain compatibility. The other model was developed to estimate the increment in flexural capacity and the ductility of the strengthened beams along with their failure mode. Both models were driven based on the ACI- 440.02R-08 and the ACI318-1 design guidelines.

5.1 Flexibility Model

Generally, the flexibility is a mechanical property of the structural cross-section, which usually used to estimate the deflection of structural elements under a certain loading. However, Appling this concept of the flexibility and predicting the load versus deflection is a bit complex especially for the structural elements that strengthened with externally bonded material like FRP, due to the difference between the mechanical properties of the FRP materials and the mild steel. Therefore, to predict the flexibility of these strengthened members the semi empirical equations that found in the ACI-440.02R-08 and the ACI318-1 design guidelines need to be used as shown below.

Equations below are used to find the predicted values for all tested beams that been carried out in this study under two point loadings scenarios:

$$\frac{1}{E_c * I_{eff}} = \frac{1}{E_c * I_c} * \left[1 + \frac{\omega}{1 + \omega}\right] \leq \frac{1}{E_c * I_g}, for\ M \geq M_{cr} \qquad (2)$$

Where:

$$\omega = \left(\frac{M_{cr}}{M}\right)^3 * \left[\frac{\beta_d * g}{I_{cr}} 1\right] \quad (3)$$

And,

$$\beta_d = \mu_d * \left[\frac{E_f}{E_s} + 1\right] \quad ,for \qquad \mu_d = 0.5 \quad (4)$$

$$\delta_{max} = \frac{P * a}{24} * \left[\frac{1}{E_c * I_{eff}}\right] * (3l^2 - 4a^2) \quad (5)$$

Where:

Ec : Modulus of elasticity for concrete

Ef : Modulus of elasticity for FRP

Es : Modulus of elasticity for steel

M : Applied bending moment on the element

Mcr: Cracking moment of reinforced concrete

Ig : Gross moment of inertia

Icr: Cracked moment of inertia

P : Applied load

a : The distance from the sup[port to the point load

In this analytical model, the gross moment of inertia is assumed before reaching the cracking moment of the element section. After that, the model used the empirical combination of the gross moment of inertia and the cracking moment to find the predicted values of the instant flexibility based on the applied loading at that specific instant as shown in the above equations. As a result of using this analytical model we examined, while the loads increased, the stiffness of the element reduced, due to the fact that the neutral axis of the section moved up.

5.2 Predicted Graphs for the Tested Specimen

Figures 5-1 to 5-25 illustrate the predicted values for load versus deflection for all tested specimens as well as compared to the results of the actual experiments carried out in the lab.

5.2.1 Group [GA]:

5.2.1.1 ***Beam A-Control***. As it can be seen in Figure 5-1 the experimental strength of control beam is the same as the predicted, but with slight difference in the ductility by 26%.

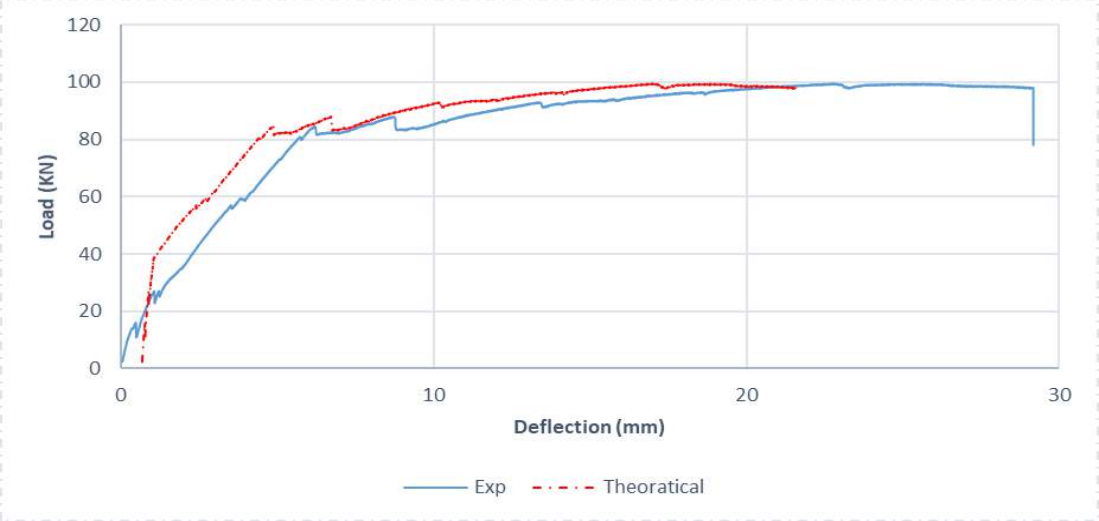

Figure 5-1: A-Control beam-experimental-theoretical results.

5.2.1.2 ***Beam A1-A***. It can be seen that in Figure 5-2 the experimental strength of beam A1-A is almost the same as the predicted, but with slight difference in the ductility by 29.9%.

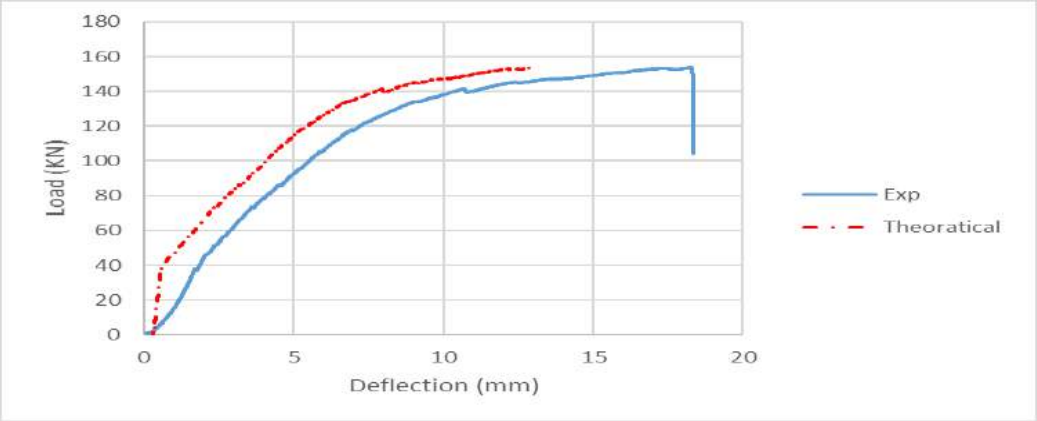

Figure 5-2: Beam A1-A-experimental-theoretical results.

5.2.1.3 ***Bam A1-C.*** It can be seen that in Figure 5-3 the experimental strength of beam A1-C is almost the same as the predicted, but with slight difference in the ductility by 16%.

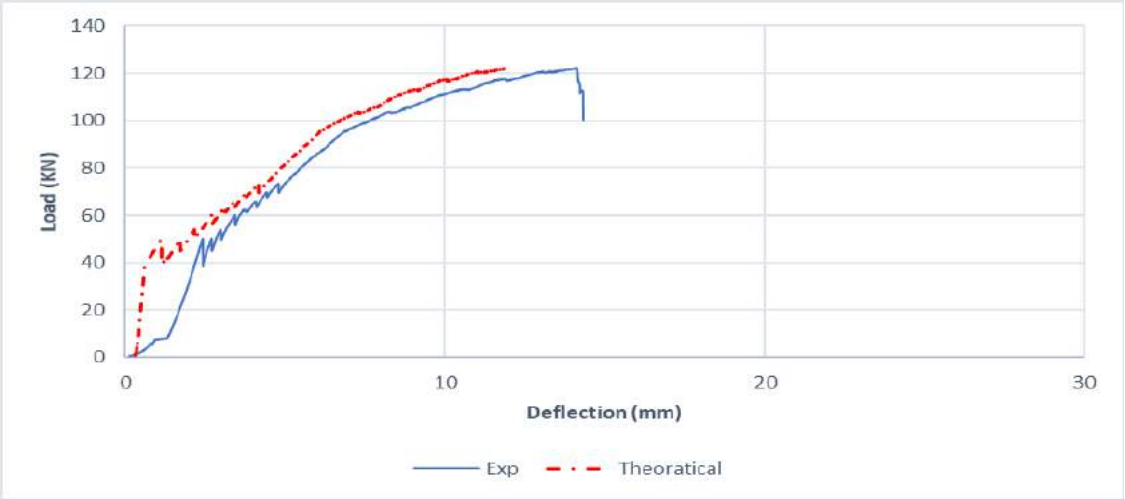

Figure 5-3: Beam A1-C-experimental-theoretical results.

5.2.1.4 ***Beam A1-S***. It can be seen that in Figure 5-4 the experimental strength of beam A1-S is almost the same as the predicted, but with slight difference in the ductility by 17%.

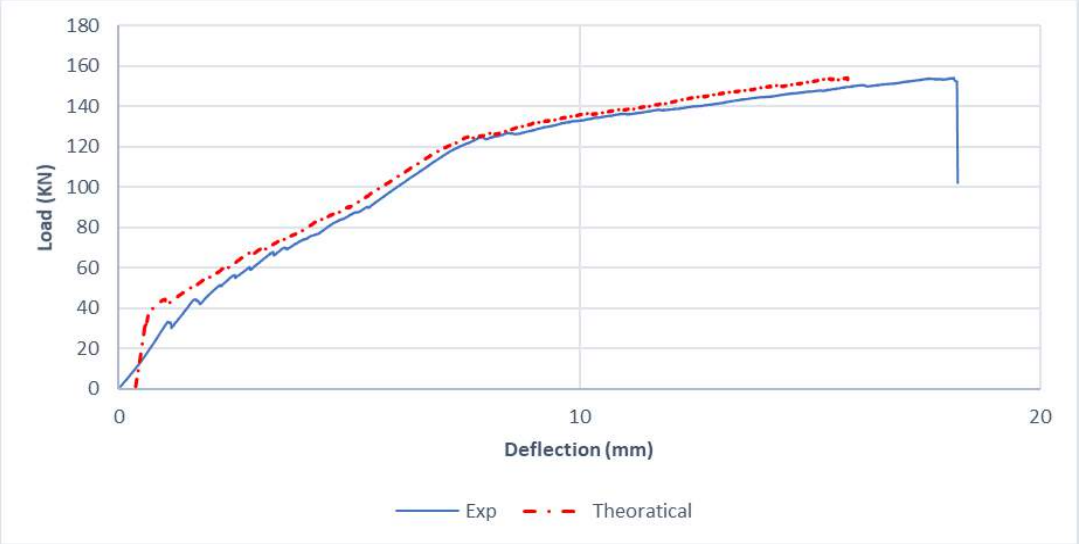

Figure 5-4: Beam A1-S-experimental-theoretical results.

5.1.2.5 *Beam A1-CA*. It can be seen that in Figure 5-5 the experimental strength of beam A1-CA is almost the same as the predicted, but with slight difference in the ductility by 32%.

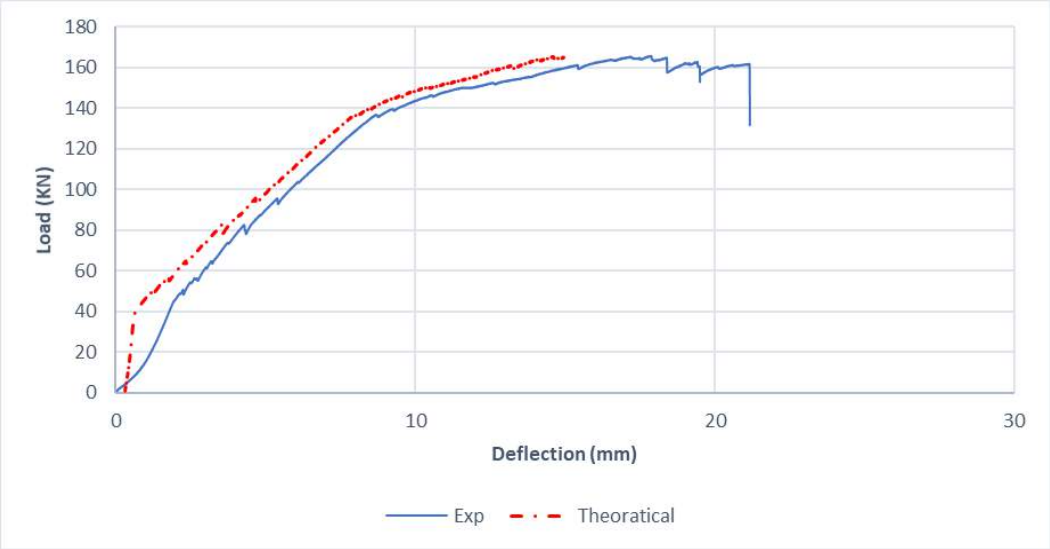

Figure 5-5: Beam A1-CA-experimental-theoretical results.

5.2.1.6 *Beam A1-SA.* It can be seen that in Figure 5-6 the experimental strength of beam A1-SA is almost the same as the predicted, but with slight difference in the ductility by 12%.

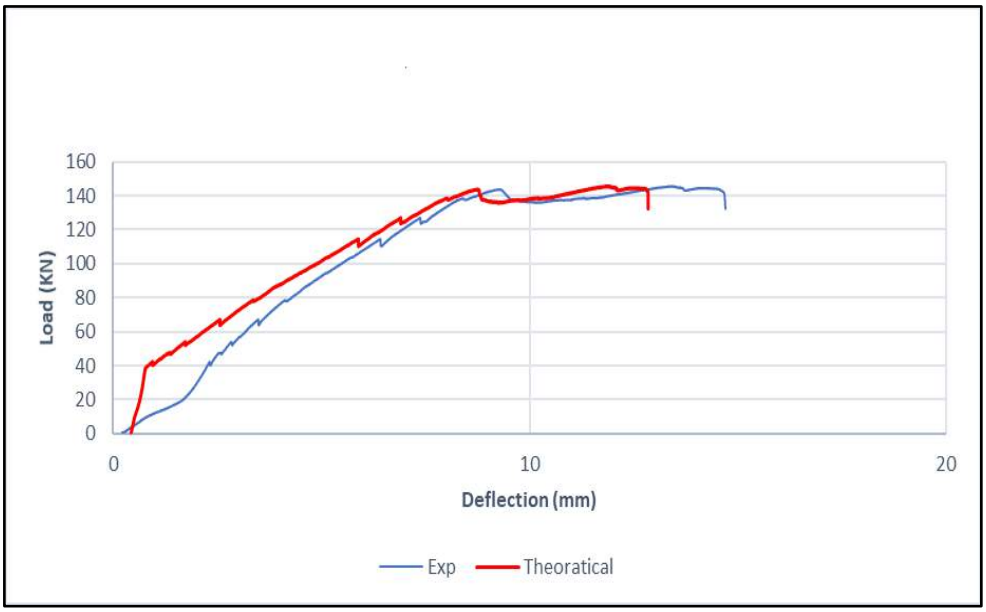

Figure 5-6: Beam A1-SA -experimental-theoretical results.

5.2.1.7 ***Beam A1-CA-W***. It can be seen that in Figure 5-7 the experimental strength of beam A1-SA is almost the same as the predicted, but with slight difference in the ductility by 11%

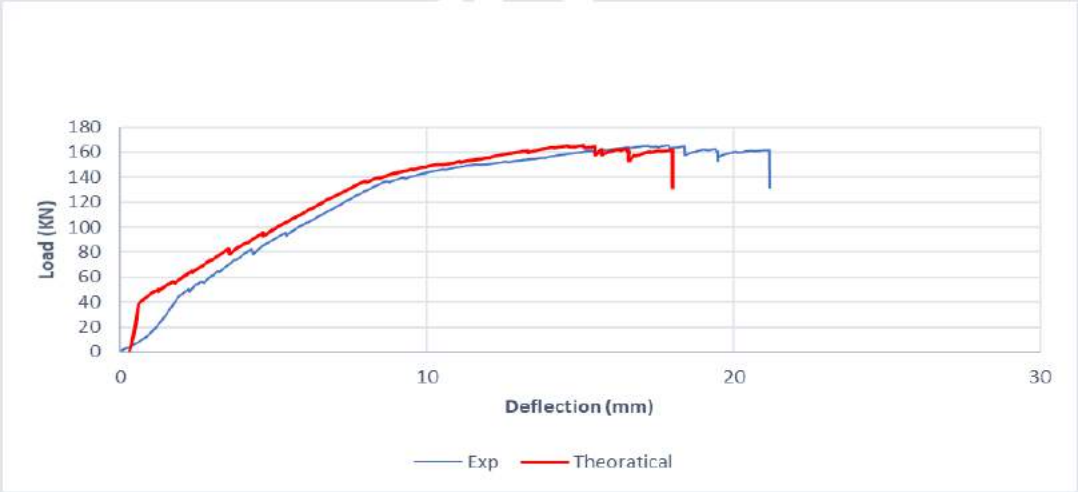

Figure 5-7: Beam A1-CA-W -experimental-theoretical results.

5.2.1.8 ***Beam A2-A.*** It can be seen that in Figure 5-8 the experimental strength of beam A2-A is almost the same as the predicted, but with slight difference in the ductility by 15%.

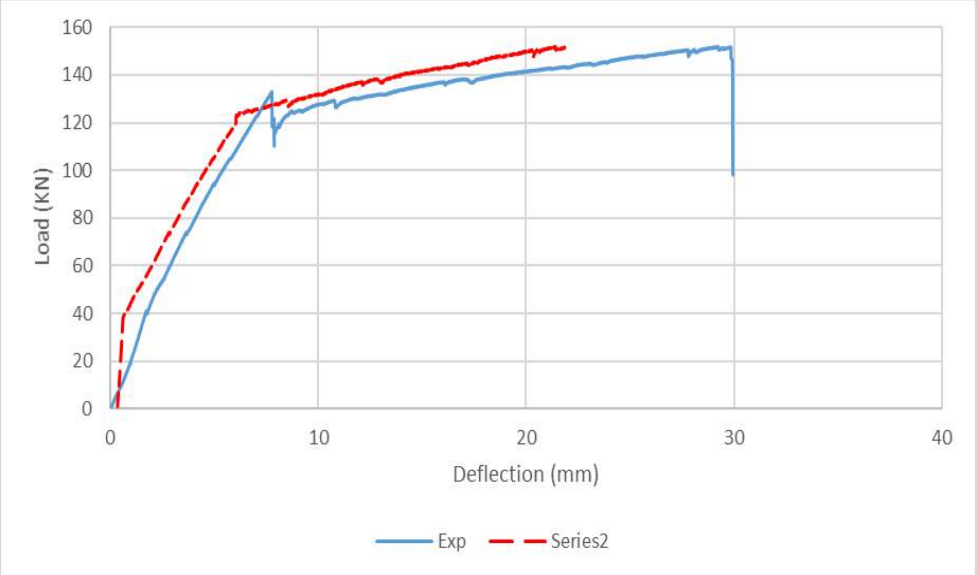

Figure 5-8: Beam A2-A -experimental-theoretical results.

5.2.1.9 ***Beam A2-C***. It can be seen that in Figure 5-9 the experimental strength of beam A2-C is almost the same as the predicted, but with slight difference in the ductility by 11%.

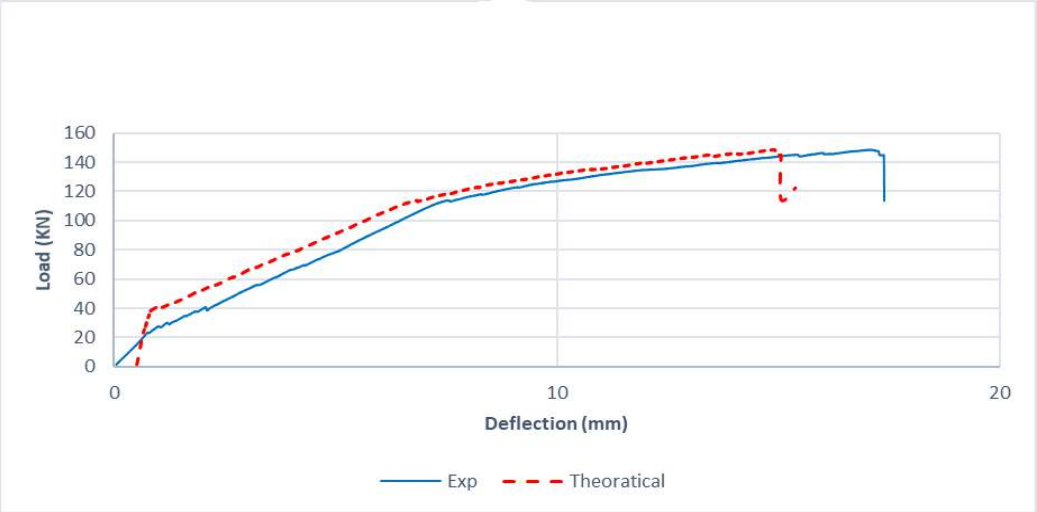

Figure 5-9: Beam A2-C-experimental-theoretical results.

5.2.1.10 ***Beam A2-S***. It can be seen that in Figure 5-10 the experimental strength of beam A2-S is almost the same as the predicted, but with slight difference in the ductility by 17%.

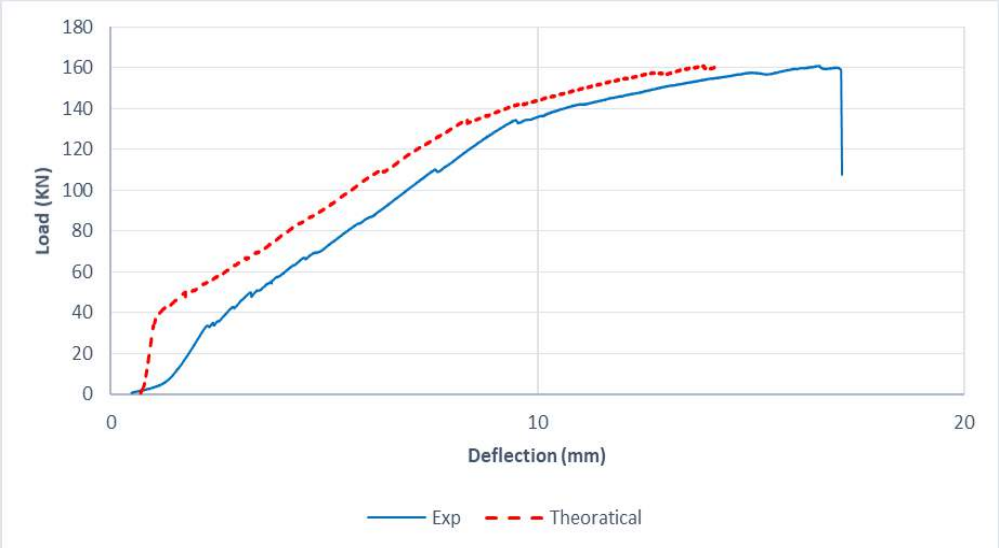

Figure 5-10: Beam A2-S -experimental-theoretical results.

5.2.1.11 ***Beam A2-CA***. It can be seen that in Figure 5-11 the experimental strength of beam A2-CA is almost the same as the predicted, but with slight difference in the ductility by 13%.

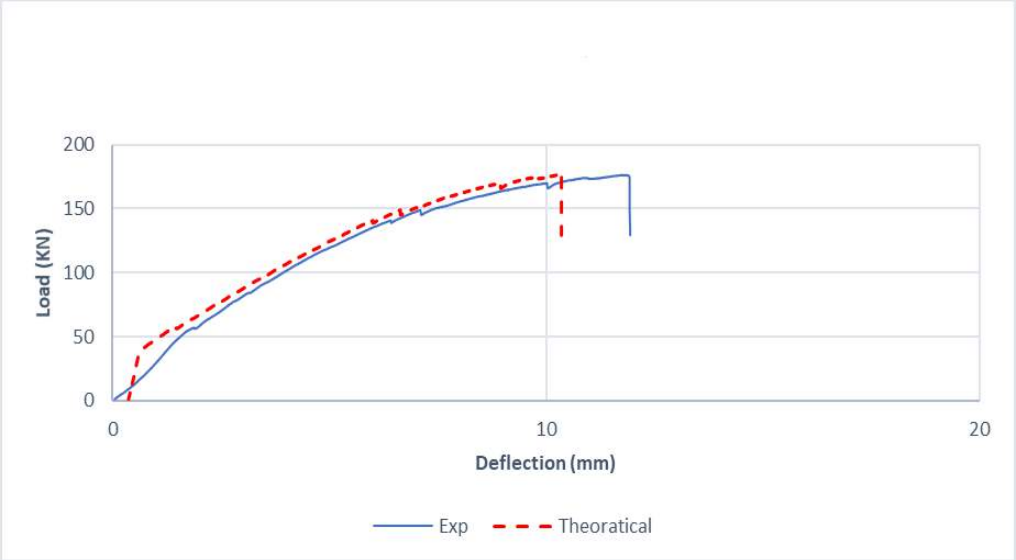

Figure 5-11: Beam A2-CA-experimental-theoretical results.

5.2.1.12 ***Beam A2-SA***. It can be seen that in Figure 5-12 the experimental strength of beam A2-SA is almost the same as the predicted, but with slight difference in the ductility by 13%.

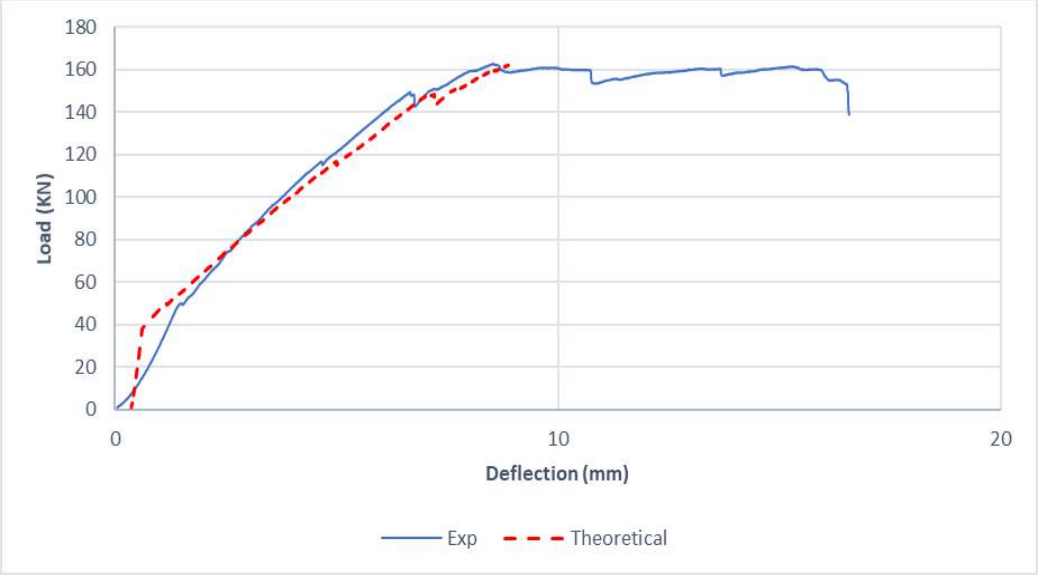

Figure 5-12: Beam A2-SA-experimental-theoretical results.

5.2.2 Group [GB]

5.2.2.1 ***Beam B- Control.*** It can be seen that in Figure 5-13 the experimental strength of B-control beam is almost the same as the predicted, but with slight difference in the ductility by 22%.

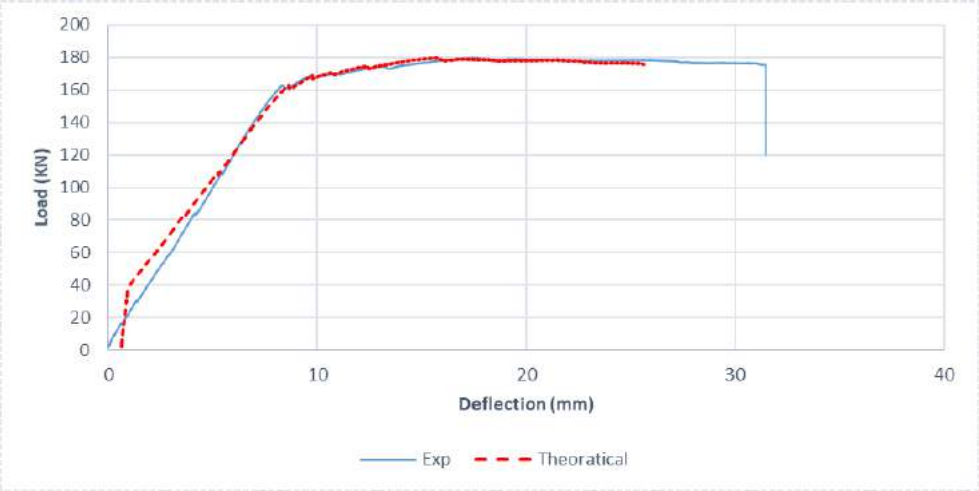

Figure 5-13: Beam B-Control-experimental-theoretical results.

5.2.2.2 ***Beam B1-A.*** It can be seen that in Figure 5-14 the experimental strength of beam B1-A is almost the same as the predicted, but with slight difference in the ductility by 7%.

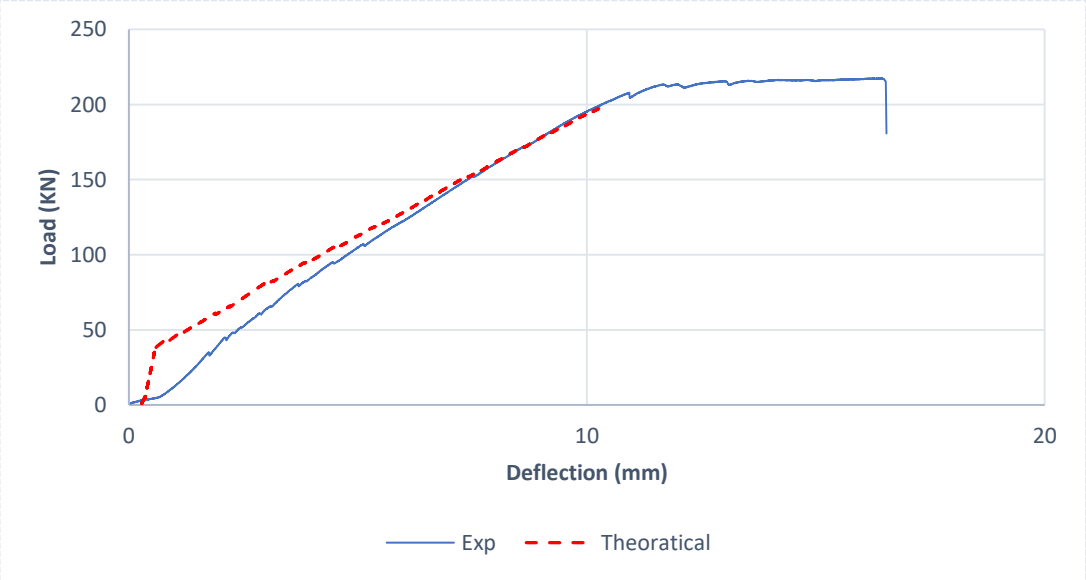

Figure 5-14: Beam B1-A -experimental-theoretical results.

5.2.2.3 *Beam B1-C.* It can be seen that in Figure 5-15 the experimental strength of beam B1-C is almost the same as the predicted, but with slight difference in the ductility by 4%.

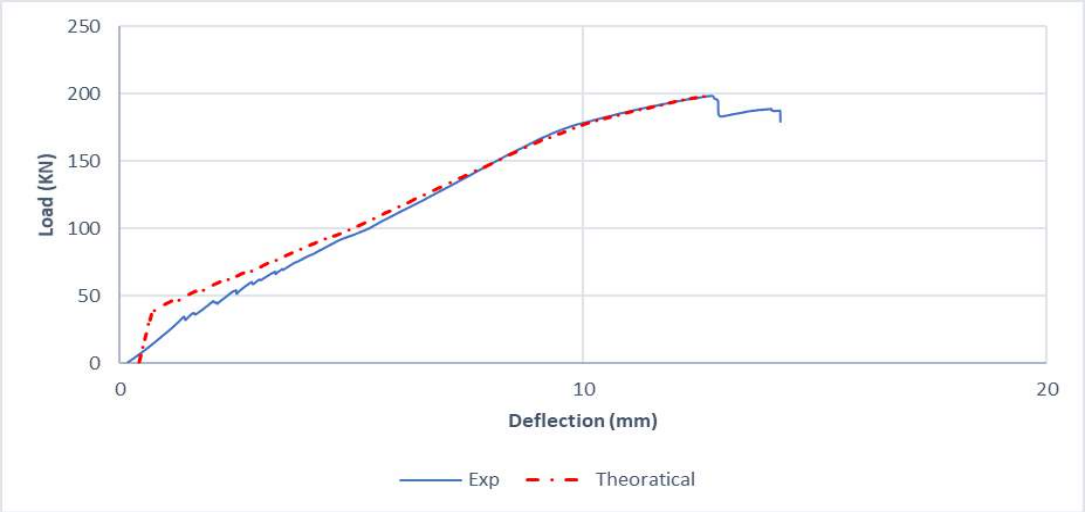

Figure 5-15: Beam B1-C -experimental-theoretical results.

5.2.2.4 *Beam B1-S.* It can be seen that in Figure 5-16 the experimental strength of beam B1-s is almost the same as the predicted, but with slight difference in the ductility by 3%.

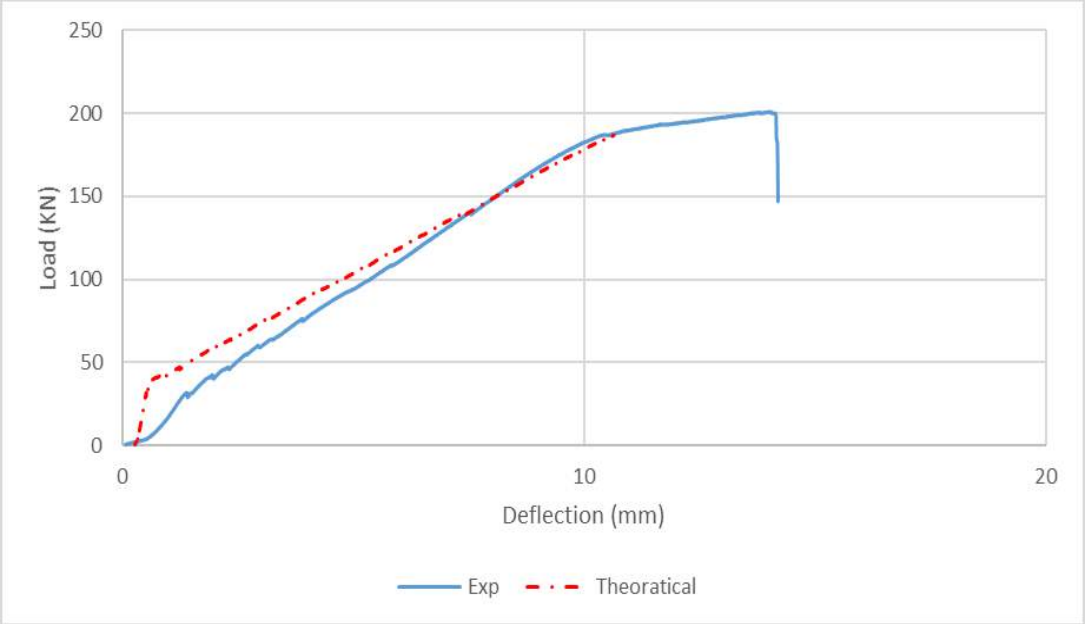

Figure 5-16: Beam B1-S -experimental-theoretical results.

5.2.2.5 ***Beam B1-CA***. It can be seen that in Figure 5-17 the experimental strength of beam B1-CA is almost the same as the predicted, but with slight difference in the ductility by 6%.

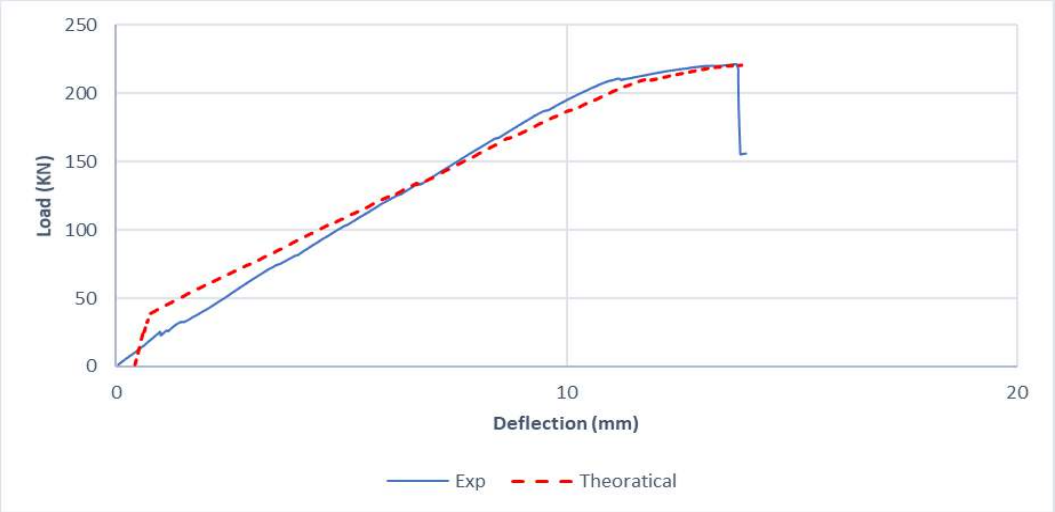

Figure 5-17: Beam B1-CA -experimental-theoretical results.

5.2.2.6 Beam B1-SA. It can be seen that in Figure 5-18 the experimental strength of beam B1-SA is almost the same as the predicted, but with slight difference in the ductility by 4%.

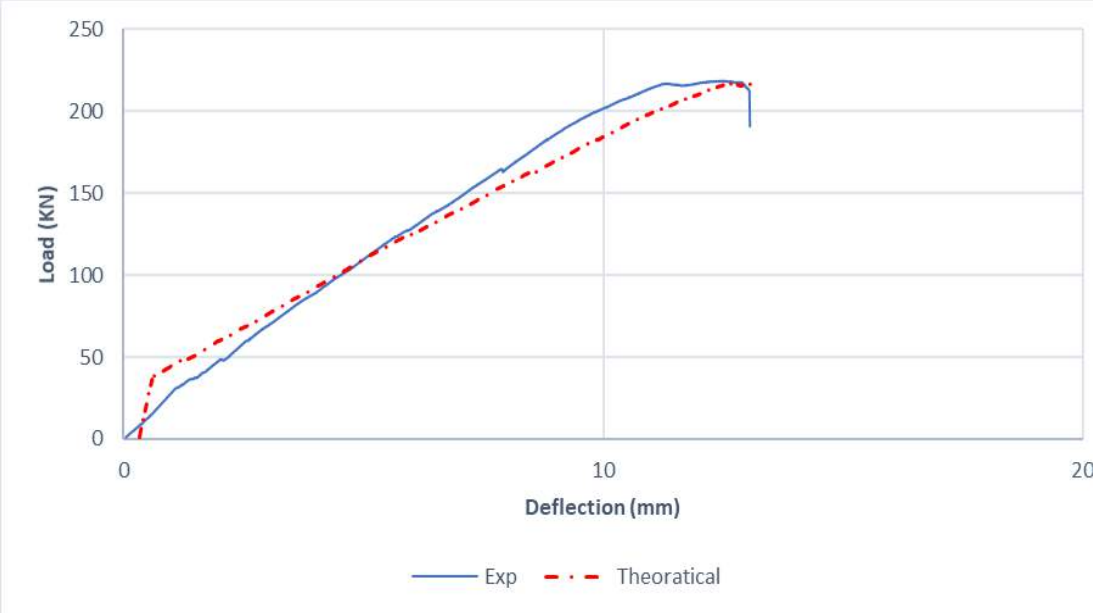

Figure 5-18: Beam B1-S A -experimental-theoretical results.

5.2.2.7 ***Beam B1-CA-W***. It can be seen that in Figure 5-19 the experimental strength of beam B1-CA-W is almost the same as the predicted, but with slight difference in the ductility by 10%.

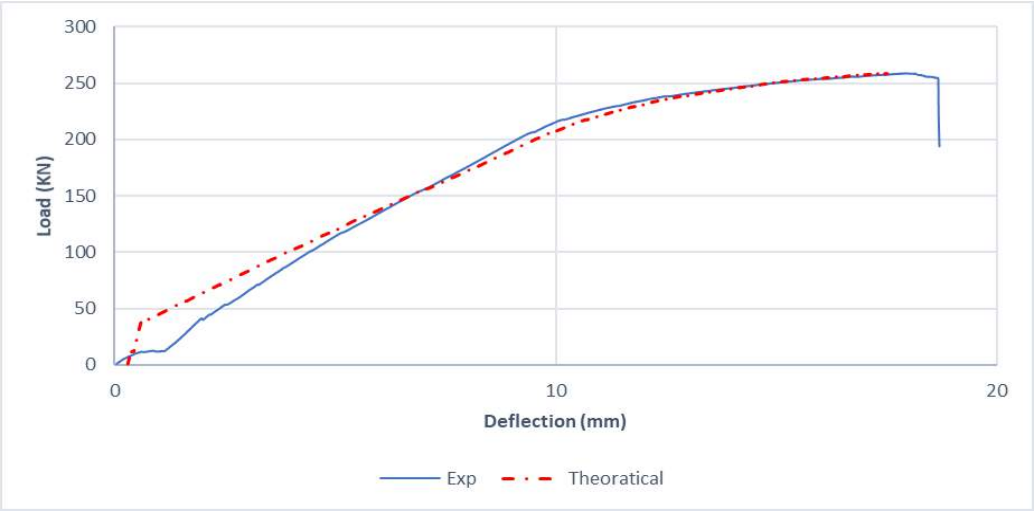

Figure 5-19: Beam B1-CA-W -experimental-theoretical results.

5.2.2.8 ***Beam B1-SA-W***. It can be seen that in Figure 5-20 the experimental strength of beam B1-SA-W is almost the same as the predicted, but with slight difference in the ductility by 12%.

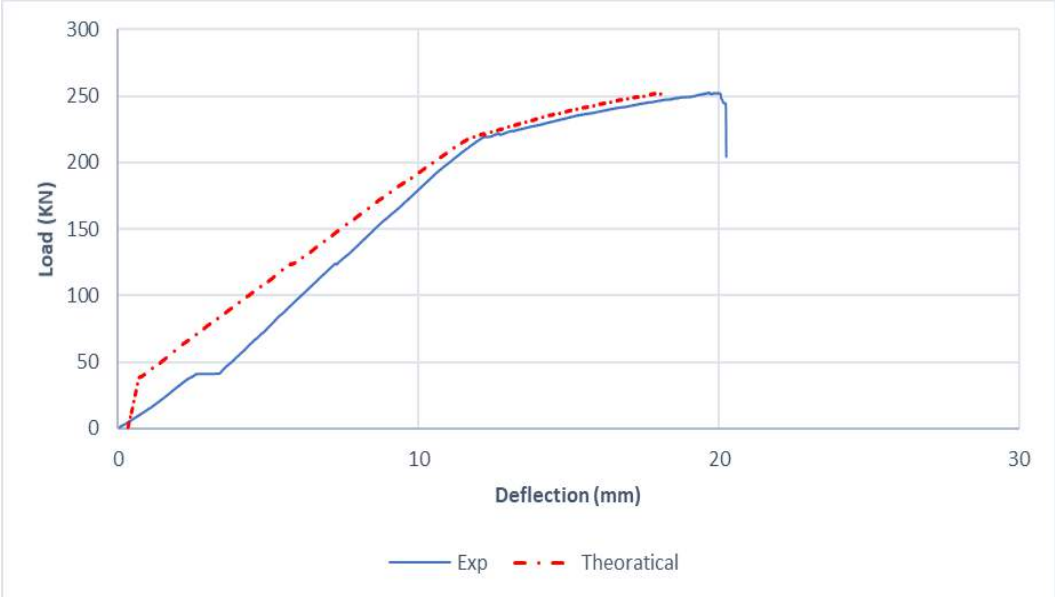

Figure 5-20: Beam B1-SA-W -experimental-theoretical results.

5.2.2.9 *Beam B2-A.* It can be seen that in Figure 5-21 the experimental strength of beam B2-A is almost the same as the predicted, but with slight difference in the ductility by 10%.

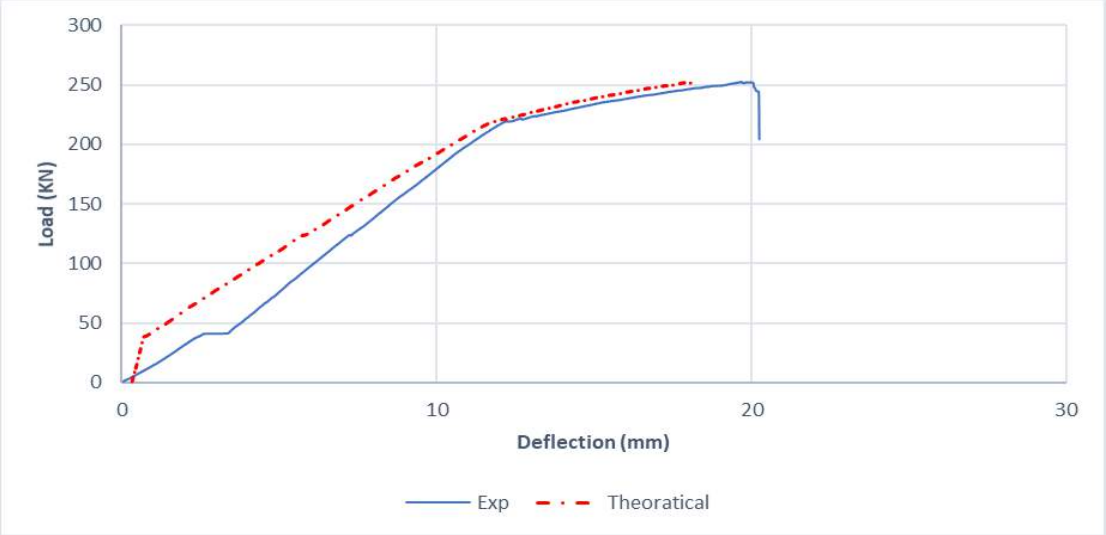

Figure 5-21: Beam B2-A -experimental-theoretical results.

5.2.2.10 *Beam B2-C*. It can be seen that in Figure 5-22 the experimental strength of beam B2-C is almost the same as the predicted, but with slight difference in the ductility by 11%.

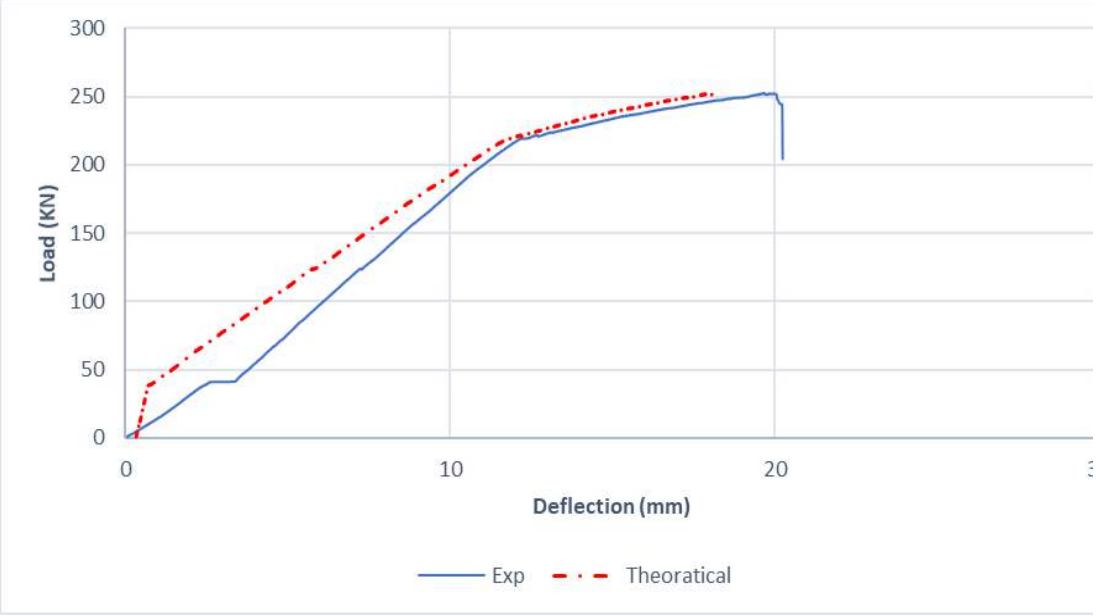

Figure 5-22: Beam B2-A -experimental-theoretical results.

5.2.2.11 ***Beam B2-S***. It can be seen that in Figure 5-23 the experimental strength of beam B2-S is almost the same as the predicted, but with slight difference in the ductility by 4%.

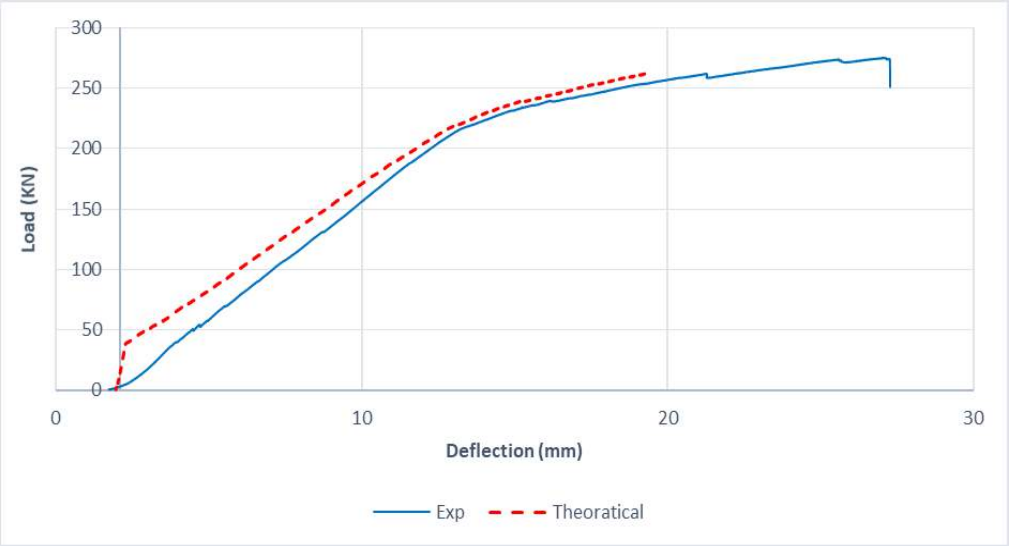

Figure 5-23: Beam B2-S -experimental-theoretical results.

5.2.2.12 ***Beam B2-CA***. It can be seen that in Figure 5-24 the experimental strength of beam B2-CA is almost the same as the predicted, but with slight difference in the ductility by 4%.

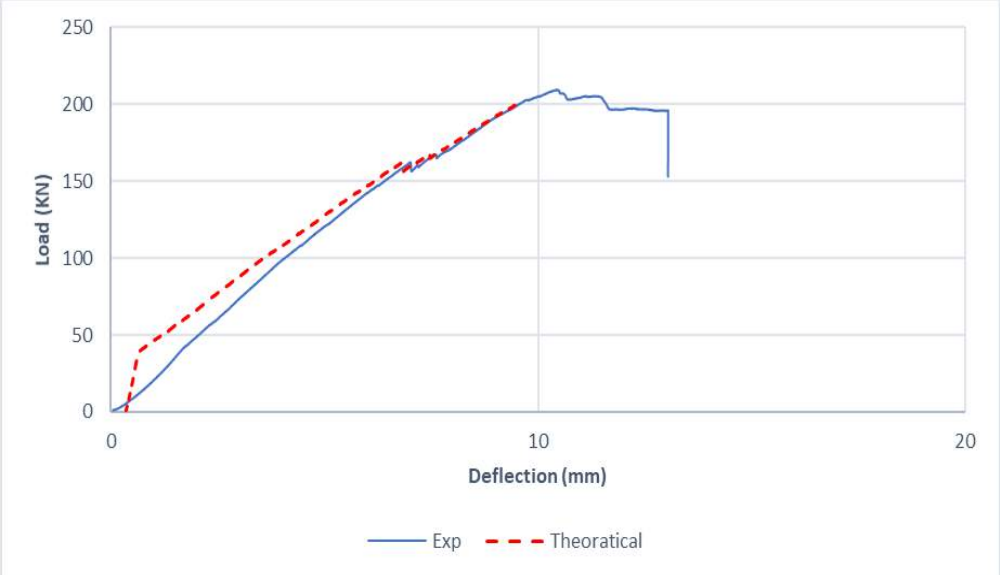

Figure 5-24: Beam B2-CA -experimental-theoretical results.

5.2.2.13 *Beam B2-SA*. It can be seen that in Figure 5-25 the experimental strength of beam B2-SA is almost the same as the predicted, but with slight difference in the ductility by 13%.

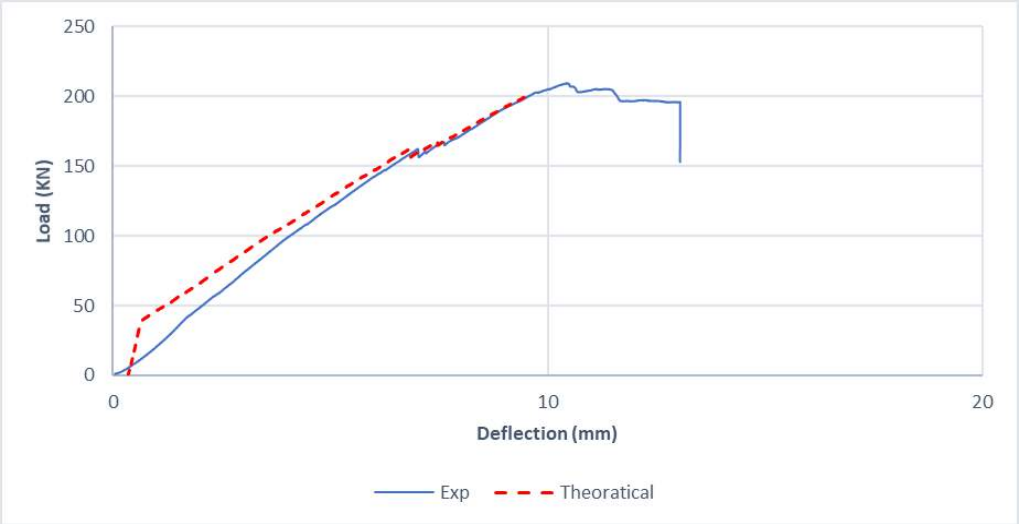

Figure 5-25: Beam B2-SA -experimental-theoretical results.

5.3 Summary of Predicted Deflection vs Experimental Deflection

5.3.1 Group A

Table5-1: Difference in predicted and experimental deflection values (GA)

Test Specimen	δ_{Pre} (mm)	δ_{Exp} (mm)	Difference (%)
A-Control	21.6	29.2	26.0
A1-A	12.9	18.4	29.9
A1-C	12.0	14.3	16.1
A1-S	15.8	13.5	-17.0
A1-CA	18.0	13.6	-32.4
A1-SA	12.9	14.7	12.2
A1-CA-W	18.0	21.2	15.1
A2-A	23.1	17.6	-31.3
A2-C	15.4	17.4	11.5
A2-S	14.2	17.1	17.0
A2-CA	10.4	11.9	12.6
A2-SA	14.4	16.6	13.3

5.3.2 Group B

Table 5-2: Difference in predicted and experimental deflection values (GB)

Test Specimen	δ_{Pre} (mm)	δ_{Exp} (mm)	Difference (%)
B-Control	24.7	31.5	21.6
B1-A	15.3	16.5	7.3
B1-C	13.8	14.3	3.5
B1-S	13.7	14.2	3.5
B1-CA	14.2	13.8	-2.9
B1-SA	13.9	13.1	-6.1
B1-CA-W	17.9	18.7	4.3
B1-SA-W	18.3	20.3	9.9
B2-A	11.9	13.5	11.9
B2-C	14.8	16.5	10.3
B2-S	16.8	18.8	10.6
B2-CA	17	16.4	-3.7
B2-SA	23.8	27.3	12.8

5.4 Results Discussion

Generally, the above graphs illustrate the results of the analytical model versus the experimental results for all tested specimens. The comparison illustrate that the predicted values were almost the same as the experimental ones, especially the curve shape at the elastic region with a small difference within in-elastic region. Moreover, the stiffness of an element overestimated as shown in the slope, which was a slightly higher than the actual values for most of the beams. However, after the load applied on the specimen reached the cracking moment, the analytical model illustrates almost a precise deflection values within the elastic range of the section. Afterwards, the section reaches the ultimate limit state where the model deviates from the actual behavior of the tested specimen with the inelastic range of the section, and it did not predict the exact failure mode as well.

Is observed from Table 5-1 that the analytical results of the beams in-group A demonstrated 30% to 32% difference in ductility compared to the experimental results. On the other hand, Table 5-2 shows that the predicted values differ by -6% to 13% from the experimental values. Moreover, all beams were strengthened with hybrid system showed higher predicted values than the experimental results by -3% to 13%. Therefore, this conclude that the developed analytical model was valid to predict the response of the strengthened RC beams that was strengthened in flexural with

externally bonded AA, CFRP, SM and their hybrid combinations, as it showed a similar behavior trends to the actual load-deflection curves.

Chapter 6: Summary and Conclusion

As previously indicated, several materials have been used as EBR materials to strength and repair aging RC structures. In this study AA, CFRP and GSM fabrics and their hybrid combinations were used as EBR materials due to their potential of overcoming the shortcomings of the current strengthening materials when used separately.

This investigation focused on exploring and understanding the effectiveness of using AA, CFRP, GSM and their hybrid combinations (AA-GSM and AA-CFRP) as new EBR materials for RC Beams. Therefore, a hybrid system which combined different types of FRP materials, resulted in enhancing composite laminate characteristics. A tensile coupon test were carried out to obtain the mechanical properties of this hybrid system, which included the values of elastic modulus, tensile strength and elongation at failure. Moreover, T-beams with different reinforcement ratio were cast and tested using four-point loading test. The beams were strengthened with AA, CFRP and GSM and their hybrid combinations. Results of the analytical models were compared to the experimental results and they were comparable.

As there are several research variables in this study, many observations and conclusion can be drawn as listed below:

1) Coupon test showed that CFRP laminates have higher tensile strength and elastic modulus than that of GSM, and lower strain rupture than AA
2) The hybrid coupon laminate that combined AA with CFRP and AA with GSM, showed a ductile behavior with elongation enhancement compared to the CFRP and GSM laminates separately.
3) Beams that strengthened with hybrid system as AA with CFRP and AA with GSM provided a better strength and ductility performance compared to strengthened beams with AA, CFRP or GSM.
4) The flexural capacity of the strengthened RC T-beams increased by 10% to 77% over the un-strengthened specimens.

5) The ductility of the strengthened RC T-beams decrease by 13%-59% compared to the un-strengthened specimen.
6) The derived analytical model showed a typical response to the Load-deflection curve of the experimental values with differ ranged from -30% to 32%, which indicated that the model was valid to predict the response of the strengthened RC beams.
7) Further studies should be carried out to obtain an optimum hybrid system that can improve the two of strength and ductility of strengthened RC beams in flexure.

References

[1] R. Hawileh, J. Abdalla, and A. Al-Tamimi, “Flexural performance of strengthened RC beams with CFRP laminates subjected to cyclic loading,” Key Eng. Mater., vol. 471–472, pp. 697–702, Feb. 2011.

[2] J. A. Abdalla, A. S. Abu-Obeidah, R. A. Hawileh, and H. A. Rasheed, “Shear strengthening of reinforced concrete beams using externally-bonded aluminum alloy plates: An experimental study,” Constr. Build. Mater., vol. 128, no. October, pp. 24–37, 2016.

[3] A. Al-Tamimi, R. Hawileh, and J. Abdalla, “Effects of ratio of CFRP plate length to shear span and end anchorage on flexural behavior of SCC RC beams,” J. Compos. vol. 15, pp. 11–17, 2011.

[4] A. Ali, J. Abdalla, R. Hawileh, and K. Galal, “CFRP mechanical anchorage for externally strengthened RC beams under flexure,” Phys. Procedia, vol. 55, pp. 10–16, 2014.

[5] R. Hawileh, H. Rasheed, J. Abdalla, and A. Al-Tamimi, “Behavior of reinforced concrete beams strengthened with externally bonded hybrid fiber reinforced polymer systems,” Mater. vol 53, pp. 972-982, Des. 2014.

[6] A. M. Mirghani, J. A. Abdalla, and R. A. Hawileh, “Modeling and simulation of bond-slip behavior of Aluminum Alloy plates adhesively bonded to concrete,” in 2017 7th International Conference on Modeling, Simulation, and Applied Optimization (ICMSAO), 2017, pp. 1–5.

[7] J. A. Abdalla, F. H. Hraib, R. A. Hawileh, and A. M. Mirghani, “Experimental investigation of bond-slip behavior of aluminum plates adhesively bonded to concrete,” J. Adhes. Sci. Technol., vol. 31, no. 1, pp. 82–99, Jan. 2017.

[8] R. A. Hawileh, M. Naser, W. Zaidan, and H. A. Rasheed, “Modeling of insulated CFRP-strengthened reinforced concrete T-beam exposed to fire,” Eng. Struct., vol. 31, no. 12, pp. 3072–3079, 2009.

[9] J. a Abdalla, A. Abu-obeidah, and R. a Hawileh, “Behaviour of Shear Deficient Reinforced Concrete Beams with Externally Bonded Aluminum Alloy Plates,” Building, pp. 18–22, June 2011.

[10] M. Naser, G. Abu-Lebdeh, and R. Hawileh, “Analysis of RC T-beams strengthened with CFRP plates under fire loading using ANN,” Constr. Build.

Mater., vol. 37, pp. 301–309, 2012.

[11] R. A. Hawileh, “Finite element modeling of reinforced concrete beams with a hybrid combination of steel and aramid reinforcement,” Mater. Des, vol. 65, pp. 831–839, November 2015.

[12] R. Hawileh, T. El-Maaddawy, and M. Naser, “Nonlinear finite element modeling of concrete deep beams with openings strengthened with externally-bonded composites,” Mater. vol 42, pp 378-387 Des, 2012.

[13] R. Hawileh, J. A. Abdalla, and A. K. Al-Tamimi, “Flexural performance of strengthened RC beams with CFRP laminates subjected to cyclic loading,” Key Eng. Mater., vol. 471–472, pp. 697–702, Feb. 2011.

[14] H. A. Rasheed, *Strengthening Design of Reinforced Concrete with FRP*. CRC Press; pp 351 2014 Dec.

[15] M. Naser, “Bond behavior of CFRP cured laminates: experimental and numerical investigation,” J. Eng. Mater. Technol., vol. 134, no. 2, pp. 5-9, 2012.

[16] J. Zhu, M. Zhu, L. Wei, and W. Li, “Bond behavior of aluminum laminates in NSM technique,” Appl. Mech., vol 501, pp.504 2014.

[17] A. F. Ashour, S. A. El-Refaie, and S. W. Garrity, “Flexural strengthening of RC continuous beams using CFRP laminates,” Cem. Concr. Compos., vol. 26, no. 7, pp. 765–775, 2004.

[18] J. Dong, Q. Wang, and Z. Guan, “Structural behaviour of RC beams with external flexural and flexural-shear strengthening by FRP sheets,” Compos. Part B Eng., vol. 44, no. 1, pp. 604–612, 2013.

[19] M. R. Esfahani, M. R. Kianoush, and R. Tajari, “Flexural behaviour of reinforced concrete beams strengthened by CFRP sheets,” Eng. Struct., vol. 29, pp. 2428–2444, 2007.

[20] R. Aboutaha, P. Wattanadechachan, and S. Kim, “Flexural Ductility of CFRP Strengthened Concrete Beams-Experimental Investigation,” Spec. Publ. vol 213, pp 207-220, 2003.

[21] H. Toutanji, L. Zhao, and Y. Zhang, “Flexural behavior of reinforced concrete beams externally strengthened with CFRP sheets bonded with an inorganic matrix,” Eng. Struct. vol 28(4), pp.557-566, 2006.

[22] A. Borri and M. Corradi, “Strengthening of timber beams with high strength steel cords,” Compos. Part B Eng., vol. 42, no. 6, pp. 1480–1491, 2011.

[23] G. de Felice, S. de Santis, A. Napoli, and R. Realfonzo, “Overview of the

experimental works on steel reinforced polymer systems," Appl. Mech. Mater., vol. 847, in November 2016, pp. 369–380, 2016.

[24] A. A. Bashandy, "Flexural strengthening of reinforced concrete beams using valid strengthening techniques," Arch. Civ. Eng., vol. 59, no. 3, pp 275-293. 2013.

[25] U. Meier, "Strengthening of structures using carbon fibre/epoxy composites," Constr. Build. Mater., vol. 9, no. 6, pp. 341–351, 1995.

[26] F. Mazzolani, "Structural applications of aluminium in civil engineering," Struct. Eng. Int., vol 16, no. 4, pp 280-285. 2006.

[27] S. Islam and B. Young, "FRP strengthened aluminium tubular sections subjected to web crippling," Thin-Walled Struct., vol 49, no. 11, pp 1392-1403, 2011.

[28] K. A. Harries, H. R. Hamilton, J. Kasan, and J. Tatar, "Development of standard bond capacity test for FRP bonded to concrete," 6th Int. Conf. fiber Reinf. Polym. Compos. Civ. Eng., no. June, pp. 1–8, 2012.

[29] N. Grace, G. Abdel-Sayed, and W. Ragheb, "Strengthening of concrete beams using innovative ductile fiber-reinforced polymer fabric," ACI Struct. J. vol 99, no. 5, pp 692-700, 2002.

[30] Z. Wu, Y. Shao, and K. Iwashita, "Strengthening of preloaded RC beams using hybrid carbon sheets," J. Compos. Vol 11(3), pp.299-307, 2007.

[31] Y. Wu and Y. Huang, "Hybrid bonding of FRP to reinforced concrete structures," J. Compos. Constr. vol 12(3), pp.266-273., 2008.

[32] A. Ahmed, M. Fayyadh, and S. Naganathan, "Reinforced concrete beams with web openings: A state of the art review," Mater. vol 40, pp 90-102. Des, 2012.

[33] H. Akbarzadeh and A. Maghsoudi, "Experimental and analytical investigation of reinforced high strength concrete continuous beams strengthened with fiber reinforced polymer," Mater. vol 31(3), pp 1130-1147 Des., 2010.

[34] O. Rabinovitch and Y. Frostig, "Experiments and analytical comparison of RC beams strengthened with CFRP composites," Compos. part B Eng. vol 34(8), pp.663-677, 2003.

[35] Y. Zhou, M. Gou, F. Zhang, S. Zhang, and D. Wang, "Reinforced concrete beams strengthened with carbon fiber reinforced polymer by friction hybrid bond technique: Experimental investigation," Mater. vol 50, pp.130-139. Des, 2013.

[36] H. Toutanji, L. Zhao, and Y. Zhang, "Flexural behavior of reinforced concrete beams externally strengthened with CFRP sheets bonded with an inorganic

matrix," Eng. Struct., vol. 28, no. 4, pp. 557–566, 2006.

[37] N. Grace, W. Ragheb, and G. Abdel-Sayed, "Developing and modeling of new ductile FRP systems for strengthening concrete structures," Development, vol 443(016), pp.383. 2004.

[38] G. J. Xiong, J. Z. Yang, and Z. B. Ji, "Behavior of reinforced concrete beams strengthened with externally bonded hybrid carbon fiber–glass fiber sheets," J. Compos. Constr., vol. 8, no. 3, pp. 275–278, Jun. 2004.

[39] N. Attari, S. Amziane, and M. Chemrouk, "Flexural strengthening of concrete beams using CFRP, GFRP and hybrid FRP sheets," Constr. Build. Mater., vol. 37, pp. 746–757, 2012

[40] ACI Committee 318, "Building Code Requirements for Reinforced Concrete," ACI Struct. J., vol. 552, pp. 503, 2011.

[41] E. J. Barbero, *Introduction to Composite Materials Design*. CRC press 2010.

[42] Sika. Technical data sheet for Sikadur® -30 -part epoxy impregnation resin. Sika Services AG, Switzerland; pp. 1–6, 2012.

[43] Sika. Technical data sheet for SikaWrap®-300 C/60 fiber fabric. Sika Services AG, Switzerland; pp. 1–3, 2003.

[44] FIDIA. Technical data sheet for FIDBASALT UNIDIR C95®, Unidirectional Ultra-High Tensile Steel Sheet for Structural Strengthening. FIDIA Technical Global Services, Milano, Italy; pp. 3–4, 2010.

[45] ASTM International, "Standard test method for tensile properties of plastics," ASTM Int., vol. 8, pp. 46–58, 2003.

[46] A. Gartner, E. P. Douglas, C. W. Dolan, and H. R. Hamilton, "Small Beam Bond Test Method for CFRP Composites Applied to Concrete," J. Compos. Constr., vol. 15, no. 1, pp. 52–61, 2011.

Vita

Abubakr Ahmed Abdelall Mohammed was born in 1990, in Madani, Sudan. Abubakr received a Bachelor of Science in Civil Engineering from University of Khartoum with first class Honors in 2013, his academic performance was ranked within the top five among 150 students in his class when he graduated. He joined the Master's program at AUS in Fall 2015, and he is a graduate research assistant at the American University of Sharjah. His research interests include design, construction, analysis and simulation of reinforced concrete and steel structures.